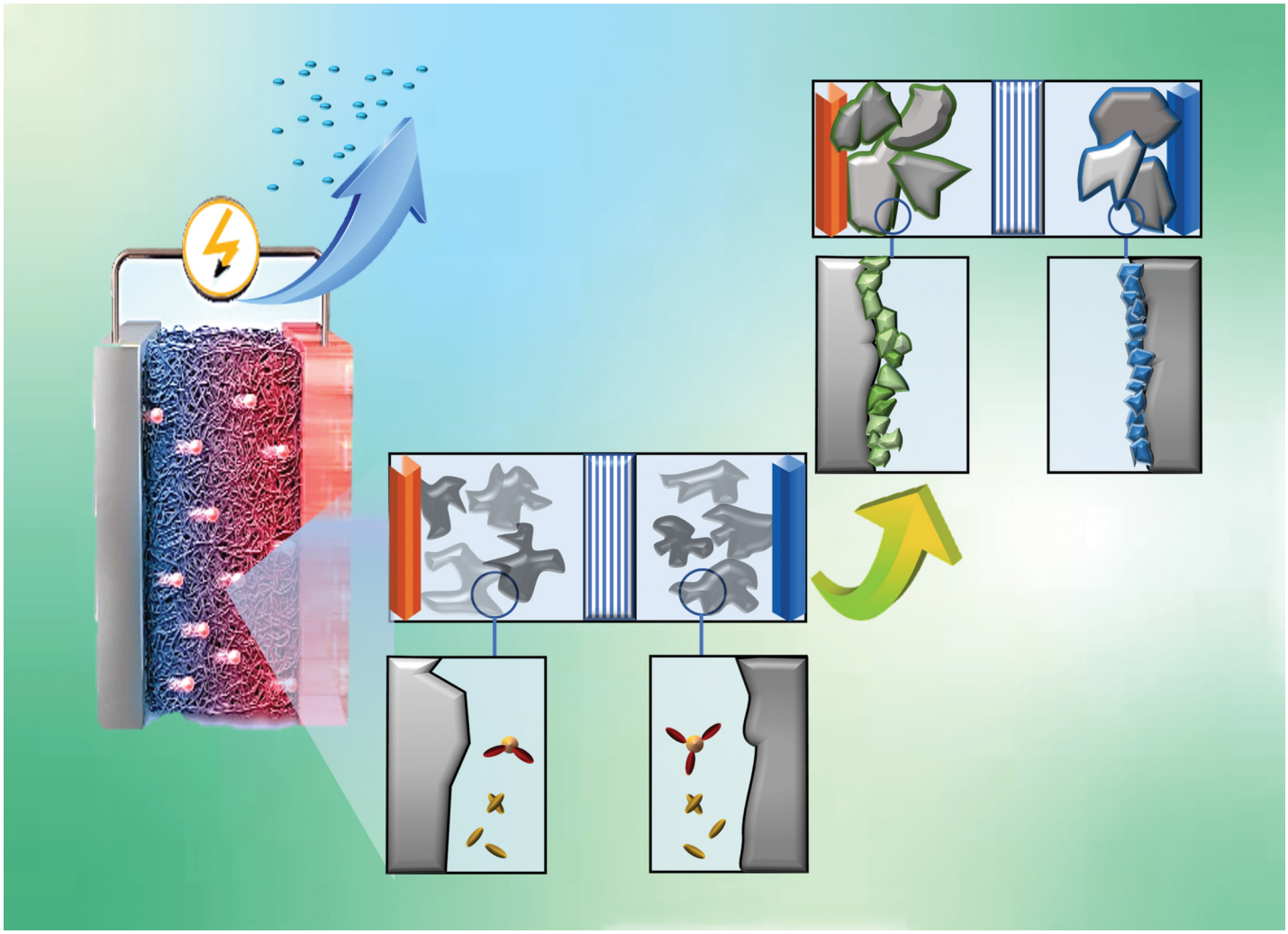

Showcasing research from Dr Cheong's and Prof. Röder's lab groups, Bavarian Center for Battery Technology (Baybatt), University of Bayreuth, Bavaria, Germany.

Lithium-ion battery cell formation: status and future directions towards a knowledge-based process design

Formation processing is one of the most intriguing processing steps that is required for the lithium-ion battery manufacturing process. The scheme addresses the objective and the role of the formation processing step within the conventional lithium-ion battery configuration. Through the formation step, there are changes in interfacial, morphological, and surficial properties of the electrode and active materials, which are expected to contribute to the safety and performance enhancement of the lithium-ion battery.

As featured in:

See Jun Young Cheong, Fridolin Röder *et al.*, *Energy Environ. Sci.*, 2024, **17**, 2686.

ROYAL SOCIETY OF CHEMISTRY

rsc.li/ees

Registered charity number: 207890

Energy & Environmental Science

ROYAL SOCIETY OF CHEMISTRY

REVIEW

View Article Online
View Journal | View Issue

Cite this: *Energy Environ. Sci.*, 2024, **17**, 2686

Lithium-ion battery cell formation: status and future directions towards a knowledge-based process design

Felix Schomburg,[a] Bastian Heidrich,[b] Sarah Wennemar,[c] Robin Drees,[def] Thomas Roth,[g] Michael Kurrat,[de] Heiner Heimes,[c] Andreas Jossen,[g] Martin Winter,[bh] Jun Young Cheong *[ai] and Fridolin Röder *[a]

Received 20th October 2023,
Accepted 5th February 2024

DOI: 10.1039/d3ee03559j

rsc.li/ees

The battery cell formation is one of the most critical process steps in lithium-ion battery (LIB) cell production, because it affects the key battery performance metrics, *e.g.* rate capability, lifetime and safety, is time-consuming and contributes significantly to energy consumption during cell production and overall cell cost. As LIBs usually exceed the electrochemical sability window of the electrolyte, formation is required to activate and stabilise the electrochemical reactions. Enhanced battery technologies are poised to further expand voltage windows and harness conversion or metal electrodes to elevate energy density, thereby magnifying the significance of cell formation in the battery realm. Despite its critical importance, even the understanding of the formation process of conventional LIBs is still incomplete due to numerous influencing factors. Complex internal processes and the associated high experimental and simulation effort make it difficult to gain a thorough understanding of the process and hence to optimise it. This review paper provides a systematic overview of the formation process and its influencing factors. It is emphasized that material and cell design and the formation process are not independent, but must interlock with each other. Promising experimental and simulative methods to gain the required understanding of the interplay for a truly knowledge-based design of the formation process are highlighted. In the concluding discussion research gaps are identified and a perspective for development of tailored cell formation processes for current and future battery technologies is outlined.

Broader context

Driven by the transition towards renewable energy sources and electromobility, the demand for cost-effective and sustainable batteries is continuously growing. Simultaneously, the demand for higher energy densities entails safety risks and challenges in maintaining long lifetime. Addressing these challanges is crucial to overcome driving anxiety and concerns against novel technology. These issues are closely linked to the formation process, which is essential to establishing stable interphase layers and utilizing materials outside the electrolyte's stability window. Challenges intensify with new materials like high-voltage cathodes and lithium metal or silicon anodes. In addition, sodium-ion technologies, seen as promising alternatives, face hurdles in establishing stable interphase layers due to high solubility. In all these technologies, a well-designed formation process is pivotal, yet complicated due to many interdependent influencing factors. This review highlights the need for a knowledge-based process design to ensure safe and durable batteries. By reviewing the status, outlining theoretical and experimental methods, the necessary foundation is laid.

[a] *Bavarian Center for Battery Technology (BayBatt), Weiherstr. 26, 95448 Bayreuth, Germany. E-mail: jun.cheong@uni-bayreuth.de, fridolin.roeder@uni-bayreuth.de*
[b] *MEET Battery Research Center, Institute of Physical Chemistry, University of Münster, Corrensstr. 46, 48149 Münster, Germany*
[c] *Production Engineering of E-Mobility Components RWTH Aachen University Bohr 12, 52072 Aachen, Germany*
[d] *elenia Institute for High Voltage Technology and Power Systems, Technische Universität Braunschweig, Schleinitzstraße 23, 38106 Braunschweig, Germany*
[e] *Battery LabFactory Braunschweig, Technische Universität Braunschweig, Langer Kamp 8, 38106 Braunschweig, Germany*
[f] *Fraunhofer Research Institution for Battery Cell Production FFB, Bergiusstraße 8, 48165 Münster, Germany*
[g] *Technical University of Munich, School of Engineering and Design, Department of Energy and Process Engineering, Chair for Electrical Energy Storage Technology, Arcisstraße 21, 80333 Munich, Germany*
[h] *Helmholtz Institute Münster, IEK-12, Forschungszentrum Jülich GmbH, Corrensstr. 46, 48149 Münster, Germany*
[i] *Department of Chemistry, University of Bayreuth, Universitätsstraße 30, 95447 Bayreuth, Germany*

Introduction

Since their first commercialisation by Sony in 1991, lithium-ion batteries (LIBs) have been used in various applications ranging from consumer electronics to electric vehicles.[1,2] Reflecting the tremendous impact of LIBs on all aspects of people's life, the Nobel Prize in Chemistry was awarded to Prof. John B. Goodenough, Prof. M. Stanley Whittingham and Prof. Akira Yoshino for the development of LIBs.[3] The demand for LIBs is set to increase dramatically in the coming years.[4] At the same time, increasing energy density poses significant challenges to ensuring safety and long lifetime.[5–9] In addition, it is vital to minimise the cost, time, energy consumption and waste associated with the manufacture of LIBs. Hence, a thorough understanding of each production step is essential to facilitate the development of current and next-generation LIBs.[10,11]

Formation is the final active process step in LIB cell manufacturing. The process affects the quality of the freshly assembled cells and contributes significantly to the overall cost, accounting for up to 33% of the production cost.[12,13] Formation typically involves multiple charge and discharge cycles. The formation cycling is required to activate the materials and establish protective interphase layers at the electrochemically active interfaces that enable a stable operation of the cell outside the electrolyte's electrochemical stability window. The drive to increase energy density will place higher demands on the formation process, as high-capacity and high-voltage materials utilize a wider voltage window and are subject to significant volume changes.

The formation process must be carried out carefully, as it is linked to influence key electrochemical and safety properties of LIB cells. However, overly cautious formation is time consuming and therefore at odds with efforts to accelerate battery cell production and reduce overall costs. There is a significant potential to improve the formation process to optimise cell quality and reduce overall costs.[14] The industry uses highly sophisticated procedures, but details are guarded as they are considered essential intellectual property of the manufacturers. Despite its importance, the formation process is not well understood due to the limited number of comprehensive studies in academia.

This review comprehensively summarises, examines and analyses the various facets of the formation process. It describes the formation process, presents the current state of knowledge on the various influencing factors, and highlights the most relevant experimental and theoretical methods for future research. In the light of future battery technologies aimed at higher energy density, a summary and suggestions for the further development of the formation process are presented. This review contributes to the overall understanding of formation and provides suggestions for methods and open questions being relevant to enable a knowledge-based process design for current and future battery technologies.

Felix Schomburg

Felix Schomburg is a research associate and PhD candidate at the University of Bayreuth and Bavarian Center for Battery Technology. He obtained a MSc at the TU Braunschweig in 2017. Afterwards he worked on several projects as a software developer and engeering consultant in the automotive industry. Since joining Prof. Röder's group in 2020, his research focuses on model-based investigations of formation procedures and their influence on the ageing behavior of lithium-ion batteries.

Jun Young Cheong

Jun Young Cheong is currently a group leader at University of Bayreuth, serving both Department of Chemistry and Bavarian Center for Battery Technology. Prior to joining University of Bayreuth, he was a staff engineer at Samsung SDI, specializing on electrode processing. He received his BS degree, MS degree, and PhD degree in materials science and engineering from KAIST in Korea (2014/2016/2020, respectively). His current research topic includes the synthesis of functional materials, energy storage and conversion, and in situ characterizations. Jun Young has published more than 80 articles and holds numerous patents and patent applications.

Fridolin Röder

Fridolin Röder is assistant professor for methods for battery management at the University of Bayreuth. After a PhD in 2019 at the TU Braunschweig (Germany) and a visiting scholar at MIT in 2015, he had a junior research group on multiscale development of batteries at TU Braunschweig until 2020. For more than 10 years he has been active in the field of modeling and characterization of energy systems with a special focus on batteries.

Description of the cell formation process

Formation within the LIB production

The production of LIBs can be divided into four parts: electrode production, cell production, cell conditioning† and system assembly.[13] For battery cell production, the system assembly is excluded. Typical design objectives are high energy density, high power density, low production cost, long lifetime and safety. Battery cell formation is part of cell conditioning. Cell conditioning also includes various quality test steps and quality sorting.

The purpose of the formation process is to electrochemically activate the cell so that its subsequent performance is positively influenced. The formation process is critical for a number of reasons. Firstly, formation is the last process step in the production of a battery cell and any scrap that is produced during formation causes the loss of value of all previous process steps.[13] Secondly, the formation process is very time consuming and energy intensive.[15,16] Finally, the process can have a significant impact on cell performance metrics such as capacity, power capability, lifetime and safety.

The formation process is often a production bottleneck due to the relatively low currents applied to individual cells.[17] Achieving high throughput requires significant investment in equipment and cell formation space. Manufacturers therefore aim to reduce the formation time.[18]

Formation time is highly dependent on cell quality requirements and cell-to-cell variation. For batteries with lower quality requirements, relatively short formation times are possible. Here the quality controls performed as part of the formation/conditioning phase are often less sophisticated.[18] Therefore, the progress of formation and individual cell quality is often not known. In applications such as electric vehicles (EV), cell quality and cell-to-cell variation are very important because the lowest cell capacity limits the total usable battery capacity. Further cell-to-cell variation within a battery system promotes ageing and is a safety concern.[19] Therefore, battery cell production for such applications requires much more sophisticated formation procedures, including quality management measures. The formation time is much longer and may include various intermediate cell tests.

The energy consumption of the formation process is significant.[16] According to Kurland *et al.*, Northvolt expects the cell production at Northvolt Ett to use 20% of the total production electricity consumption for the formation step.[20] In general, the electricity consumption can vary significantly between laboratory scale and industrial plants. According to Erakca *et al.* this is because recuperation is commonly used in industrial production facilitities.[21] Recuperation is the process of recovering energy released during battery discharge. Consumption also depends on the energy consumption of the electrical equipment, which is usually higher for laboratory equipment. Thus, the energy consumption of the formation process can vary from 0.6 Wh of Wh cell capacity produced in pilot plants to 42.6 Wh of Wh cell capacity produced in laboratory cell productions.[21]

The formation process is influenced by several factors. These include material and cell design, as well as the electrochemical conditions during formation. Some of these factors, such as electrode properties or moisture contamination, also depend on previous manufacturing steps. Therefore, the entire process chain and its interdependencies must be considered when optimising the formation process.[22,23]

Description of the process

Before the formation process, the cell is filled with electrolyte. This places the active and inactive materials of the electrode in direct contact with the electrolyte, as shown on the left in Fig. 1. Electrochemical reactions and passivation of the interface take place only if the electrolyte and the electrode are in direct contact. Therefore, complete wetting, *i.e.* filling of the electrode pores with electrolyte, is required for formation.[24–27] As the battery is initially in a completely discharged state, there is limited interaction between the electrodes and the electrolyte. The start of formation can be defined as the point at which the cell is electrically connected, and the first charge is initiated.

During formation several processes take place that lead to significant changes in the cell properties. The main processes observed are shown in the centre of Fig. 1. These processes include solid electrolyte interphase (SEI) formation,[28] cathode electrolyte interphase (CEI) formation,[29] structural changes in the active material,[30–32] copper (Cu) corrosion[33–37] and aluminium (Al) dissolution.[36,38–40]

The interfacial layers formed on the negative and positive electrodes can be expressed in terms of low unoccupied molecular orbitals (LUMO) and high occupied molecular orbitals (HOMO), as shown in Fig. 2.[41,42] Both electrodes can reach potentials that exceed the electrochemical stability window of the electrolyte triggering electrochemical side reactions.

Among the processes during the formation, SEI formation is the most widely studied. This process is initiated by an irreversible electrochemical reduction reaction that consumes electrical charge, lithium (Li), solvent and other electrolyte components at the negative electrode. The reaction products can precipitate on the electrode surface inhibiting further side reactions. The ideal passivation layer exhibits strong electrical insulation, high ion conductivity, mechanical and thermal stability.[43–47] The most commonly reported SEI components are lithium fluoride (LiF),[48–53] lithium carbonate (Li_2CO_3),[48,53–58] lithium oxide (Li_2O),[48,53,55] litihium ethylene dicarbonate (LEDC)[51,52,59] and lithium alkyl (bi)carbonates ($ROCO_2Li/RCO_2Li$).[50,53,55,58]

CEI formation is another side-reaction that is first initiated during formation. The process is initiated by an oxidation reaction that releases electrical charge to the positive electrode.[60,61] Like SEI, CEI inhibits further degradation.[62] The CEI is thinner than the SEI,[55,63,64] suggesting a lower magnitude of charge transfer due to CEI formation compared to SEI formation. Typical CEI components are LiF,[55,65–68]

† Cell conditioning is also occasionally called cell finalisation. Both refer to the same part of the manufacturing process. Throughout the rest of the script, we only use cell conditioning.

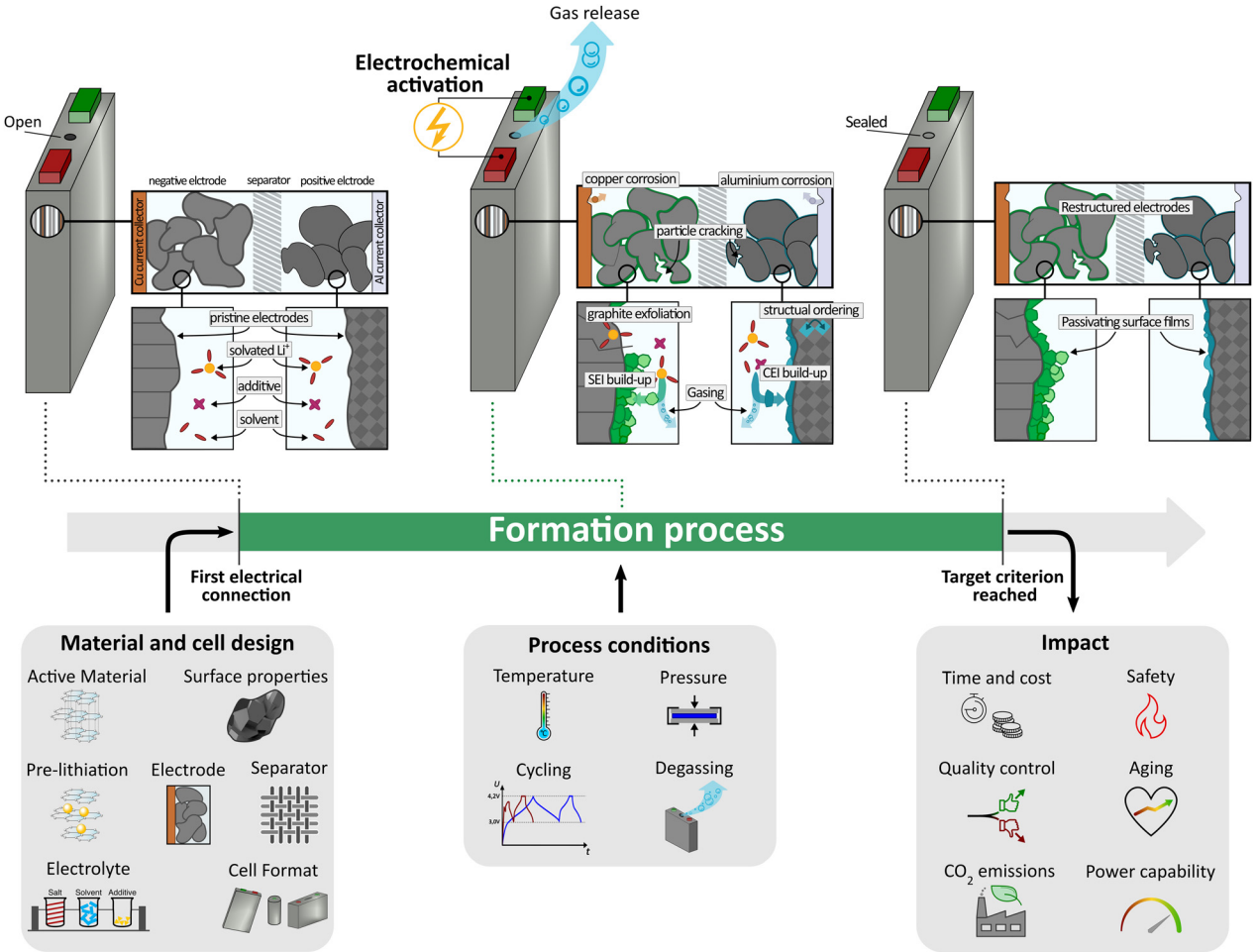

Fig. 1 Schematic overview of the formation process and manuscript. The formation begins with a freshly assembled cell (top left battery). The formation of state-of.art LIBs starts with its first connection of the cell. During formation, a number of processes take place within the cell that are required to electrochemically activate the cell and establish passivation layers on the electrodes (top centre battery). After reaching a target criterion, the formation is finished. Within the battery the electrodes have been restructured and passivating surface films have formed (top right battery). The formation process is influenced by a variety of factors. These can be categorised into *Material and cell design* properties (left box) and *Process conditions* (centre box). The first part of this review is structured according to this categorisation. The impact (right box) of the individual influencing factors is discussed in the respective chapters.

$Li_xPO_yF_z$,[65,67–69] Li_2CO_3[65–67,69,70] and $ROCO_2Li$.[66–71] For both interface processes, reaction products can also be gaseous species.[72–74]

Despite the interfacial processes, structural changes have also been observed during the first cycles. Agglomeration of nanoparticles,[75] particle cracking[76–81] or exfoliation of particles[82–84] can lead to significant changes of the active material. Structural changes have also been observed at the material level. Here, irreversible rearrangement of the material can cause significant heat release and voltage hysteresis during the first cycle.[31,85–87]

After the end of formation, the cell characteristics should stabilise. A commonly used indicator of this stabilisation is the coulombic efficiency (CE), which approaches 100% towards the end of formation.[18] CE is therefore useful in defining a target criterion for the end of formation.

After formation, the cell properties have changed significantly. Firstly, the formation results in a loss of cyclable Li, which has been immobilised mainly by the side reactions forming SEI.[88–90] Secondly, the loss of cyclable Li results in a reduced cell capacity[91] and a relative shift in the electrode open circuit potentials.[92] Thirdly, there is an increase in interfacial resistance.[93–96] In addition, the grown passivation layer and structural changes are likely to lead to a decrease of porosity. Further, electrode restructuring leads to a decrease in conductivity as seen in ageing studies.[97–99] Similarly, the electrolyte composition is changed after formation,[100,101] which impacts the Li-ion diffusivity and ionic conductivity.[99,102,103]

All of these changes can have a significant impact on cell performance in terms of ageing,[104–106] power capability,[107–111] safety,[112–118] energy consumption,[12,13,17] cost[12,13,17] and CO_2 emissions[12,13] as shown in Fig. 1.

Procedures

To influence cell quality and process time, several procedures are possible during formation. The formation procedure is

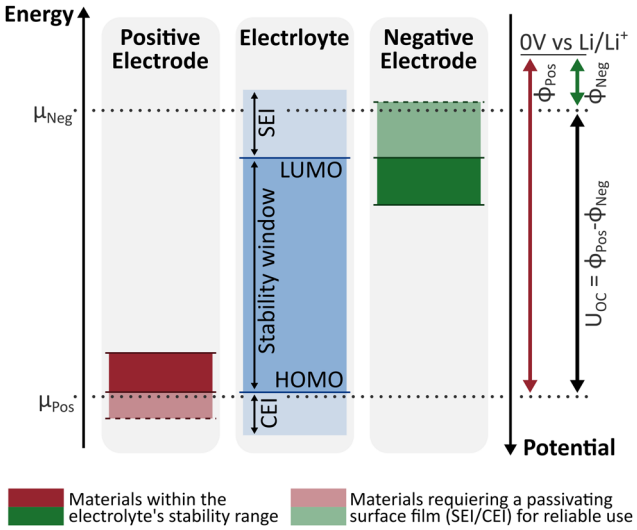

Fig. 2 Schematic representation of the thermodynamic stability window of the electrolyte|electrode interface. Φ and μ represent the electrodes potential and chemical potential, respectively. The indices Neg and Pos denote the negative and positive electrodes, repectively. Stabilising passivation layers, *i.e.* SEI and CEI, are formed when Φ_{Neg} < LUMO and Φ_{Pos} > HOMO, respectively. The passivation layers extend the operating stability range, allowing the use of low voltage materials on the negative and high voltage materials on positive electrode. Redrawn from Goodenough and Kim,[41] as well as Horstman *et al.*[42]

initiated after the initial wetting and includes several possible steps, *i.e.* pre-charging, formation cycling, degassing, 2nd wetting and ageing. The procedure may vary depending on the cell format and size.[119,120] A possible procedure, applicable to hard-case cell formats and high-quality requirements, *e.g.* for the automotive industry, is described below. The process and the steps involved are illustrated in Fig. 3.

Prior to the start of the formation process, initial wetting is carried out. This can be done by a high temperature soaking process, in which the cells are exposed to high temperatures, typically between 30–50 °C, for several hours to change the viscosity of the electrolyte and reduce the time between the electrolyte filling process and reaching the optimum wetting level to start the formation.[121] Formation is initiated by the so-called pre-charging process,[122] in which a low charging current is applied to the cell until a low voltage, *e.g.* 1.5 V, is reached. Low currents and voltage limits are necessary to protect the Cu-based current collector from corrosion.[12] The voltage limit during pre-charging can also be increased to a state where most of the gas generation during the first cycle has been completed. This is followed by the degassing step. The gases are usually removed by applying a vacuum. The cell is then sealed.[123] Generally, the housing is sealed as early as possible to minimise evaporation of volatile electrolyte components.[119] If there is no pre-charging step, degassing is carried out after the formation is complete or before shipping to the customers. After degassing, a second wetting and possibly electrolyte filling process may be added to compensate for any electrolyte loss during pre-charging. This is followed by the formation cycling, which includes at least one and possibly several charge and discharge cycles with a defined current and voltage limit. Finally, the cell is aged. During ageing the cells are stored at a defined state of charge (SOC) and temperature. The ageing process completes cell formation. It also serves as a self-discharge test. In this context, the ageing process can also be considered as part of the end-of-line (EOL) cell quality test since an increased capacity loss during storage indicates unwanted self-discharge.

Without the ageing test, industrial formation procedures typically take less than 20 hours.[4,119] The ageing test alone can take up to three weeks.[12,17,119] For application with low quality requirements, formation procedures are significantly shorter.[13,122,124] Once the formation procedure is complete, further EOL testing is performed.[123]

The EOL test protocol can vary, but can include electrochemical tests for discharge capacity, CE, internal resistance, self-discharge test if not already covered by ageing process, impedance, as well as leakage, weighing and optical tests. Depending on the material, size, type and format of the cell, the formation procedure varies in terms of sequence, duration, and quantity from one cell manufacturer to another. The main objective is to find procedures, cycling protocols and evaluation methods that reduce the overall process time, while ideally performing formation and cell quality testing simultaneously.

Required equipment

The formation area in a battery cell production plant consists of large formation towers with either individual racks or chamber systems, each with one individually controlled channel per cell.[124] In these areas, the cells are transported in fully automated bundles by product carriers, which also serve a contact

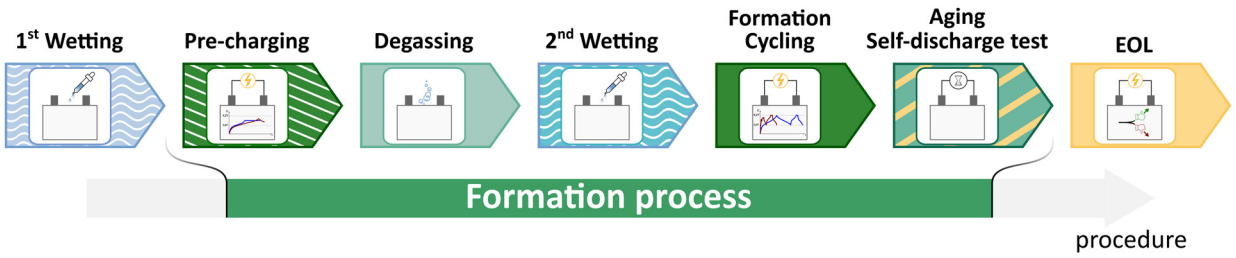

Fig. 3 Schematic overview of an example cell formation procedure. The procedure may vary significantly from manufacturer to manufacturer. The bars show the sequence of process steps. The bars for the 1st wetting and the EOL are only shown to delimit the formation process.

to the formation equipment.[124] Battery formation equipment, also called battery testers, with the correct power system, often AC–DC or DC–DC stage, is required to carry out the formation protocol. If the cells remain unsealed during formation, the formation must either take place in a dry and clean room or a special type of carrier with a suction device must be used. Such open formation procedures are currently only used for large prismatic cells. For closed cells, formation does not take place in a dry and clean room, but under controlled temperature conditions.

To address the high energy consumption and the move towards greener battery production, new formation equipment with a recuperation function has been developed to use the discharge energy from one cell to charge another. Controlling and precisely delivering power to the formation equipment for an entire Gigafactory is a significant challenge. Recently, Tesla announced an innovation to reduce the cost of the formation process by leveraging the production design to allow a group of cells, rather than individual cells, to undergo this formation process resulting in an 86% reduction in formation investment.[125] In addition, Müller *et al.* proposed an optimised formation step for serially connected cells.[126] Thus, serial formation techniques could potentially reduce processing costs. In principle, parallel connection of cells is also possible. However, this reduces the maximum current that can be applied and is therefore only useful for smaller cell formats.

Influencing factors

The formation process is influenced by process conditions, material and cell design. The process conditions are mostly considered for optimizing the formation process. However, the material and cell design must also be tailored to improve the formation process. A comprehensive overview of the most important influencing factors is given below.

Process conditions

The side reactions and structural changes during formation can be controlled in several ways. The main factors to be considered are the formation cycling, *i.e.* current and voltage profiles, temperature, pressure, and degassing.

Formation cycling. On the one hand, the protocol used during the formation cycling affects the duration of a formation process. On the other hand, it can have a significant impact on cell quality in terms of rate capability, safety, and lifetime. Therefore, the optimization of formation cycling is a complex multi-objective optimization problem.

Stages of SEI formation. Most of the literature focuses on the aspect of SEI formation, which mostly takes place in the first cycle.[45,127] Fig. 4 shows the potential of the negative graphite (Gr) electrode during the cycle at low current rate, *i.e.* 1/20C. The potential of the negative electrode can only be measured by a reference electrode inside a battery cell and is specified *vs.* $Li|Li^+$. According to An *et al.*,[45] the initial charge can be classified in three stages based on the negative electrode potential. Initially the potential of the negative electrode is high and within the stability window of the electrolyte. This is shown as position 1 in Fig. 4. Various additives are added to the electrolyte which have been found to have a positive effect on the SEI properties.[45,128,129] Additive decomposition starts at potentials of about 1.4 V *vs.* $Li|Li^+$, which is indicated as position 2 in Fig. 4, and is the first stage of SEI formation. Below about 0.9 V *vs.* $Li|Li^+$, the next stage of SEI formation begins, which is shown as position 3. At this potential, commonly used electrolytes are not stable, and their reduction reactions start. Below about 0.2 V *vs.* $Li|Li^+$, *i.e.* shown as position 4, the Li-ion intercalation rate increases, but is accompanied by further SEI formation.[45,130] Therefore, in this third stage of SEI formation, intercalation and SEI formation run in parallel. The lowest potential is reached at position 5. During discharge, the Li-ions de-intercalate. As a result, the Li flux direction reverses and the potential of the negative electrode rises. In low potential regions, the SEI continues to grow. At potentials above 0.3 V, the SEI can partially re-oxidize.[52,131] These stages should be considered when designing formation cycling protocols.

Challenges for fast formation. One way to reduce formation process time is to reduce the duration of this first charge, where most of the SEI is formed. However, this faces similar challenges as fast charging of LIBs. Similar to conventional charging of LIBs, plating of metallic Li on the negative electrode during formation must be avoided as it has been shown to degrade subsequent cell performance and safety.[132] In both cases, therefore, a major challenge is to develop protocols that reduce the charging time while avoiding Li plating.[133] Li plating on a Gr-based negative electrode surface requires sufficiently low potentials, *i.e.* it is thermodynamically favourable at electrode potentials below 0 V *vs.* $Li|Li^+$. Under open circuit conditions and with the correct ratio of negative to positive electrode capacity (N : P ratio),[134] plating can be prevented by setting an appropriate upper cut-off voltage to ensure that the negative electrode does not reach too low potentials. However, this idealised assessment ignores the presence of overpotentials. Increasing the charge rates will result in higher polarisation overpotentials. These can cause Li plating even when the cell voltage is in a range where it is not thermodynamically favourable under open circuit conditions. In addition, in contrast to fast charging, significant interference with reduction reactions, gas evolution and layer deposition is expected, requiring lower charging limits compared to cells after formation to mitigate Li plating.[135]

Influence of voltage. Several studies suggest that rapid attainment of low negative electrode potentials is beneficial. Zhang *et al.* found that SEI generated between 0.25 V and 0.04 V *vs.* $Li|Li^+$ combines the desired properties: electronically insulating but ionically conductive.[136] This observation is consistent with other studies reporting that only low potential reduction products are beneficial for LIB operation in a typical $LiPF_6$/organic carbonate-based electrolyte.[137,138] The same effect can be seen in full cells by variation of the upper

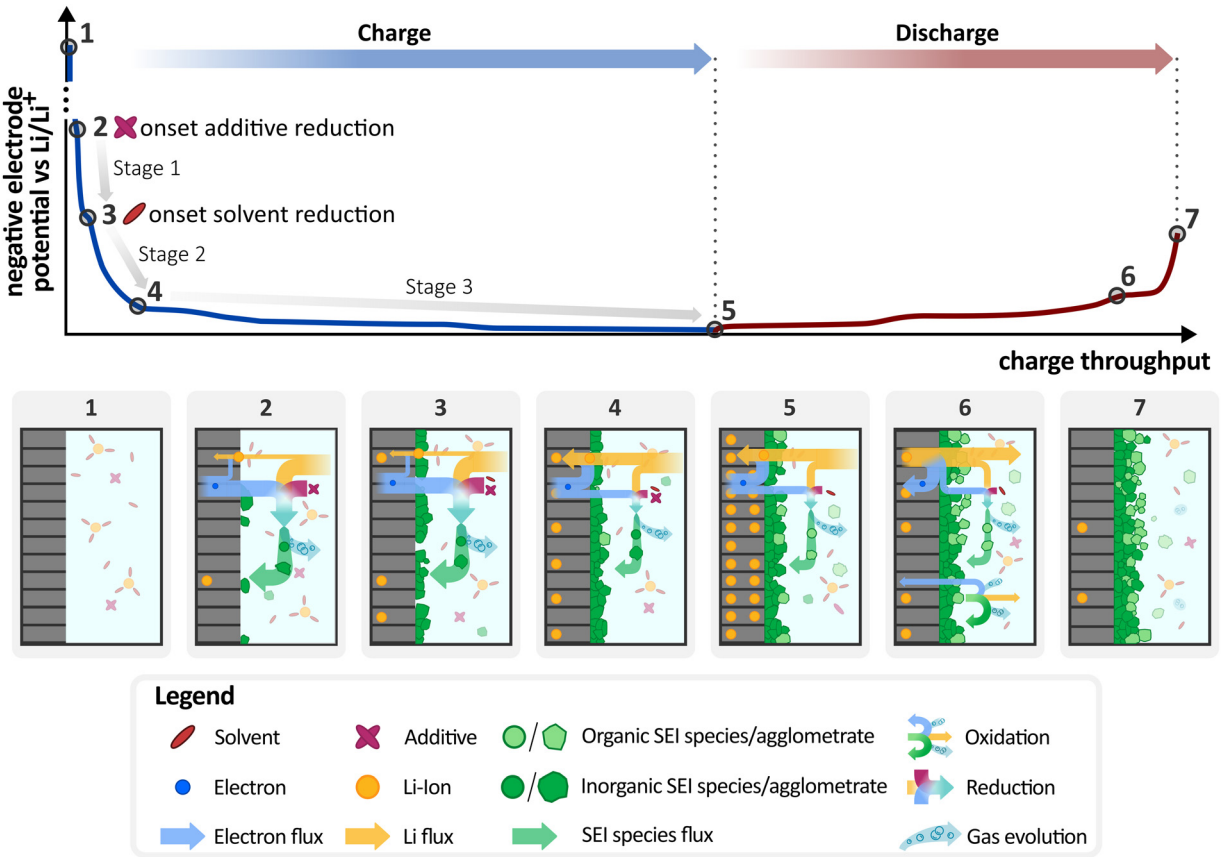

Fig. 4 Schematic of the negative electrode potential curve as a function of charge throughput and SEI growth at the electrode|electrolyte interface. The fluxes of charge carriers, intercalation and reduction reactions and precipitation are shown for a slow (1/20C) initial formation cycle. Characteristic points during the initial cycle are numbered 1–7.

cut-off voltage. Lee *et al.* investigated the effect of different upper cut-off voltages in MesoCarbon MicroBeads (MCMB)||Li or LCO||MCMB coin cells and commercial 18 650 cylindrical cells.[139] When the cut-off voltage was varied between 4.15 V and 3.70 V, no significant differences were observed in the subsequently conducted 200 cycles. In contrast, at a cut-off voltage of only 3.6 V, the cells showed accelerated capacity fading. However, this effect seems not be permanent as shown by German *et al.* with a similar study of NMC111||Gr pouch cells.[37] When cells were initially charged to less than 3.8 V, some of the capacity loss during the first formation cycle was shifted to the second cycle. After a few full charge/discharge cycles in a subsequent cycling experiment, the authors observed no differences in performance regardless of the cut-off voltage of the first charge. Thus, numerous studies show that low potentials of the negative electrode are important to form a stable SEI layer. However, it is less clear to what extent the structure of the SEI is affected. Further insight is given by Antonopoulos *et al.*, who investigated the influence of the negative electrode potential on SEI in more detail.[140] They revealed differences in the surface composition of electrodes formed at high potentials, *i.e.* 0.6 V or 0.45 V *vs.* Li|Li$^+$, and low potentials, *i.e.* 0.3 V or 0.1 V *vs.* Li|Li$^+$. In a ferrocenium-containing model system, the authors were able to confirm the influence of the electrode potential by finding different diffusion coefficients and heterogeneous reaction rate constants of the SEIs formed at different potentials. Therefore, there are strong indications that the potential influences the SEI properties, which can be influenced by the formation cycling strategy.

While the potential of the negative electrode clearly exceeds the electrochemical stability window, the positive electrode exceeds the stability window only at high cell voltages.[141] However, recent experimental work has shown that HOMO energies do not necessarily correspond to the oxidation stability of the organic electrolyte, and that the CEI layer is observed at potentials below those traditionally considered thermodynamically stable.[142] Nevertheless, the CEI is receiving little attention today with respect to formation cycling. However, this should be reconsidered, in particular if high-voltage materials are investigated as discussed below.

As can be seen, the voltage level is an important factor influencing the formation process and the SEI structure. It has been shown that SEI formation takes place in different stages, while low potentials of the negative electrode seem to be favourable for the formation of a stable SEI for common electrodes and electrolytes. At the same time, charging rates must be limited to mitigate Li plating. These principles should

be considered while developing formation strategies that can be muti-cycle or single-cycle strategies.

Multi-cycle formation strategies. The Li intercalation and deintercalation processes cause volume changes and mechanical stress to the Gr particles.[143,144] This results in a break and repair mechanism that affects also the SEI covering the particles.[144,145] As a result, multiple cycles may be required to establish a stable layer.[146]

Conservative formation strategies use multiple full cycles at low C-rates and therefore can last several days.[17,105] To include multiple cycles while accelerating the formation process, decreasing the difference between upper and lower cut-off voltage, *i.e.* sub-cycles, or increasing the C-rates is possible. Pathan *et al.* investigated different formation variants within ten 0.05C cycles between different cut-off voltages.[147] A positive correlation was found between increased lower cut-off voltage and capacity retention (CR). Furthermore, CR was improved when the difference between the upper and lower cut-off voltages was the smallest. These results suggest that the main influencing factor is the cell voltage and formation at high voltages is beneficial. This is utilized also in other studies that aim to decrease formation time. An *et al.* investigated a fast formation strategy with four repeated sub-cycles between 3.9 V and 4.2 V at high C-rates, *i.e.* 0.2C, and showed improved surface layer resistances compared to two cycles at lower C-rates, *i.e.* 0.05C. With this strategy, formation time was reduced from 80 h to 21 h. These formation times were even further reduced in consecutive studies. Wood *et al.* were able to reduce the duration to approximately 14 h by increasing the C-Rate to 1C for the initial charging until 3.9 V and for the final discharge from 3.9 V to the lower cut-off voltage.[17] Drees *et al.* compared the protocol of An *et al.*[148] with another sub-cycling formation protocol.[149] The new protocol used 0.8C and removed the constant voltage (CV) phases during the sub-cycles, resulting in a reduced formation time of only 10 h, without significant impact on the cell performance. Thus, multiple studies show that formation time can be reduced without significantly compromising the cell quality.

Weng *et al.* investigated the influence of these cycling strategies on lifetime in more detail by comparing the average lifetime of cells subjected to the fast formation strategy of An *et al.*[148] and Wood *et al.*[17] with a slower baseline formation strategy at different temperatures.[104] The results indicate, that the fast formation strategy even improved cycling performance at both 45 °C and room temperature. However, swelling was observed at the end of life at 45 °C for the fast formation strategies.[104]

A comprehensive comparative study of five different formation protocols with different cycle numbers and currents was performed by Mao *et al.*[105] The total formation time ranged from 10 h to 86 h. The main results of this study are shown in Fig. 5. Analysing the first cycle CE (Fig. 5A), rate capabilities (Fig. 5B), and cycle retention (Fig. 5C), the authors conclude that neither long, 86 h, nor short, 10 h, formation times provide the optimal electrochemical performance. Instead, intermediate formation times, *i.e.* 26 h and 30 h, resulted in the lowest electrode resistance after formation (Fig. 5D), lower capacity losses for 300 ageing cycles at a cell voltage of 3.8 V (Fig. 5E) and lower area specific resistance (ASI) of cells at different cycles (Fig. 5F). The morphology of material of three protocols was

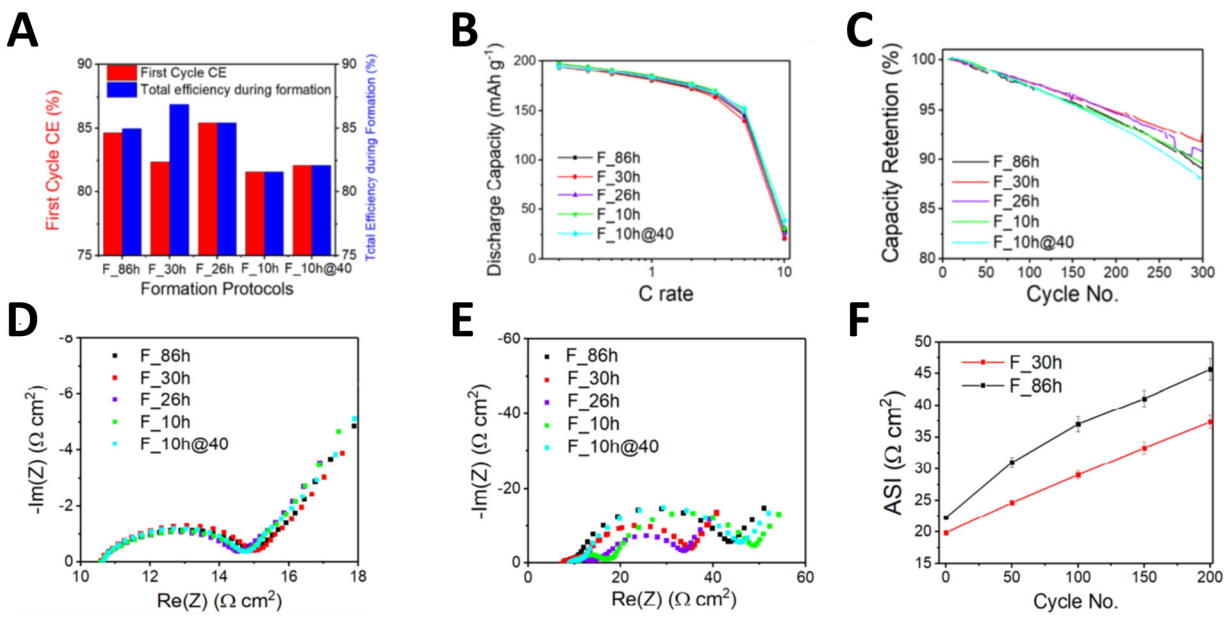

Fig. 5 (A) Comparison of first cycle CE and total efficiency during formation with respect to different formation protocols. Comparison of the (B) rate capablity and (C) cycle retention characteristics with respect to different formation times. Nyquist plots of cells with different formation times (D) after formation cycle and (E) after 300 ageing cycles at 3.8 V cell voltage. (F) Area specific resistance of cells with formation time of 30 h and 86 h as a function of the number of cycles. Reprinted with permission from *Mao et al.*,[105] Elsevier, Copyright 2018.

further investigated by scanning electron microscope (SEM) and X-ray photoelectron spectroscopy (XPS). The atomic compositional profiles of the four elements, *i.e.* surface Carbon (C), Oxygen (O), Li, and Phosphorus (P), were used to estimate the SEI thickness of the electrodes formed with the different formation protocols. Among the electrodes studied in detail, the medium formation time of 30 h showed the thinnest SEI layer thickness of 54 nm. Even though the effect of the cycling strategy is not obvious in some studies, the formation cycling can influence the SEI structure and properties. However, whether one structure or the other is beneficial is often not well understood, as evidenced by the results of Lee *et al.*, who investigate the influence of SOC and number of formation cycles with a fluoroethylene carbonate (FEC) based electrolyte.[150] Cells were charged to SOC 10% (3.5 V), 20% (3.7 V), 30% (3.9 V), and 100% (4.2 V) and then fully discharged (2.7 V). Cells formed with three cycles in a narrow SOC range at low voltages, *i.e.* 10% to 30%, showed improved CE after 180 cycles. These results are in contrast to many other studies, as they suggest that lower negative electrode potentials during formation result in a less stable SEI. This is probably due to FEC, which was not used in the other studies. Based on the morphological analysis, this effect was attributed to a higher proportion of interlinked particles on the particle surface, which is illustrated in Fig. 6. Based on these results, it is emphasized that the cycling strategy is not independent of the material and cell design but must be adjusted individually.

Therefore, also other active materials must be investigated. Rago *et al.*[33] investigated the fast formation protocol of An *et al.*[148] for cells with Si–Gr composite electrodes. For this material, no performance differences compared to five-cycle formation strategy with C-rate of 0.05C were found. However, the authors also reported that the negative electrode surfaces for different formation protocols had different optical appearances and different chemical SEI compositions. Faster multi-cycle-based formation resulted in suppressed Cu and Al dissolution and thinner SEI.[33]

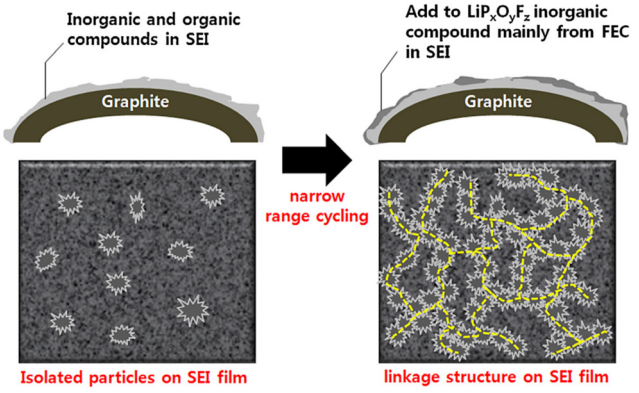

Fig. 6 Illustration of the effect of performaming formation cycels within a narrow votlage range at low SOC with a FEC containing electrolyte on the SEI on graphite negative electrode. Reproduced with permission from Lee,[150] Elsevier, Copyright 2014.

The effect of the upper cut-off voltage on the CEI in a multi-cycle formation was investigated by Phraewphiphat *et al.* for nitrogen-doped Li_2MnSiO_4/C positive electrodes.[151] Five formation cycles were used with 4.5 V and 4.6 V as the respective upper voltage limit during the formation cycling. The cells formed at the lower potential showed improved cycling stability. The improved ageing behaviour was attributed to the improved structural stability of the CEI. Zhang *et al.* observed that during normal cycling the CEI does not form as a conformal surface layer completely covering the interface.[152] However, by brief electrical shorting of their NMC||Li cells, they were able to form a conformal surface layer.

For multi-cycle formation strategies, cell voltage was confirmed to be an important factor influencing for both CEI and SEI formation. In contrast, the influence of cycle number and applied current is less obvious. Most studies found no significant influence on the cell properties. However, some studies report an influence on interphase properties such as thickness, composition, and resistance. The influence of the choice of material and electrolyte makes it difficult to draw general conclusions und rather suggests that cycling strategy must be adjusted to material and cell design.

Single-cycle formation strategies. A single-cycle formation strategy promises to reduce formation time compared to multi-cycle formation strategies. There are many ways to implement a single-cycle strategy, as it may involve a varying charge rate, charging/discharging modes or perform special fast charge procedures.

Drees *et al.* compared several multi-cycle formation strategies with fast single-cycle formation strategies.[149] Fig. 7 shows (A) a slow multi-cycle, (B) a multi-sub-cycle and (C) a fast single-cycle formation strategy that have been investigated. The slow multi-cycle formation consists of two full cycles with low currents, *i.e.* 0.05C, in the first cycle and moderate currents, *i.e.* 0.2C, in the second cycle. This conventional approach is very time consuming. The multi-sub-cycle formation approach involves multiple sub-cycles at high SOC to enable faster SEI growth while reducing the formation time compared to full cycles. Fast single-cycle formation uses constant current (CC) charging at 1.5C followed by a constant negative electrode potential phase. Using cells in a three-electrode setup,[134] the potential of the negative Gr electrode was limited to 0.02 V *vs.* $Li|Li^+$. The potential limit was chosen slightly above 0 V *vs.* $Li|Li^+$ to accelerate SEI growth while effectively preventing Li plating. Charging was stopped at 80% SOC. The cells were then discharged at 1C. The single-cycle formation strategy was clearly the fastest formation as it took only 1.7 h. Nevertheless, the different formation strategies achieved similar discharge capacities, internal resistances, and electrochemical impedance spectra immediately after formation and during 250 cycles. Differences were observed in a high temperature storage test at 60 °C, 80% SOC and 28 days storage time. Variants with the highest initial charge rate resulted in the lowest cell degradation, while the fast single cycle formation was one of them.[149] A similar single-cycle fast charge formation approach was upscaled from three-electrode coin cells to 5 Ah

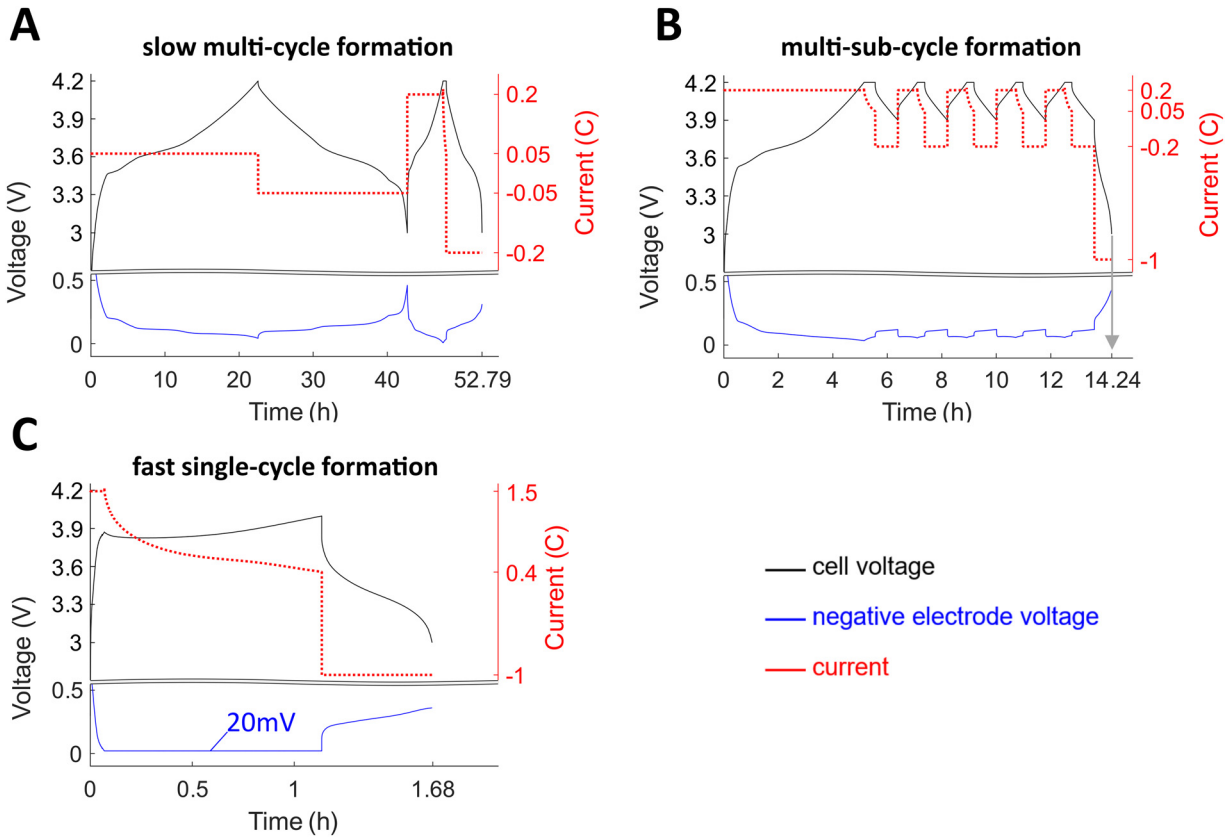

Fig. 7 Formation strategies with different speeds and number of cycles. (A) Conventional slow multi-cycle formation. Very slow first full cycle and moderate second full cycle. (B) Multi-sub-cycle formation with periodic sub-cycles at high SOC (low NE potentials).[33,147–149] (C) Fast single-cycle formation with high currents at low NE potentials.[27,135,149,153] Reprinted with permission from Drees *et al.*,[149] John Wiley and Sons, Copyright 2022.

pouch cells using a look-up-table based current control.[153] The maximum C-rate was 3C and the total formation time was below 1 h. These fast formed cells resulted in similar cycling performance over 1000 cycles to various slower reference formations. The fast formation approach using the look-up-table based method was also successfully applied to the formation of 25 Ah prismatic cells.[27] These results indicate that single cycling formation is promising approach to reduce formation time and possibly also improve cell quality.

The influence of the current within the first charging cycle seems to be the key influencing factor and was investigated further by Chiang *et al.*[154] They investigated the influence of the current by comparing three single-cycle formation protocols with LCO||Gr-based cells.[154] They also proposed a dual current procedure which limited the rate to 0.1C for 1 h and then increased the rate to 1.0 C for the remaining first cycle. Long-term cycling experiments showed that the rate of capacity loss was not affected by either protocol. In addition, Zhang *et al.* studied the influence of the current rate.[155] They used the second cycle CE to evaluate the formation protocols of Gr||Li cells at different current densities and observed that as the current density increased, the first cycle CE increased while the second cycle CE decreased. According to these findings, a high current density contradicts the idea of a single-cycle formation, as more cycles are required to complete the formation process. They further investigated the cycling performance and found that it was slightly better for cells after formation at low or medium current densities. Moretti *et al.* observed a compositional difference when comparing the effect of three formation protocols.[156] They studied a single current formation protocol, which includes a single 0.05C constant current followed by constant voltage (CC–CV) cycle between 3.9 V and 2.5 V, a dual current formation protocol, which includes a slow 3 h, 0.05C pre-charge step, a subsequent 3.6 V CV charge phase and a 0.1C discharge to 2.5 V, and an advanced industrial protocol, which includes multiple steps, *i.e.* a pre-charge to 3.0 V, a long rest and a 0.1C CC–CV cycle between 3.6 V and 2.5 V at 40 °C as well as a final 1 h rest at 20 °C. Comparing the effect of formation protocols on SEI in LFP||Gr coin cells, the authors observed the highest LiF content and cycling performance in cells formed with the dual current protocol. Antonopoulos *et al.* reported improved Li-ion transport rates for formation protocols with high initial charge rates. They applied a current rate of 1C until the negative electrode potential reached 0.24 V *vs.* Li|Li^+, followed by a 0.1C charge.[138] The authors also found improved C-rate capability for currents higher than 1C when applying 1C during formation until 0.24 V *vs.* Li|Li^+.

Besides the formation of passivating layers, structural changes are also possible. Although most of the research on the formation process focuses on the interfacial layers and the

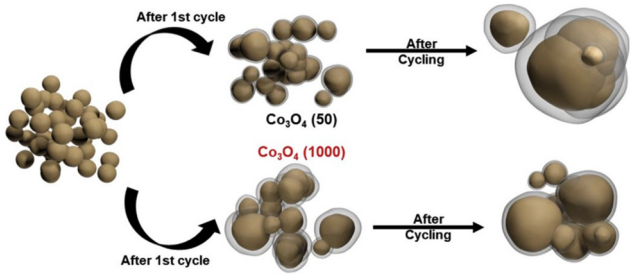

Fig. 8 Structural evolution of Co_3O_4 nanoparticles after a single formation cycle with different current densities and subsequent cycling. Reprinted with permission from Cheong *et al.*,[74] Elsevier, Copyright 2019.

decomposition of the electrolytes, the degradation effects of the active material particles have also been investigated. Cheong *et al.* adopted different current densities in the initial formation cycle and observed how the morphological evolution takes place for Co_3O_4 nanoparticles as shown in Fig. 8.[75] It was found that a fast formation cycle, *i.e.* with a current density of 1000 mA g^{-1}, resulted in initial agglomeration of nanoparticles, which ultimately led to improved structural integrity of the active material particle. In contrast, the formation cycle with a current density of 50 mA g^{-1} resulted in increased agglomeration after cycling.

These studies indicate that the composition and properties of the SEI as well as of active material structures can be influenced by single-cycle formations strategies. However, it remains unclear whether faster current rates are beneficial or not.

As can be seen, it is not possible to draw general conclusions and make direct comparisons between different studies. This may be due to the influence of material and cell design. This can also be seen from the different current limits reported to mitigate Li plating.[157] Drees *et al.* reported Li plating after 1.5C CC–CV charging, which correlated with reduced discharge capacity.[149] Mao *et al.* reported Li plating at much lower rates. They used a 0.5C CC–CV formation and found increased impedances and decreased cycling stablity.[105] In contrast, Münster *et al.* also found Li plating only at higher rates, *i.e.* a 2C CC–CV formation. However, this did not affect cycling stability compared to a slow 0.2C formation protocol that did not resulted in Li plating.[132]

Single-cycle strategies promise to significantly reduce process time compared to multi-cycle strategies. However, avoidance of Li plating and incomplete formation are important limiting factors. There is also evidence that charge rates affect cell properties such as charge rate capability and self-discharge, but the mechanisms behind this are not well understood. Formation strategies must always be tailored to the material and cell design. For single formation strategies, the design of the first charge allows to influence the SEI composition and properties, while dual current formation is a possible approach.

Degassing

The formation of the passivation layers produces gaseous species as by-products.[45] The evolved gas can isolate active material or displace electrolyte from the pores, affecing the homogeneity of the passivation layer and safety.[158,159] One possible measure to handle gas evolution is to implement appropriate degassing steps within the formation process. Various factors the influence the gas evolution must be considered when implementing degassing during the formation process.

The quantity of gas generated is linked to the active material on both electrodes.[160,161] Similar gas species are reported for common negative electrodes, *i.e.* Gr and silicon (Si). For both active materials the release of ethylene (C_2H_4), carbon monoxide (CO) and carbon dioxide (CO_2) has been reported for pure ethylene carbonate (EC) or EC-based electrolyte solutions.[58,161–166] Additionally, ethane (C_2H_6), methane (CH_4) and hydrogen (H_2) may be formed as by-products of EC on Gr negative electrodes. These gases are related to the specific SEI formation mechanism on Gr and Si-based negative electrodes. The gas species may differ for other negative electrodes.[167] On the positive electrode side, mainly CO and CO_2 are reported as by-products of oxidation reactions.[72,73,168] According to density functional theory (DFT) simulations by Leung *et al.*, EC decomposition on $Li_{0.6}Mn_2O_4$ leads to CO_2 production only at high voltages.[169] In contrast, Jung *et al.* hypothesise that the CO and CO_2 evolution is due to a chemical reaction of the lattice oxygen with the electrolyte by analysing the gas evolution of different NMC||Gr cells for different cut-off voltages.[73] In addition, the CO_2 evolution may result from material impurities,[72] *e.g.* due to the oxidation of Li_2CO_3 at high potentials of the positive electrode.[170,171]

Electrolyte composition has a significant effect on the total gas volume and relative species content. For example, it has been found that EC-based electrolytes generate a higher volume of gas compared to propylene carbonate (PC) based electrolytes.[172] Increased amounts of CO_2 and CH_4 were observed for solutions containing EC and dimethyl carbonate (DMC), respectively.[172] The choice and ratio of solvant as well as of additive on the gassing behaviour was also reported in other experimental studies.[164,166,173–177]

Bernhard *et al.* found that the C_2H_4 gas production starts at around 0.9 V *vs.* $Li|Li^+$, with the rate of production peaking at around 0.5 V *vs.* $Li|Li^+$ before decreasing until the end of the first charge cycle. Significant amounts of C_2H_4 were found only in the first cycle.[178] These results were confirmed by Jung *et al.* at room temperature.[179] However, at 40 °C or 50 °C the C_2H_4 gassing extended into the subsequent cycles. In addition, the total amount of gas increased at elevated temperatures. Jung *et al.* also found significant amounts of CO and CO_2 gas within the first formation cycle, but the CO_2 was attributed to the NMC positive electrode.[179] Xiong *et al.* reported increased gas volume for NMC electrodes when stored at elevated temperatures.[74,164,180]

It was found that some gases are consumed by SEI reduction reactions,[165,178,179,181] and, to some extent, cross over from the positive to the negative electrode.[182] Ellis *et al.* investigated the influence of gas consumption by comparing cells with and without degassing.[165] After an initial 0.05C pre-charge to 3.5 V, the gas was removed. However, the degassed cells resulted in

the same performance as the non-degassed cells.[165] In contrast, Bläubaum *et al.* reported improved cell performance when CO_2 gas was added to the electrolyte prior to formation.[183] A positive effect of CO_2 on the SEI was also reported in other studies.[173,174] Thorton *et al.* hypothesis that stabilising effect of CO_2 origins from a reduction reaction, which forms stable solid species and C_2H_4.[181] CO_2 injection to actively modify the resulting SEI composition was also suggested by Spotte-Smith *et al.* in a theoretical study.[162]

The produced gas amount also depends on the formation current and voltage.[182,184–186] Leißing *et al.* investigated the influence of different C-rates on gassing.[184] Gassing was found to be caused by both SEI formation and unspecific decomposition. Both very slow and very fast formation led to an increase in non-specific gassing, but the species observed differed.[185]

The gas amount was also seen to limit the ability for fast-charging formation. When Drees *et al.* scaled a single-cycle fast charging strategy (Fig. 7C) from three-electrode coin cells to pouch cells, irregular plating was detected.[135] By introducing a moderate pre-charge and early degassing step before continuing with the same fast charging protocol, Li plating was successfully prevented. The efficieny of the gas removal was improved by applying external compression on the pouch cells, which also resulted in lower overpotentials.

Significant gas evolution occurs during battery cell formation. The amount and composition of the gas is influenced by the formation protocol, the active material, the electrolyte composition, and cell design. Gas formation can be a limiting factor for fast formation strategies, especially with thick electrodes and larger cell formats. Possible countermeasures are adequate degassing steps, external compression and reduction of gas evolution by selection of suitable electrolytes. Gas injection may also be used as an active measure to influence reactions during the formation process.

Pressure

With respect to pressure influence, a distinction is made between internal and external loads. Internal loads occur, for example, as a result of electrode volume changes during Li insertion and removal, resulting in dynamic stresses. Also, the previously discussed gas evolution can increase the internal cell pressure. External loads can be applied by the housing, *e.g.* in cylindrical or prismatic hard-case cells, or by external compression *via* product carrier systems in pouch cells. Cannarella and Arnold analysed mechanical pressure in context of battery lifetime of pouch cells and found that the negative electrode surface area and separator expansion were dependent on the stack pressure applied during the cycle life.[187] Studies of the influence of mechanical stress on formation are rare. However, external pressure is also relevant to the formation process. Heimes *et al.* investigated the effect of external compression within single-cycle formations by applying a compressive force up to 1.9 kN.[188] This effect is shown in Fig. 9A and B. Higher pressure resulted in lower overpotentials and reduced formation times. They conclude that by mechanically compressing the electrode and separator, electrolyte diffusion in the cell can be optimised. This allows the SEI formation process to be accelerated and cell impedance to be reduced up to 50%, depending on the cell chemistry and pressure range. It has been found that the formation time can be reduced by compressing the cells with longer CC and shorter CV phases.[188]

Currently, pressure is rarely studied in the context of formation. However, for novel materials that undergo significant structural changes and volume expansion, pressure requires more attention.

Temperature

The influence of different temperature settings during formation has been investigated in numerous studies. According to the Arrhenius equation, temperature affects the reaction kinetic. This also applies to side reactions in the battery cell, such as the SEI and CEI formation.

An *et al.* describe that elevated formation temperatures accelerate SEI formation, resulting in a reduction in formation time.[45] SEI formation at 40 °C results in a layer consisting of compact, inorganic components instead of a less compact,

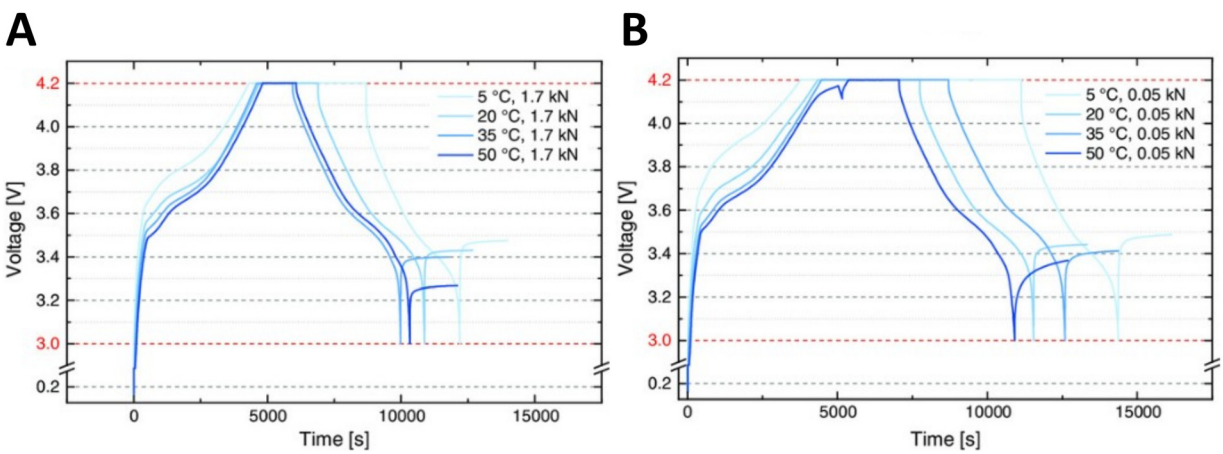

Fig. 9 Cell voltage curves of the first formation cycle (CC-CV-CC) for different ambient temperatures and external pressures of (A) 1.7 kN and (B) 0.05 kN. Reprinted with permission from Heimes *et al.*,[188] John Wiley and Sons, Copyright 2019.

organic structure. Bhattacharya *et al.* performed formation at 25 °C and 60 °C.[189] They compared the morphology and composition of the SEI layers and concluded that formation at higher temperatures resulted in a more homogeneous layer due to higher diffusion rates. He *et al.* elaborate that formation at 50 °C resulted in lower total internal resistances during and after formation in comparison to a formation at 25 °C.[190] At 50 °C, the formation time was reduced to 15 h, compared to the formation time at 25 °C of more than 16.5 h.

Heimes *et al.* discovered similar relationships by investigating the influence of temperature on formation time.[188] Fig. 9 shows results for formation at different temperatures and pressure. Fig. 9A and B show that as temperature increases, the overpotentials decrease and the formation time decreases. The authors describe that higher ambient temperatures increase the effective conductivity of the electrolyte in the separator, improve the solid diffusivity in the active material and reduce the charge transfer resistance, which increases the reaction rate and reduces the internal resistance. Therefore, the formation time can be reduced by increasing the temperature.

In contrast to studies that suggest an advantage of elevated temperature, Lee and Pyun describe that as the formation temperature increases, so do capacity losses.[191] They conclude that at elevated temperatures the SEI is formed with more defects, resulting in more transport pathways for solvent co-intercalation. Furthermore, the formation of Li_2CO_3 is accompanied by gas evolution which can damage the Gr layer. This is in contrast to an extensive follow-up study, the microstructure of SEI was investigated when formed at different temperatures.[189] This study showed that when formed at 60 °C, the SEI morphology was more homogeneous and the surface composition differed significantly. It was found that formation or pre-treatment at higher temperatures could also be beneficial.

Ellis *et al.* found no significant influence of the formation protocol on either SEI thickness or the long-term cycling behaviour when they varied the temperature and CV step time during formation cycling.[192] Moretti also analysed the SEI and found no major compositional differences when comparing two formation protocols where the first charge was performed only at 20 °C and partially at 40 °C, respectively.[156]

Elevated temperatures have been shown to be useful in reducing formation time by increasing the side reaction rate. However, there are conflicting results regarding possible improvements in cell quality. Both negative effects due capacity loss and positive effects due to improved interfacial homogeneity have been observed.

Material and cell design

In addition to the electrochemical and environmental conditions, design choices, *i.e.* active material, electrolyte, and cell type, also influence the formation process. The effect of material and cell design on the formation process are outlined below.

Active materials. Further enhancing battery energy density requires new materials with higher specific capacity or voltage.[193] Increasing capacity requires moving from intercalation to alloying or conversion type materials, which involves significant structural changes that affect interphase integrity. Increasing voltage strains electrolyte stability and requires good passivation properties of the interphase layers. Both will have significant implications on the formation process.

Many high-voltage or high-capacity materials, such as Nickel, Li or Mn rich layered oxides, high-voltage spinel oxides, and high voltage polyanionic compounds offer potential for advancement for the positive electrode.[31,193] However, this can lead to thick interphase layers as shown on Fig. 10A. Achieving stability under highly oxidizing conditions is critical to suppress unwanted side reactions. The goal is to construct interphases that provide chemical and mechanical stability to promote long-term battery performance and safety. Potential strategies include new electrolytes that are more stable against oxidation or form effective passivating surface layers.[194–196] In particular, the development of additives represents a promising way to improve layer properties without compromising the gains in the negative electrode. In addition, significant heat generation during formation cycling was observed for example in Mn-rich layered oxides.[31] This unusual heat release was attributed to structural rearrangement of the active material and was also accompanied by pronounced voltage hysteresis. This indicates that focusing on the negative electrode might not be suitable when using high-voltage positive electrode materials that also require passivating interphases and undergo significant structural changes. This significantly complicates the optimization process as both electrodes must be addressed simultaneously in a full cell setup.

Silicon-based active materials, such as Si or silicon dioxide (SiO_x), offer higher energy density potential, which can be up to ten times the theoretical capacity of Gr.[197–199] However, large volume changes of up to 300% place significant demands and can lead to pulverization, lithiation retardation, and unstable SEI growth, as can be seen in Fig. 10B. The SEI on Si tends to be thick, non-uniform, oligomeric and susceptible to HF attacks.[200] In contrast to Gr electrodes, the interphase structure of Si evolves significantly during cycling.[201] However, the formation of a stable layer is critical to prevent thick SEI and continuous capacity loss. This challenge can be addressed by the development of new electrolytes[202,203] or additives,[197,200,204] material design strategies,[205] the cycling strategy[206] and the surface properties.[207–209] In addition, Si electrodes undergo significant morphological changes, including crystalline-to-amorphous phase transitions, especially during initial charge–discharge cycles.[210–212] Overall Si-based negative electrode materials will significantly increase the demand for sophisticated formation strategies.

Li metal is promising to achieve the highest energy density in Li-based batteries due to its low potential and high specific capacity.[213–217] Unlike other electrode materials, Li metal immediately forms a SEI in a corrosion-like process within a few μs,[218,219] as can be seen in simulation results shown in Fig. 10C. Therefore, the initial layer formation cannot be

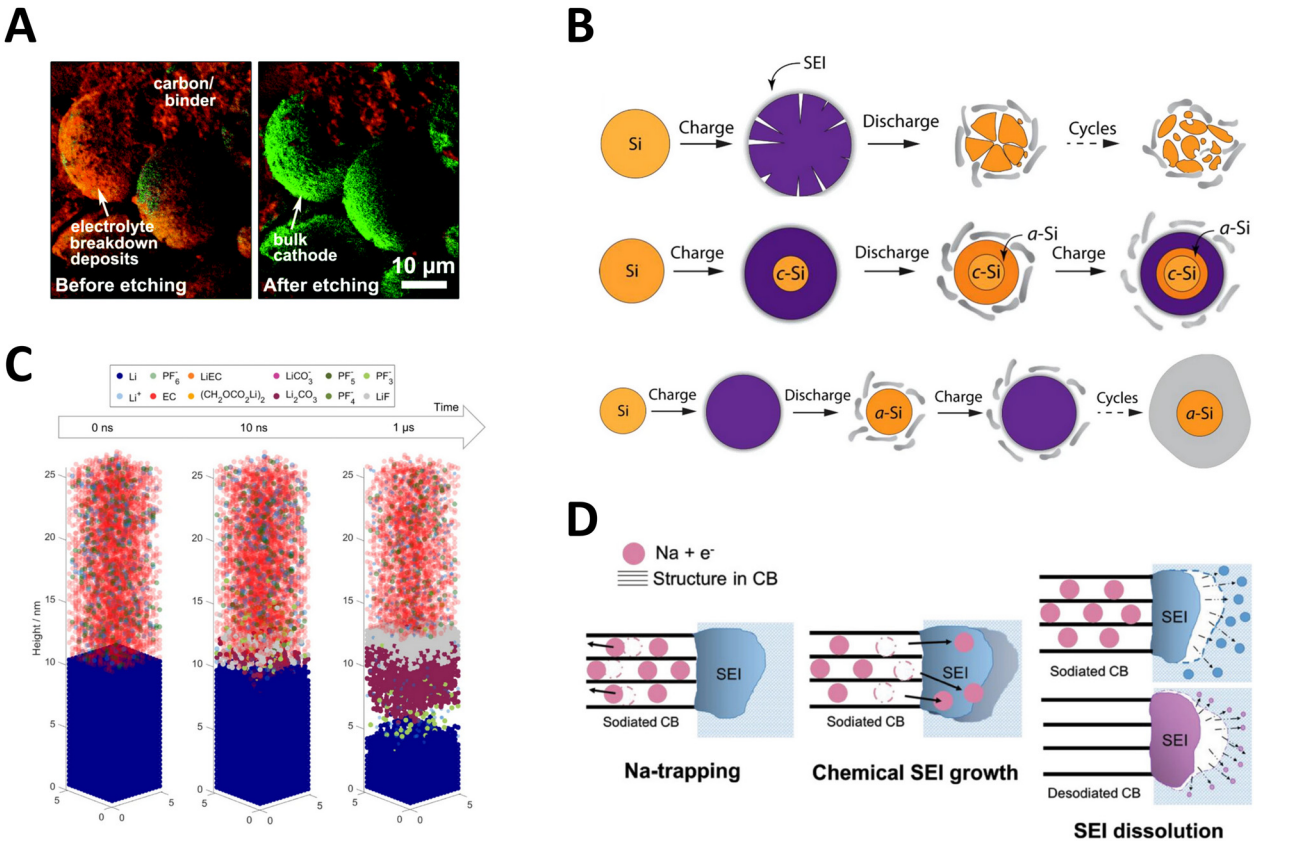

Fig. 10 Next generation pose significant challenges on the formation process which can be seen in (A) Surface layers in high voltage $Ni_{0.7}Co_{0.15}Mn_{0.15}O_2$ as depicted by TOF-SIM mapping. Reprinted with permission from Li *et al.*,[193] Royal Society of Chemistry, Copyright 2017. (B) Illustration of different degradation mechanisms in silicon electrodes associated with significant volume changes. Reproduced with permission from Zhang,[205] Springer Nature, Copyright 2017. (C) Snapshots of kinetic Monte Carlo simulation of SEI formation on a lithium metal electrode. Reproduced with permission from Wagner-Henke *et al.*,[218] Springer Nature, Copyright 2023. (D) Illustration of the aging mechanisms in sodium-ion batteries. Reproduced with permission from Le Ma *et al.*,[230] John Wiley and Sons, Copyright 2023.

influenced by formation protocols. Nevertheless, a controlled subsequent formation cycle is often performed,[4] which induces high volume expansions during plating and stripping of Li, associated with significant morphological changes of the interfacial layer.[220] This places high mechanical stress on the SEI layer and poses a significant safety risk as Li can penetrate the separator and cause a short circuit. The development of a formation process that creates a robust SEI layer holds promise for enabling stable cycling and managing these morphological changes, as it can prevent uneven Li deposition.[220] Therefore, the design of electrolytes[195,221–225] or additives[226–229] that promote the formation of more stable and homogeneous SEI layers appears to be a promising approach to enable Li metal for next generation batteries.

The challenges of formation are not unique to Li-based batteries, but also apply to sodium-ion batteries, for example. This battery technology promises to be a next-generation alternative due to the abundance of sodium. However, their formation process presents significant hurdles. Solid products in sodium-ion batteries exhibit higher solubility compared to Li-ion counterparts, resulting in dissolution that necessitates interface reformation, leading to significant capacity loss[230] as illustrated in Fig. 10D. Therefore, the key objective is to develop a SEI that is predominantly insoluble. Studies also highlight the positive impact of formation cycling on film properties.[231,232] For example, electrochemical reactions in high voltage regions may not effectively form the SEI, emphasizing the importance of specific voltage ranges.[231] In addition, studies show that different electrolytes require different approaches: for example, NaBOB-based can benefit from lower C-rates and higher temperatures,[231] while ionic liquids can benefit from higher C-rates.[232]

As outlined above, for many next generation materials the formation process can be considered pivotal and similar challenges arises. However, the possible influencing factors and solution can significantly differ. The development of all materials would significantly benefit from a better mechanistic understanding of the underlying processes, while often a complex interplay between electrochemical kinetics and mechanical stress needs to be considered.

Surface properties. The preparation and pre-treatment of the active material surface will also affect the formation process and is offers a possibility to tailor the material properties for an optimized formation process.

Cui *et al.* used a surface treatment of Gr with 0.5 mol L^{-1} Li_2SO_4 aqueous solution, which resulted in the formation of thinner, more stable and elastic SEI layer capable of accommodating structural changes during cycling.[233] The study suggests that surface properties play an important role in the formation process. Further studies have found a correlation between Gr surface properties and first cycle specific charge loss, confirming the importance of the surface properties of active material. A key factor in determining the initial capacity loss is the active surface area.[90,234,235] The study of Ng *et al.* also highlights the importance of oxygen groups as an influencing factor when the active surface area becomes greater than 0.2 m^2 g^{-1}.[234]

Different types of Gr in EC- and PC-based electrolytes were investigated by Spahr *et al.*[236] They show that active surface area was a main factor determining the surface passivation.[236] Further insights into the importance of the active surface area of Gr was gained by Märkle *et al.* who investigated SEI formation on pristine and heat-treated Gr.[237] Using SEM, the surface coverage and extent of exfoliation of Gr particles was investigated for different specific currents. Differences were reported between electrolytes and Gr type. The pristine Gr showed no exfoliation due to the larger number of oxygen-containing surface groups and hence high active surface area. The heat-treated Gr suffered from exfoliation regardless of the current in EC-based electrolytes. However, the exfoliation was less severe at higher current rates. This is attributed to suppressed solvent co-intercalation due to faster SEI coverage[237] and is in agreement with other studies.[137,236,238] In PC-based electrolytes, both Gr types suffered exfoliation regardless of current density, but again was more pronounced for the heat-treated Gr.[236,237] *Post mortem* SEM images of heat-treated and untreated Gr after a single charge are depicted in Fig. 11.

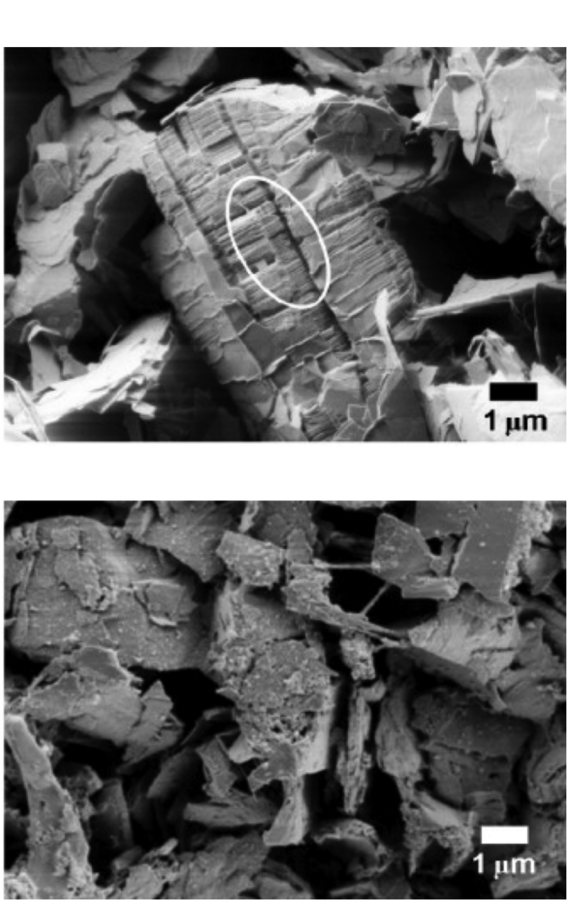

Fig. 11 *Post mortem* SEM images of heat-treated (A) and untreated (B) graphite (SFG6) in 1 M $LiPF_6$ in EC/PC 1 : 1 (w:w) after a single charge to 0.005 V with a constant current of 0.01 Ag^{-1}. A region suffering from exfoliation is indicated with a white circle. Reprinted with permission from Spahr *et al.*,[236] Elsevir, Copyright 2010.

Further exfoliation was found to be influenced by temperature and electrolyte composition by Zhang *et al.* in LFP||Gr cells.[239] When formation occurred at 20 °C with certain solvent combinations and Gr types with few electrochemically active sites, a reduced first cycle efficiency was observed due to solvent co-intercalation. Increasing the temperature improved the desolvation kinetics and no exfoliation was observed. The addition of vinylene carbonate (VC) to the electrolyte also effectively mitigated solvent co-intercalation.[239–241]

In addition to the surface properties, the surface heterogeneity of the active materials influences the electrochemical properties during and after formation. Placke *et al.* reported that the absolute and relative extent of the basal/non-basal planes has a critical effect on SEI layer formation and leads to different initial capacity losses.[242] The effect of current on Gr exfoliation was further investigated by Goers *et al.*[238] Varying the current resulted in different local current densities, which played a significant role in the local overpotential that affected the electrochemical performance.[238] Such partial local current density variations were found to be a key parameter in the exfoliation behaviour of Gr and emphasised the crucial role of exfoliation in the initial electrochemical performance of active materials.[238] Tang *et al.* investigated the orientation of the Gr and the influence of the Li salt with respect to their effect on the quality of SEI after the formation.[243] They found that the electrochemical activity is higher on the basal plane of the Gr, resulting in slower formation of the SEI.

While a strong dependence surface modifications of Gr negative electrodes on SEI formation has been reported in experimental[236–238,244] and simulative studies,[245] the reduction of EC on pristine Si has been simulated to be unaffected by surface modifications.[246] However, differences between pristine and oxidised Si on the SEI formation were observed by Yun *et al.*,[161] who modelled the reduction EC-based electrolyte on the two types of Si. The results showed that although an interaction between Li and passivated oxygen atoms on the Si surface leads to an increased presence of Li_2O on the SiO_x negative electrode, overall the two negative electrodes showed similar behavior.[161]

An important factor influencing the formation is the surface properties of the active material where the interfacial layers are formed. Exfoliation and slower surface layer formation are possible negative effects. Specific surface area, surface groups,

e.g. oxygen groups and material homogeneity have been shown to be important factors. Some problems such as exfoliation or structural rearrangements are material specific and may vary betwenn vendors.[239] Therefore, surface and material pretreatment must be considered individually for each material group.

Pre-lithiation. In addition to surface properties, electrochemical or chemical pre-lithiation can affect the formation process. In this process, additional Li is introduced into the cell to compensate for the high capacity loss in the first cycle, resulting in improved SEI qualities and cell metrics.[247–250] For example, Chevrier *et al.* employed pre-lithiation to a Si alloy, which helped to improve CR and CE.[251] A cylindrical cell with a pre-lithiated Si alloy showed a CR of 80% after 500 cycles and CE of 99% after 700 cycles.[251] Esen *et al.* compared differences between SiC electrodes with and without pre-lithiation in NMC811||SiC cells in terms of formation and ageing behaviour.[252] As a result of pre-lithiation, a more stable SEI consisting of a higher proportion of LiF, Li_3PO_4 and organic species was obtained compared to the non-pre-lithiated reference. They also showed a significant increase in cycle stability.[252] Sun *et al.* added nanocomposites, *i.e.* transition metals and lithium oxides, to the positive $LiFePO_4$ electrode.[253] In Gr||$LiFePO_4$ coin cells, pre-lithiation resulted in a 11% capacity increase in comparison to the cells build with pristine electrodes.[253]

Electrode. To increase the energy density, the coating can be densified or increased in thickness.[254] These high energy electrodes may lead to an inhomogeneous electrolyte wetting, resulting in an uneven formation and poor cycling performance.[255–257]

With thicker electrodes also the risk of Li-plating rises during formation.[135] In addition, Li-plating is also associated with an increase in the volume of gas generated during formation, which can further exacerbate the problem in larger cells.

The increased polarisation due to thick electrodes can be addressed by structuring the electrodes,[258] *e.g. via* mechanical embossing,[259] laser ablation,[260–262] or a gradient film design,[263] enabling the production of thick high energy electrodes without sacrificing significant power capability.[257] The maximum current and the degassing steps must be adjustd to the electrode design, especially for high-energy cells.

Electrolyte. The electrolyte plays a key role in the formation process. The electrolyte typically consists of several components, *i.e.*, salts, solvents, and additives. Typical weight proportions of components in an electrolyte mixture are 12.6 wt% salt, 0–10 wt% additives, and approximately 85 wt% solvent.[264] Overall approximately 2%–5% of the electrolyte mass is reduced during the first two formation cycles.[100,101]

A basic requirement for successful formation is a sufficient electrolyte availability.[24] This is achieved by maintaining an electrolyte volume factor that exceeds the total pore volume of the cell components. Recent research underscores the importance of achieving a 98% wetting degree before formation, as the quality of cells post-formation cycling was seen to be closely tied to the degree of wetting.[27]

There are several comprehensive reviews covering different aspects of battery electrolytes. Xu provided a review of electrolytes in LIBs and post-Li batteries and electrode|electrolyte interactions.[141,265] The status and progress toward the realization of high-voltage electrolytes was reviewed by Fan and Weng.[266] Electrolyte design principles for achieving high-energy Li batteries are summarized by Wan *et al.*[7] Zhang *et al.* provide a summary and guidelines on the development of non-flammable electrolytes.[5] Chemical and enviromental design guidelines for organic-based electrolyt are provided by Flamme *et al.*[267] Additives were reviewed by Zhang,[268] Zhao *et al.*[269] and Haregewoin *et al.*[270] Aravindan *et al.* review conductive salts used in Li-based batteries.[271] Advances and future directions in the design of electrolytes for fast-charging is provided by Lei *et al.*[272] and Zhang *et al.*[273] The decomposition of electrolyte components has been the subject to many earlier reviews covering the impact on the SEI[43,46,88,145,274] and CEI.[275–277] Heisaken *et al.*[89] and An *et al.*[45] provide details of the initial SEI formation.

This summary focuses on electrolyte aspects that influence the formation process.

Conductive salt. The conductive salt can significantly affect the composition of the SEI. In salts that contain fluoride (F) such as $LiPF_6$ or $LiBF_4$, typically LiF is observed as one of the main SEI components, however with in different weight percentages.[278–280]

It is also possible to combine multiple conductive salts. For example, Yan *et al.* dissolved a blend of different salts.[281] The electrolyte with the blended salts resulted in an increased cycling stability and lower impedance, both of which are attributed to the formation of uniform and stable passivation layer.

Varying the salt concentration affects the SEI/CEI layer composition. By elevating the concentration of F-containing salts the content of LiF can be increased at both electrodes, leading to a improved impedance and cycling stability, even at high voltages.[282–285] Borodin *et al.* observed that in the case of highly concentrated electrolytes, solvent molecules were effectively excluded from direct interactions with the positive electrode surface.[286]

As can be seen, adjusting the salt and its concentration can be an effective measure to enable the formation of stable interphases. However, it must be taken into account that the salt and its concentration also significantly influence relevant properties such as the conductivity of the electrolyte.

Conductivity. The ionic conductivity is an intrinsic property of the electrolyte composition and affects the power capability of the cell.[102] However, it also influences the homogeneity of the formation process along the electrode.[141,287] The ionic conductivity depends mainly on the salt and its concentration, but also on the solvent and the temperature.[102,288,289]

Solvent. Besides the salt also the solvent can significantly influence the formation process as it reacts at the interface as soon as the electrochemical stability window is exceeded.

EC is the most widely used solvent. It is known to form mainly oligomeric products, which are unfavourable due to

their poor mechanical and thermodynamic stability.[290,291] Accordingly, solvent decomposition should be suppressed to prevent the formation of an ineffective SEI/CEI.[7] Differences in SEI morphology for typical solvent combinations on LTO electrodes are shown in Fig. 12. As can be seen, the use of PC/EMC (Fig. 12A) resulted in a smoother but thicker SEI compared to EC/EMC (Fig. 12B).[172]

The decomposition reactions also depend on the components in the Li^+ primary solvation shell.[7,286] As the predominant species in solution changes as a function of the salt concentration,[282,292] this also elucidates the influence of the conductive salt concentration on the resultant passivation layer compositions.[7] Balbuena *et al.* found that the spatial distribution of the reduction reaction product is influenced by the local solvent concentration.[293] Their *ab initio* molecular dynamics (AMID) simulations suggest that Li_2CO_3 is more likely to be found in regions of low EC concentration, whereas LEDC is more likely to be found in regions of high EC concentration.

Since the solvent is the main educt for the decomposition reactions during formation, the choice of solvent has a significant impact on the composition and morphology. In addition, decomposition is strongly associated with salt and also indirectly affects interphase stability by determining the solubility of the solid reaction products, as discussed below.

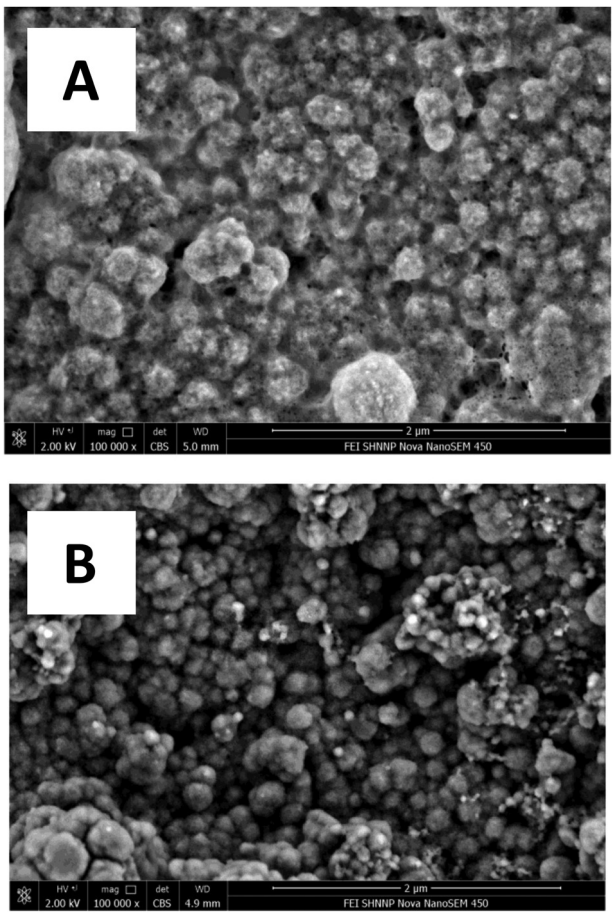

Fig. 12 SEM images of LTO electrodes after five formation cycles between 1.5 V and 2.8 V (CC-CV, with a CC rate of 0.1C and CV termination criterion of 1/20C) of the two solvent mixtures PC/EMC 1 : 1 and (B) EC/EMC 1 : 1. Reprinted with permission from Liu *et al.*,[172] Elsevier, Copyright 2015.

Solubility. The SEI species exhibit varying solubilities in dependence on the solvant.[89,294–296] High solubility can be problematic as it compromises a stable interfacial layer. In theoretical studies, the solubility of different SEI species in pure solvents DMC and EC has been investigated.[297,298] Irrespective of the solvent, the heat of dissolution was determined to be exothermic for organic species and endothermic for inorganic species.[297,298] This indicates that inorganic species are less favoured to be dissolved in the electrolyte. A higher solubility of LiF in EC compared to PC and DMC has been observed experimentally.[294,295] Other SEI species, *e.g.*, Li_2CO_3, Li_2O $LiOCH_3$ were found to be only weakly soluble in the tested akylcarbonates solutions, *i.e.*, EC, PC, DMC and EC/PC/DMC 1 : 1 : 3.[295]

During cycling, the solubility of the SEI species leads to dissolution and redeposition.[127,296,299,300] Due to the higher solubility of organic species, dissolution is more pronounced for solvent-derived SEIs, which may also result in accelerated aging.[296,301–303] By choosing a suitable solvent, the solubility of the SEI species in the electrolyte can also be used to selectively dissolve unfavourable species and form an SEI with a higher content of inorganic species.[304]

Solubilities may also affect initial formation, as suggested by Ushirogata *et al.*[305] Analysing the solubility of SEI species often reported in the near-particle region, the authors question the often assumed immediate deposition of SEI species on the particle surface, which they call surface growth mechanism (Fig. 13A). Instead, a near-shore aggregation mechanism is proposed, which precedes in two successive steps (Fig. 13B). Upon reaction, the SEI species first diffuse into the electrolyte and agglomerate in the bulk phase. Agglomerates coalesce before being deposited on the electrode. This theory is supported by another recent simulation study, which indicates that the passivation layer grows by the aggregation of precursors within the electrolyte bulk.[306] The strong aggregation of dissolved LEDC[307] and the varying solubility of SEI species[297,298] confirm the importance of the solvation state[308] and support the hypothesis of a near-shore aggregation mechanism.

The discussion indicates that solubility is an important aspect of the electrolyte to consider, as it can affect the stability of the interfacial layer as well as the formation process.

Additives. Additives can perform a variety of functions, including overvoltage protection and flame retardance.[5,64] In the formation process they are used as sacrificial donors to modify and to improve SEI and CEI properties.[45,309–311] A large number of additives have been reported to yield favourable electrochemical metrics.[312] A selection of additives and reported effects is given in Table 1.

Widely used are VC[241,291,313–317] and FEC,[226,316–322] which have been shown to improve SEI properties. VC can also effectively surpress co-solvant intercalation, improving first cycle CEs.[239–241] Under certain conditions, the reduction of

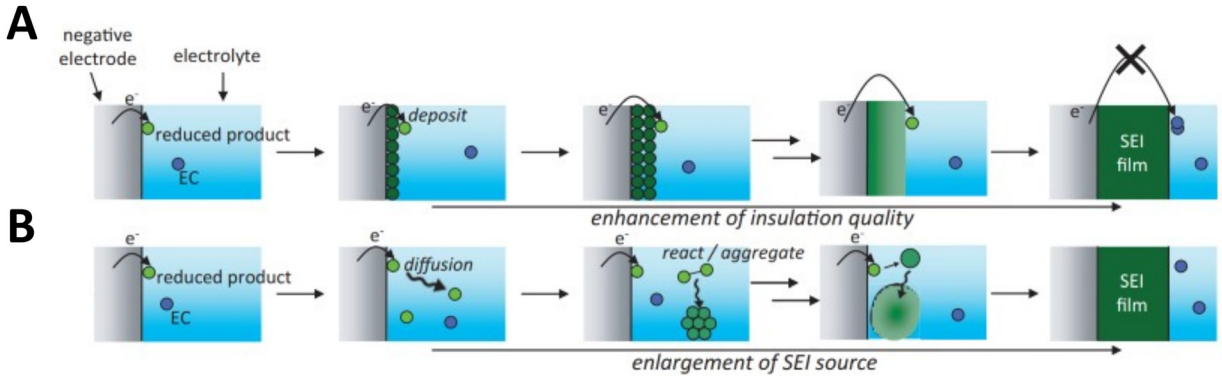

Fig. 13 Schematic representation of the (A) surface growth mechanisms and (B) near-shore aggregation mechanisms. Reprinted with permission from Ushirogata *et al.*,[305] IOP Publishing, Copyright 2015.

Table 1 Exemplary selection of electrolyte additives used to promote the electrode|electrolyte passivation layers. Effects on the interphases are taken from the listed references and briefly summarized

Additive	Effect	Ref.
Vinylene carbonate (VC)	Compact but rigid sei Improved thermal stability Polycarbonate-rich sei	118 314
Fluoroethylene carbonate (FEC)	Smooth, compact sei structure Mechanically strong (less factures) Improved thermal stability poly(carbonate)- and lif-rich inner sei	118 313 318
Aminosilane-based (TMS-ON)	Reduction of transition-metal dissolution due to stable cei Enhanced sei integrity with low interfacial resistance HF scavenger	310
Lithium difluorophosphate (lidfp)	Uniform, mechanically stable sei and cei High li_2co_3 and lif contents Mitigation of near-surface reconstructions Transition metal scavenger High ionic conductivity	324–331
5-Methyl-4-((trifluoromethoxy)methyl)-1,3-dioxol-2-one (DMVC-OCF3)	Mechanically deformable SEI Lif-rich inner SEI	334
5-Methyl-4-((trimethylsilyloxy)methyl)-1,3-dioxol-2-one (DMVC-OTMS)	Mechanically deformable SEI Improved structural integrity of the CEI and SEI HF scavenger	334
Lithium fluoromalonato(difluoro)borate (lifmdfb) + fluoroethylene carbonate (FEC)	Uniform, thin, compact sei and cei Improved positive electrode integrity and reduction of transition-metal dissolution High mechanical stress tolerance of the sei	332
Hexafluorocyclotriphosphazene (HFPN) + fluoroethylene carbonate (FEC)	Lowered gas evolution Less alkyl carbonates in the electrolyte after aging Smooth, homogeneous sei with less organic species Improved structural integrity of the negative electrode	333

FEC and VC results in identical products, which may explain the beneficial properties of the resulting SEI layers.[323] VC can also effectively surpress co-solvant intercalation, improving first cycle CEs.[240,241]

Another commonly studied additive is lithium difluorophosphate (LiDFP). In Gr||NMC full cells, LiDFP has been observed to improve rate capability and aging, which is attributed to improved stability and ionic conductivity of the SEI due to higher Li_2CO_3 and LiF content.[324,325] The addition of LiDFP in NMC||Li half cells was also found to improve the stability of the positive electrodes and the CEI. The formed CEIs are reported to be more uniform, reducing mechanical stress in the layer and its transfer resistance.[326–328] In addition, it mitigates near-surface reconstructions of the active material and acts as a transition metal scavenger, enabling stable operation of the NMC over a wider voltage range.[327–331]

Recently, electrolytes with multiple additives have been tested to take advantage of synergistic effects.[332–335] For example, by combining LiDFP with other additives, the improvements in terms of rate capability, CR and calendric ageing of the individual additives were further enhanced.[326,335–337] Combinations of addtives were systemetically assessed by Song *et al.*[338] and Wang *et al.*[312,339,340] with regards to electrochemical performance metrics and gas evolution.

Computational first-principles studies can provide insight into the functionality of additives. Wang *et al.* show that VC has

a higher reduction potential than EC and produces more stable intermediates during reduction than EC.[341] The effect on the oligomerization process of EC was also studied, showing that the introduction of FEC or VC modifies the process.[342,343] This modification results in an increase in the formation of polymeric species and a decrease in the formation of unstable oligomeric products.[342] In addition, in the presence of LiDFP, the LUMO and HOMO levels of EC and EMC are higher, indicating facilitated oxidation and hindered reduction of the solvents at the negative and positive electrodes, respectively.[328]

To conclude, additives can be used to influence the reactions during formation and to achieve interfacial layers with improved properties. As can be seen in Table 1, there is a wide variety of additives. Some are associated with specific properties. However, there is little understanding of the underlying mechanisms, which hinders to provide design principles. Nevertheless, in contrast to solvents and salts, additives promise a targeted improvement of the interphase properties without affecting the electrolyte properties.

Electrolyte design. The influence of the electrolyte on the formation process is manifold, which results in a huge design space. The incorporation of next generation materials increases the requirements. Electrolyte design is a promising strategy to improve stability for wider voltage windows and more significant volume expansion. However, the design process is complecated due to many interdependencies. For example, salt concentration affects ionic conductivity and interphase formation, making it difficult to tune these aspects separately. Key challenges for rational electrolyte design have recently been summarized by Wan *et al.*[7] and comprise the composition, solvation structure and bulk properties as shown in Fig. 14A.

The development of electrolytes is further complicated by the complexity of SEI/CEI, the ideal composition of which is unclear. Overall, a passivation layer with a high inorganic and low alkyl carbonate content seems to improve the aging performance of conventional Gr-based electrodes.[333] The advantages of inorganic over organic SEI species are mainly due to their low solubility and thermodynamic stability, both of which ensure protection of the electrodes, resulting in improved safety and aging.

Among the inorganic components, high LiF content is increasingly associated with favourable SEI/CEI properties, especially for high-capacity materials.[344] LiF is characterized by high mechanical stability.[7,344] The mechanical stability results from low Young's modulus and high interfacial energy with alloy negative electrodes,[7,222,334] which tolerates high active material expansions. This prevents breakage of the passivation layer, which would lead to increased electrolyte consumption. The mechanical stability and high lithiophilicity also prevent dendrite growth.[344] Further, LiF exhibits good ionic transport properties[229,345] and electronic insulation capabilities,[346,347] resulting in a thin layer. This results in high first cycle CEs and low interfacial resistances. Lastly, LiF posses a high thermodynamical stability due to a wide band gap.[348] These intrinsic properties result in an improved ageing, fast-charge performance and safety.[5,7]

To increase the content of inorganics in the SEI/CEI various electrolyte compostitions were tested. Multiple recent studies point out that inorganic-rich SEI/CEIs can be acheived by preferentially decomposing anions instead of the solvent. To foster the decomposition of anions over solvents, an increased number of anions in the primary solvation shell is key.[7] Elevating the reduction potential of the anion and lowering the solvent's reduction potential (Fig. 14B) by tuning the electrolyte composition can augment the formation further to yield more inorganic species.[222] By applying these design principles, tailored electrolyte solutions that promote F-rich SEI/CEIs already have developed and shown to improve the electrochemical performance.[222,223,349]

Despite the progress, improvements are still needed to achieve the high CEs (>99.9%) required for long-term use of high-capacity negative electrodes and high-voltage positive electrodes in many applications.[350] Therefore, the search for electrolyte components and formation protocols that further promote the formation of the F-rich inorganic passivation

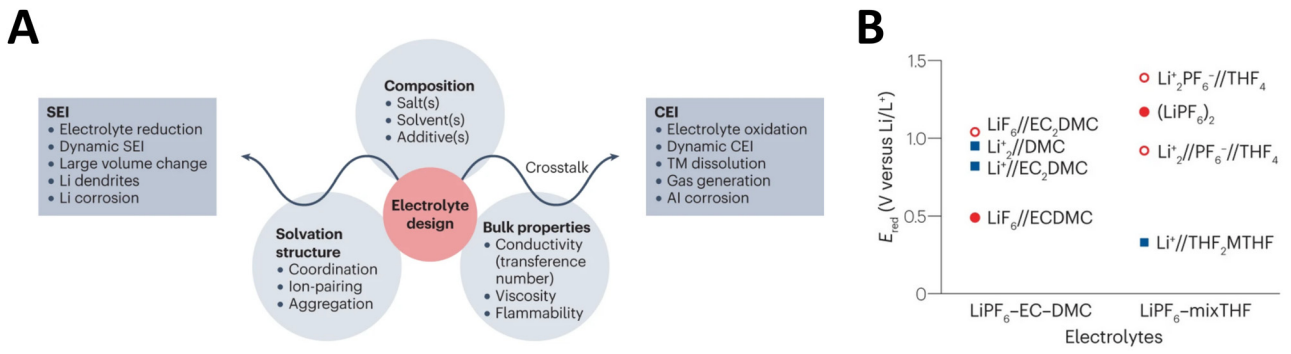

Fig. 14 (A) Key scientific challengens reagarding the design of electrolyte involved in improving the SEI and CEI to enbale high-energy LIBs. Factors that need to be considered in designing an electrode include electrolyte compositio, bulk properties and the solvation structure. (B) Reduction potentials of various electrolyte composnents calculated *via* DFT simulations by Chen *et al.*[222] The colors denote a preferential reduction of an anion (red) and solvant (blue). The marker denote species undergoing ionic aggregation (circels) and completely dissociated Li^+ species. Reprinted with permission from Wan *et al.*,[7] Springer Nature, Copyright 2023.

layer is an important task.[7,47] This requires a more in-depth understanding of the influence of individual electrolyte components on SEI/CEI composition, which is currently incomplete. This is due to the complexity of the interactions, the many contributing parameters. As a result, optimizing the electrolyte design remains one of the major challenges for improving the formation process. To address this challenge, more systematic research is needed to gain a more fundamental understanding of how to tune the electrolyte to achieve improved SEI/CEI compositions.

Separator. The separator has a major influence on the quality, safety and performance of a battery cell.[351] The effect of the separator material on formation quality has been little studied. However, it is expected that the separator also plays a key role in the formation due to its high influence on the Li transport within the cell. Some investigations of the separator with respect to wettability, mechanical strength and cycle stability have been reported.[352,353] We will discuss these findings in the context of the requirements for the formation process.

Man *et al.* describe the relationship between the degree of wetting of the separator and the effective current density in the battery cell.[352] Inadequate wetting impedes ion transport and is resulting in higher internal resistances and inhomogeneous current distributions in the cell. During formation, inhomogeneous current densities can lead to inhomogeneous SEI formation, resulting in varying SEI and CEI thicknesses and structures.[352]

Ladadec et al. investigated the effect of the separator material on the local compressive stresses.[353] They found that a given compressive stress has a greater negative effect, *e.g.* pore closure limiting Li transport, on polyethylene separator than on others separators such as a polypropylene separator. Therefore, some separator materials may also be more sensitive to internal and external compressive stresses during formation. This is relevant when external compression is applied during formation.

Frankenberger *et al.* investigated the effect of lamination on the formation process and electrochemical performance. They found that laminated cells exhibited reduced capacity fade at all formation rates and cycling rates.[354] The authors attribute the reduced capacity fade of the laminated cells to either inhomogeneous SEI growth or significantly reduced additional surface reactions at fast formation cycles.[354]

The separator mainly influences cell performance and maximum applicable rates, which is also relevant to the formation process, *e.g.* fast formation cycles. Furthermore, only an indirect correlation has been reported due to incomplete wetting. It can be speculated that wettability might also correlate with degassing properties. However, currently there are no dedicated studies on this aspect.

Cell format. Different cell formats and designs exhibit different characteristics due to temperature, pressure or current density distributions resulting from the internal layout.[355] This also affects the formation, as suggested by recent studies.

In the work of Lee *et al.*, half cells, coin cells and cylindrical cells were formed at different cut-off voltages.[139] While the half cells and coin cells did not show any increased capacity fade during cycling at any specific voltage cut-off voltage, the cylindrical cells at a cut-off voltage of 3.6 V showed a reduced CR.[139] Bridgewater *et al.* show a slightly increased capacity loss in the first cycle, but an improved CR for multi-layer pouch cells compared to coin and single layer cells.[356] Both results suggest that cell performance is affected by formation in different cell formats.

Drees *et al.* investigated a fast formation protocol with three-electrode coin cells and multilayer pouch cells.[153] The cells showed a slight voltage deviation for the different cell formats during formation, but showed similar voltage curves in later cycles at 1C.[153] These voltage deviations were attributed to temperature and manufacturing inhomogeneities.[153]

In addition, the cell format influences the liquid and gas transport pathways, which also affect the formation process, as shown in a study by Hagemeister *et al.*[27] They observed differences in the capacity decay after formation between pouch and hardcase cells for different wetting degrees. While there was a clear correlation between the ageing behaviour and the degree of wetting for the hardcase cells, there was no correlation for the pouch cells.[27]

Heidrich *et al.* investigated the SEI at the positive and negative electrodes of coin cells, laboratory-scale pouch cells and larger multi-layer pouch cells and found variations in the composition and thickness of the passivation layers.[63] These were associated with differences in the residual water content, mainly of the casing used for each cell format. Higher initial water content in the cells resulted in lower CE during formation.[63]

In smaller cells, gas generation is uncritical, and formation can be performed in a sealed cell.[119] In larger cells, gas bubbles interfere with the formation process by blocking Li-ion transport and interfering with electrolyte contact with the electrode surfaces,[135,357,358] necessitating gas venting.[119,120] In industry various gas venting methods are applied.[359–362] The procedure may differ depending on the cell format. Hard case formats are usually sealed after gas venting.[363,364] Pouch cell formats and occasionally hard case formats can be sealed, then opened and sealed again.[12,119,365,366]

In addition to the effect of cell format, there are also geometric differences between the cell types used in formation studies. In most commercial cells, the negative electrode is larger than the positive electrode, known as negative electrode overhang. This causes additional equalisation processes and interferes capacity,[367] CE,[367,368] and self-discharge tests.[369,370] However, the effect of size differences is often neglected in formation studies and can lead to confounded conclusions when comparing laboratory and industrial scale cells. Roth *et al.* investigated the effect of SOC and negative electrode overhang size on self-discharge behaviour after formation in single-layer pouch cells. They attributed the transient self-discharge to SEI growth and equalisation processes, and showed that both effects were less pronounced at low SOCs.[371]

The cell format and design can influence the formation process. However, detailed studies and a mechanistic insight into this influence are currently not available.

Experimental characterisation

Various techniques are used to analyse and evaluate the effects and interdependencies of the influencing factors on the formation process. This chapter summarises the applied experimental methods that have been successfully used to study formation processes or closely related aspects.

Characterisation of the formation process varies in level of detail and scope. Some characterisation techniques can be integrated into battery cell production and are then applied to each individual cell produced, others provide more detail but are typically limited to a small number of samples due to time-consuming preparation or the need for special setups. The latter are therefore most commonly used in research and development activities. This distinction is also used to group available studies:

1. In-line testing: non-destructive characterisation of full cells. Applicable as a quality control measure in cell production.

2. Sample testing: destructive experiments (*ex situ*, post-mortem or special cell design required). Sample size is limited to small numbers, but in-depth material characterisation is possible.

This chapter aims to illustrate the options available for characterising the various aspects and properties affected by the process. Existing methods with their main results related to the formation process are summarised in Fig. 15.

In-line testing – non-destructive characterization of full cells

Non-destructive or *operando* characterisation can be used to characterise the battery cell during and after formation. These methods can be integrated into the battery cell production as quality control and integral part of the EOL testing.

Capacity test. Cell capacity testing is essential in assessing battery quality. Before measuring capacity, the battery cell must be fully charged to the upper cut-off voltage. The charge should be a CC–CV charge followed by a rest period. The cell is then discharged to the lower cut-off voltage with a specified C-rate, *e.g.* C/3. A static capacity test measures the discharge capacity in ampere-hours.[372] The test should be repeated until three consecutive discharge capacities are stable within a defined range. To measure full capacity, either very low C-rates or a CV phase must be applied after CC discharge. The capacity test is performed along with other tests after the ageing process. The current trend in large-scale production is to measure the capacity either before the ageing phase or in the formation phase. This allows early quality check and helps reduce process time.[373]

The capacity is influenced by the formation process, because during the process Li is consumed, which reduces the amount of cyclable lithium inventory (CLI). Therefore, differences in the loss of CLI can be assessed by comparing discharge capacities.

Coulombic efficiency and capacity retention test. The progress of the formation process can be assessed using the CE and CR. In the first cycle, the CE is rather low, usually less than 0.9.[374] After the formation process is complete, the surface layers are passivated and capacity loss due to side reactions is largely inhibited. At the beginning of their life, LIBs typically achieve coulombic efficiencies greater than 0.996,[375] which

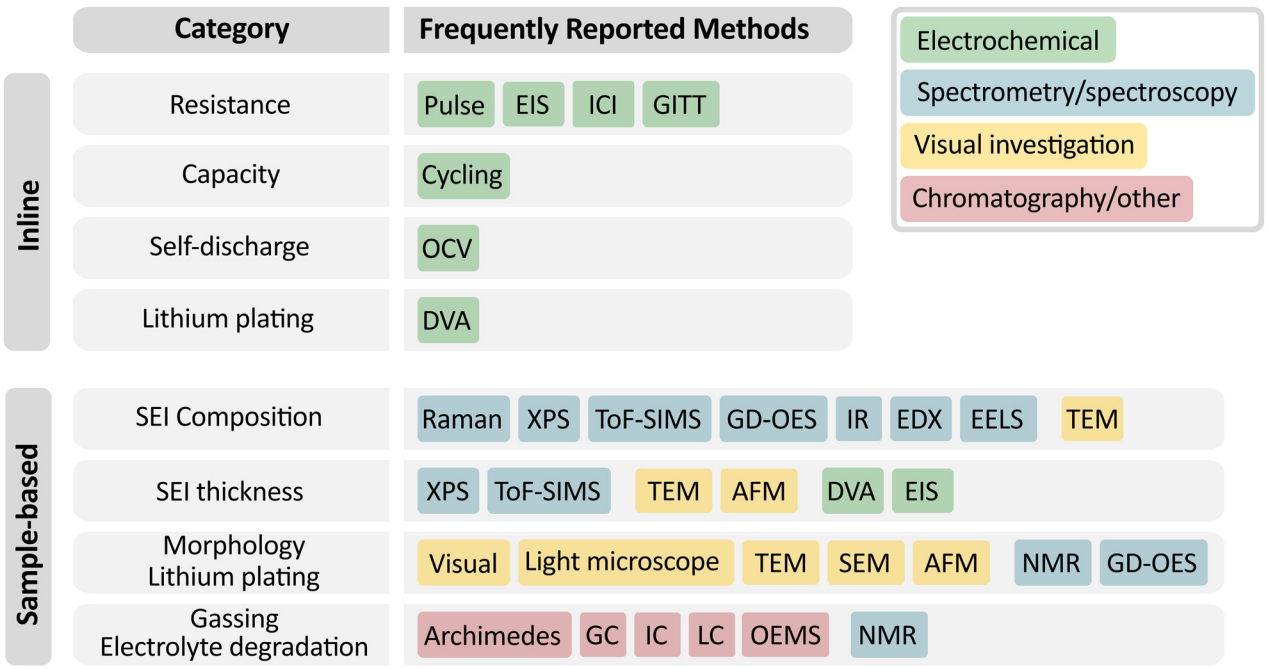

Fig. 15 Schematic overview of frequently reported methods and their application in the characterisation of the formation process. The figure is devided into methods that can be integrated into in-line quality control and methods that are typically only for sample-based characterisation.

continue to increase over the first cycles of the battery. Towards the end of the battery's life, the CE may decrease significantly.[375,376]

CE is defined as the ratio between the capacity during the charging process and the capacity of the subsequent discharge process:

$$\mathrm{CE} = \frac{\text{Ah capacity for } n\text{th discharge cycle}}{\text{Ah capacity for } n\text{th charge cycle}}$$

Capacity is usually measured by current counting, *i.e.* integrating the applied current, in CC charge and discharge cycles using low C-rates, *e.g.* C/22.[367] However, it is important that the SOC before charging is equal to the SOC after discharging, which is ideally 0% SOC. This can be achieved by discharging the cell prior to the CE test using the same discharge procedure as for the CE measurement. CR is the ratio between the capacity of two successive discharges:

$$\mathrm{CR} = \frac{\text{Ah capacity for } (n+1)\text{th discharging}}{\text{Ah capacity for } n\text{th discharge}}$$

CE and CR are both useful for assessing side reactions at the negative and positive electrode. CE is also a useful value for estimating the cycle stability of a battery cell without long-term battery cycling tests.[375,377] However, it has been pointed out that very high measurement accuracy is required for cycle life assessment. According to Smith *et al.*[377] CE measurement accuracies of at least 0.01% are required, while standard measurement equipment is not sufficient. The requirements for CE measurement accuracy may be lower when evaluating the progress of the formation process, as the changes in CE during formation are significantly greater as discussed above.

CE and CR can be used to study irreversible side reactions at the negative and positive electrode, as studied by Tornheim *et al.*[378] However, it is necessary to distinguish between cells with different type of limitation. Typically, LIBs are inventory limited, which means that cyclable Li inventory (CLI) determines the charge and discharge capacity. This is illustrated in Fig. 16. It can be seen that for a fully discharged cell the CLI is only in the positive electrode (Fig. 16A) and for a fully charged cell the CLI is only in the negative electrode (Fig. 16B). Therefore, the discharge and charge capacities are only determined by the CLI of the negative and positive electrodes, respectively.

Reduction reactions at the negative electrode reduce the CLI of the negative electrode, while oxidation reaction at the positive electrode increase the CLI of the positive electrode, as shown in Fig. 16. Therefore, the reduction reaction at the negative electrode reduces the discharge capacity but does not directly affect the charge capacity. Conversely, the oxidation reaction at the positive electrode increases the CLI and thus increases charge capacity but does not directly affect discharge capacity.

As shown by Tornheim *et al.*,[378] this can be used to distinguish between oxidation and reduction reactions. CE is only affected by the reduction reaction at the negative electrode,

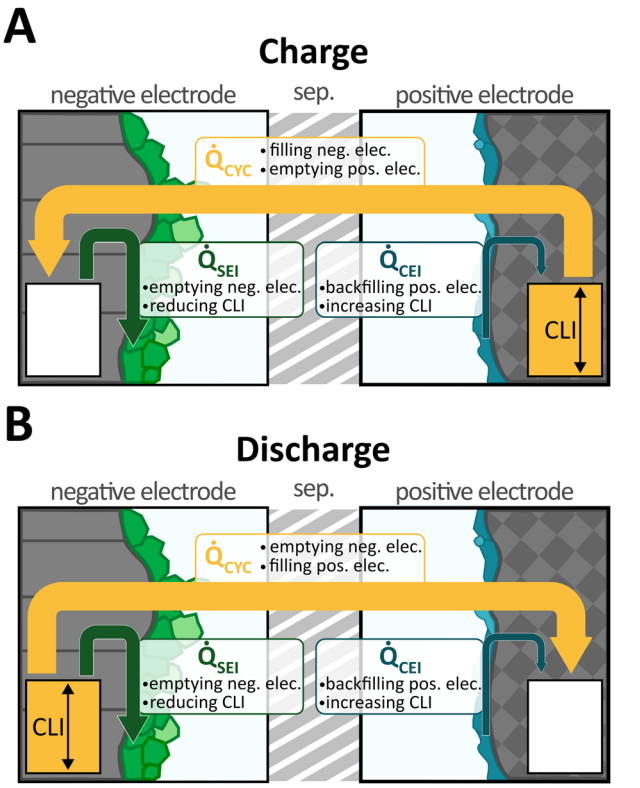

Fig. 16 Schematic of CLI fluxes during (A) charge and (B) discharge. The amount and location of CLI is indicated by the reservoirs in the negative and positive electrodes at the beginning of the charge and discharge, respectively. Li fluxes are shown as arrows. The size of the arrow indicates the magnitude of the flux. The colours indicate the de/intercalation reaction (yellow), the loss of CLI due to the SEI reduction reaction at the negative electrode (green) and the gain of CLI due to the oxidation reaction at the positive electrode (blue).

giving CE <1. CR is affected by both reactions, but in opposite directions. Reduction reactions at the negative electrodes result in a decrease in CR. Oxidation reaction at the positive electrode result in an increase in CR.

The situation is more complicated for site-limited cells. Here the capacity is determined by the available sites at one electrode. Cells using Li metal as the negative electrode are a typical example.[379,380] Here, Li metal provides a large reservoir for CLI. Thus, as long as sufficient Li metal is available, the capacity is determined only by the available sites of the positive electrode.[379,380]

Another important issue is anomalies in the measurements, such as these caused by the aforementioned negative electrode overhang.[367] Here the measured CE depends on the initial state and resting time prior the CE measurement, which can be classified as a short-term path dependency phenomenon.[381] As this anomaly can significantly distort the measured value, it must be considered carefully when using CE to evaluate formation progress.

While the capacity measurement mainly evaluates the loss of CLI due to the formation process. Evaluation of the CR and CE provides further insight into the stability and passivation properties of the interfacial layers and allows differentiation

between positive and negative electrode passivation. Despite the limitations for inventory limited cells and the bias due to negative electrode overhang, it is a simple yet useful method to evaluate the progression and success of the formation process.

Self-discharge measurements. Self-discharge measurements are very time consuming and can take many days or even weeks.[13,17,119] This long duration is due to low self-discharge rates and transient behaviour caused by relaxation effects, making early detection of electrochemical defects and micro-shorts in the early phase of the measurement difficult.[17,369,370] However, the decay of the self-discharge current, which is mainly attributed to the continuous growth of the SEI,[382,383] directly indicates the passivating properties of the interphases after the formation cycling and is used to identify cells with increased leakage currents.[17,119]

There are three methods for determining self-discharge: the capacity loss method, the voltage hold method and the voltage decay method.[369,384] The methods are depicted in Fig. 17. The capacity loss method (Fig. 17A) compares the capacity before and after a period of storage, allowing the separation of reversible and irreversible capacity losses. Disadvantages of this method are that it does not provide information during storage, which limits its ability to identify early rejects, and it requires the cell to be cycled before and after storage.[369] The voltage hold or float current method (Fig. 17B) directly measures the current required to maintain a given cell voltage.[370,385] This measurement shows time-resolved self-discharge and allows early rejects to be identified. However, it requires continuous and accurate voltage control and the measurement equipment is occupied for the entire test duration.[369] The voltage decay method (Fig. 17C) tracks the cell voltage over the storage period. The voltage can be measured at intervals and does not require a battery cycler. Although the voltage drop during storage already provides information about self-discharge, it has been shown that calculating the actual self-discharge current from the differential capacity *vs.* voltage plot provides time-resolved information comparable to the voltage hold method.[369,385] Liao *et al.* recently developed a detection method that can quickly assess the self-discharge rate of the battery cells by observing the OCV difference during the battery resting process. The OCV threshold is then compared with the OCV difference, and the ratio of the threshold is normalised. When the threshold ratio is compared with the self-discharge analysis results, it is concluded that the OCV detection method is reliable and can therefore be used to quickly analyse the self-discharge behaviour of the battery cells.[386]

Overall, the voltage decay method offers greater flexibility in terms of measurement equipment, while still providing a detailed and time-resolved self-discharge measurement. This makes the decay method well suited for cell manufacturing and formation analysis. The voltage hold method, on the other hand, provides reliable and direct measurement of self-discharge. Separation of reversible and irreversible effects can only be achieved by the capacity loss method, making it a suitable complement to voltage-based methods. When interpreting self-discharge measurements, it is also important to consider the influence of intermediate check-ups and cell design on relaxation behaviour, which can distort the evaluation.[371,387,388]

To conclude, self-discharge measurements also provide information on the passivation properties of the interfacial layers. In contrast to CE and CR measurements, it is much more time consuming, but offers a higher sensitivity. Sometimes it is the only in-line method that shows significant differences for different formation processes.[149]

Electrochemical impedance spectroscopy. EIS allows the unravelling of complex processes in full cells[389] and can be used *operando* within the cell manufacturing process.

Often, EIS spectra are used primarily to qualitatively assess differences between different formation process conditions and material impacts. In general, higher impedances indicate less favourable conditions. Similarly, EIS spectra can be used to assess the completion of SEI formation.[139]

In addition, EIS allows to distinguish between different process due to varying contributions at different time constants.[389,390] In addition, EIS can enable to distinguish between different process contributions, such as interface or diffusion processes.[389] However, sometimes process separation is difficult due to similar time constants.[389,391] An overview on different processes and their typical frequency domains is provided by Krewer *et al.*[392]

To separate the process contributions, equivalent circuit models are often fitted to the impedance spectra. By applying

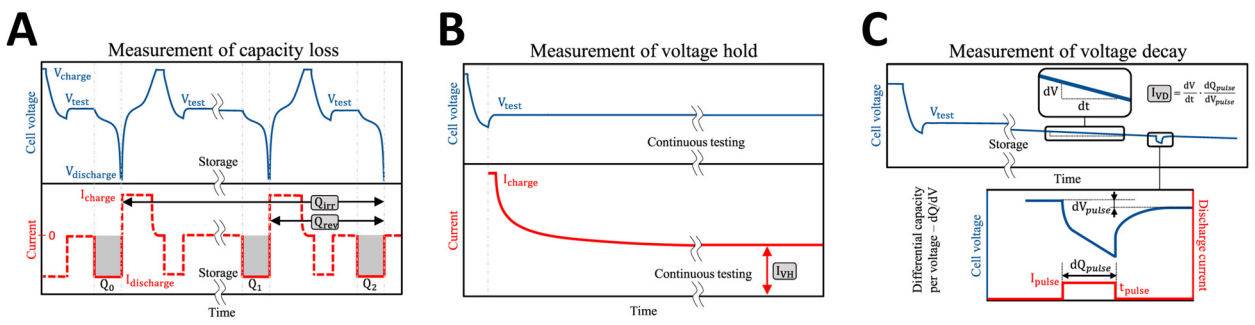

Fig. 17 Illustrations of different self-discharge measurement approaches: (A) Voltage decay method, (B) voltage hold method, and (C) capacity loss method. Reprinted with permission from Roth *et al.*,[369] IOP Publishing, Copyright 2023.

distribution of relaxation time (DRT) analysis to the frequency data, improved identification of the underlying process contributions and definition of more robust models can be achieved.[391] Separation of processes *via* equivalent circuit models allows, for example, to evaluate cell-to-cell differences and to assess the SEI film resistance separate from other process contributions.[393]

However, some challenges remain. For example, an increase in film resistance could be related to thicker surface films but could also indicate slower ion transport within the film. In addition, interface resistivity is strongly related to specific surface area, which is often unknown and subject to significant uncertainty.

EIS can also be used in combination with other electrochemical techniques. For example, EIS has been combined with cyclic voltammetry.[190] Here, it is used to identify distinct regions for subsequent EIS analysis.

EIS provides complementary information to the previously discussed measurements, as it does not evaluate the interfacial layer based on the loss of Li inventory, but directly on the interfacial properties, *e.g.* the interfacial or film resistances. In particular, a combined evaluation of CLI and interface resistivity using impedance spectra can be used to infer film properties such as ion transport.

Differential voltage analysis. SEI formation and Li plating can be studied *operando* using differential voltage analysis (DVA).

DVA can be useful to identify undesired SEI formations. This was shown by Müller *et al.* who identified differences in the differential voltage curves of NMC622||Gr-based cells formed with and without a CV step and were able to correlate these observations with *ex situ* analysis.[394] It was revealed that the SEI appeared to be more heterogeneous and porous in the cell formed without a CV step, which was also reflected in the appearance of the differential voltage profiles.

To investigate Li plating/stripping, an *operando* analysis *via* DVA was introduced by Petzl and Danzer.[395] It associates a particular minimum in the DVA curves with stripping of previously plated Li. However, some challenges to the general applicability of using DVA to quantify Li stripping have been raised in the recent work of O'Kane *et al.*[396]

In conclusion, DVA is another technique complementary to CLI based techniques. It provides additional information and can be applied as a manufacturing process control measure,[397] but the interpretation of measurement results is more demanding.

Internal resistance measurements. The internal resistance of LIB cells is an important parameter for assessing cell quality and is routinely determined as part of the EOL to identify scrap. After formation, the internal resistances should have a low standard deviation as it correlates with the cell internal heating,[398,399] which may cause heterogeneous ageing.[400] Further, the internal resistance at low SOCs was found to correlate with cycle life in lab scale NMC111||Gr cells and to be a better predictive feature in comparison to the CE or changes in discharge voltage curves, which are often used to assess the impact of formation protocols.[104]

The determination of the internal resistance can be carried out using a direct current (DC), *i.e.* galvanostatic intermittent titration technique (GITT)[401,402] and intermittent current interruption (ICI),[403] or a alternating current (AC), *i.e.* EIS.[401,404] Barai *et al.* compared the internal resistance of 20 Ah LFP||Gr-based LIB pouch cells obtained with GITT and EIS.[405] The determined resistances were found to be in good agreement.[405] In pulse-based resistance investigations, however, the time-based measurement resolution of typical cyclers, limits the distinction of different process contributions to the overall resistance.[405]

In summary, measuring the internal resistance provides information about the cell quality. Resistance can be determined using both DC and AC measurements. While AC-based determination is more time-consuming and requires more precise equipment, DC-based techniques can be easily performed in-line by typical cyclers and provide comparable information on the total cell resistance. However, an EIS measurement is required to differentiate between individual process components.

Sample testing – *ex situ*, *post mortem* or special cell design required

Although much valuable data on the formation outcome can be obtained in-line, other techniques can provide further insight. These methods may require sophisticated preparation, special experimental setups, or destructive post-mortem analysis.

Comprehensive discussions of the analytical techniques that can be used to investigate LIBs can be found in other available reviews. Verma *et al.* published a review giving insight into many methods, which can be used to characterise the SEI.[88] The review by Zampardi and La Mantia summarises current and emerging techniques applied to analyse the CEI.[406] Waldmann *et al.* provided an overview article on *post-mortem* analysis methods of LIBs in general.[407] Here we will focus on discussing some tests specifically informative about the formation process.

Characterisation of experimental cells. Special cell setups can provide valuable additional information that cannot be obtained from a classical fully assembled cell. Investigations of electrodes with a Li metal reference electrode or in symmetrical cells, *i.e.* cells composed of electrodes of the same type, can have the advantage of isolating an electrode of interest.[134] Experimental cells can be assembled before or after formation, *e.g.* by extracting the electrodes of a full cell after formation. As an alternative, inclusion of reference electrodes in special cell setups is possible, but not typically done in commercial cell production. Such studies are therefore most useful to accompany the production process or to investigate the influence of changes/adjustments to the formation process.

Three-electrode cells allow the individual impedance of the negative and positive electrodes to be evaluated. For example, in the formation study by Chiang *et al.* the CEI and SEI were examined separately and it was shown that the impedance of the negative electrode was affected by different formation processes, while no significant changes were found for the

positive electrode.[154] Huang *et al.* aimed to investigate impedance contributions, but assembled a three-electrode setup by plating Li metal reference electrode *in situ* on a Cu wire located inside the cell prior to formation.[106]

Schomburg *et al.* introduced a novel DVA-based approach to determine the growth behaviour of SEI using three-electrode setup with Li metal reference electrode.[408] This allowed to derive continuous SEI growth curves for different electrolytes. The growth curves are shown in Fig. 18. As differences between electrolytes were observed, this method is useful for analysing new electrolyte formulations. The data can also be used to parametrise SEI growth models.[408] Potentially the method can also be used as an early quality control measure in production lines, as the DVA has also been used in ageing studies based solely on full cell voltage.[409–414]

Similar to three-electrode cells, half cells can be used to study electrode formation individually. Half cells are used in combination with EIS and cyclic voltametry measurements to study initial SEI formation[95,131] as well as effects of material pretreatments[415] and electrolyte compositions.[416] Solchenbach *et al.*[96] used EIS at 0% SOC before and after formation to obtain the SEI resistance R_{SEI} for various electrolyte solutions in of Gr||Li half cells. The measured impedance spectra are depicted in Fig. 19A and B. The low SOC (blocking condition) was chosen because charge transfer is slow in fully discharged Gr electrodes, which allows the clear separation of R_{SEI} by fitting a transmission line model (Fig. 19C) to the impedance data, which is not possible at high SOCs (non-blocking condition). Although there are variations due to electrolyte dependence, the resistances between the non-blocking (Fig. 19D) and blocking (Fig. 19E) conditions are similar, suggesting that the SEI resistance plays a significant role in the overall intercalation resistance of a Gr electrode under non-blocking conditions.[96]

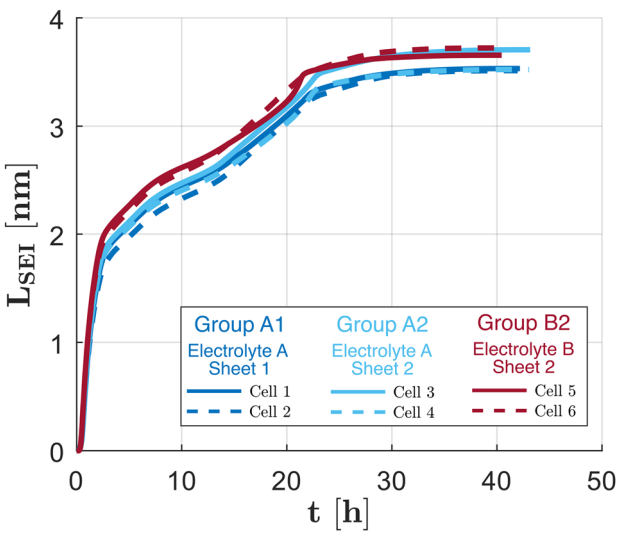

Fig. 18 SEI thickness growth identified by a combined DVA and model-based analysis method for two electrolytes. Reprinted with permission from Schomburg *et al.*,[408] John Wiley and Sons, Copyright 2022.

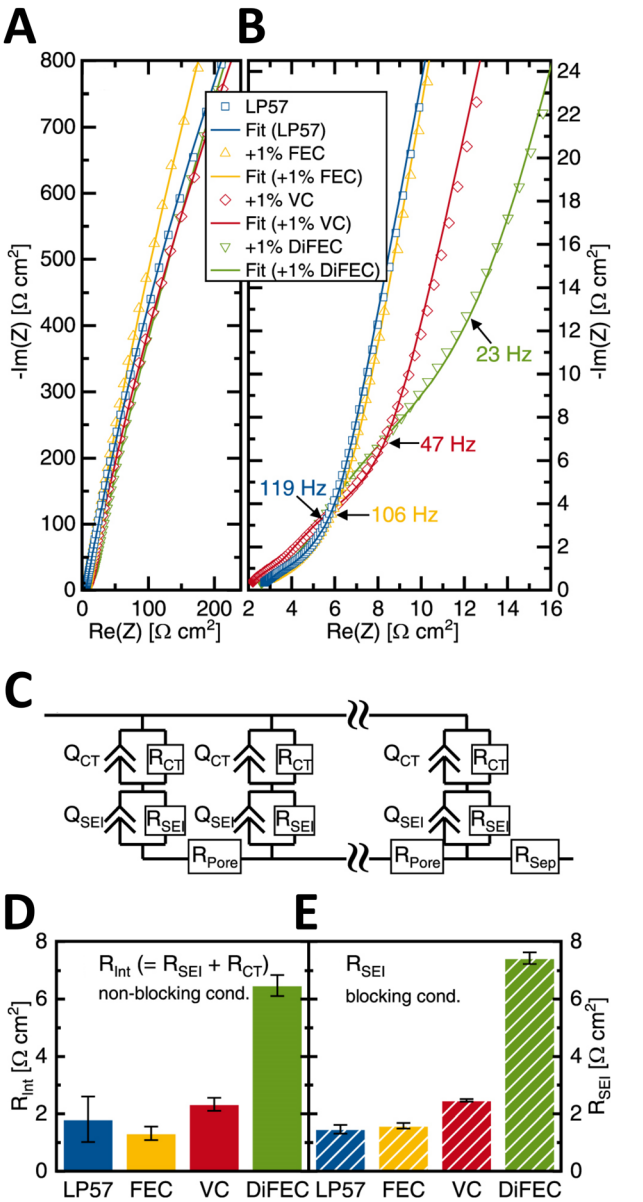

Fig. 19 (A) Normalized impedance of graphite||Li half cell at 0% SOC (*ca.* 2.01 V *vs.* Li^+/Li) at 25 °C after formation (2× C/10 CC full cycels) for the base electrolyte solution 1 M $LiPF_6$ EC/EMC 3 : 7 (blue squares) and with 1 wt% of the respective additives FEC (yellow triangles), VC (red diamonds) and DiFEC (green triangles) (B) Enlarged view of high-frequency area of the entire impedance spectrum. (C) Used transmission line model (TLM) with two *R*/*Q*-elements to fit R_{SEI} to the impedance data. The value of R_{Pore} was obtained by analysing additional impedance data and was kept fixed during the R_{SEI} fit. (D) Intercalation resistance R_{Int} (=R_{SEI} + R_{CT}) obtained by fitting the impedance data in non-blocking conditions at 40% SOC. (E) SEI resistance R_{SEI} determined in blocking conditions at 0% SOC. Reprinted with permission from Solchenbach *et al.*,[96] IOP Publishing, Copyright 2021.

Symmetric cells are often used for EIS experiments and are a useful tool for formation studies. This setup allows the contribution of the negative and positive electrode to be separated. For example, it can be used to investigate whether the SEI has formed completely without interference from the impedance of

the positive electrode. Momma *et al.* provided a detailed review of symmetrical cells.[417] Heidrich *et al.* used electrodes from NMC622||Gr-based cells after formation in symmetrical cells for EIS experiments.[418] This showed that the impedance of the negative electrodes did not increase much as the impedance of the positive electrodes as a result of long-term cycling, implying a different growth behaviour of the SEI and the CEI. Further, symmetric cells can be used to sudy the impact of electrolyte compositions on the SEI and cell performance. Analysing EIS and cyclic voltametry mesurements of various electrolytes in Li||Li cells, Hobold *et al.* found a correlation between a fast Li^+ exchange trough the SEI to a stable cycling performance.[419]

Three-electrode, half cell, and symmetrical cell setups can be used to examine individual electrode contributions separately. This is useful for identifying material-dependent changes. Symmetrical cells are suitable as a post-mortem analysis technique to analyze full cells after formation but can also provide information on the evolution of the passivation layer.

Surface analysis techniques. Most relevant processes during formation take place at the interfaces between the active material and the electrolyte. The composition and thickness of the interphase layers are critical to cell performance. Due to their low thickness, bulk-sensitive techniques cannot be used to characterise the layers, and surface analysis is mainly used instead. Surface analytical methods cannot usually be used in-line and require the cell to be opened. Here, an overview of techniques that have been used to characterise battery electrodes after formation is given.

Microscopy based techniques. Many studies on formation strongly rely on microscopy-based techniques to reveal the morphology of the interphase layers.

SEM is a powerful and widely available microscopic technique. After formation, typical applications of SEM include morphological studies of the electrode particles, including their coverage, deposition of residues or plated Li. For example, Märkle *et al.* used SEM in their study of different Gr types and electrolytes to identify the surface coverage and extent of exfoliation of Gr particles.[237] Schweidler *et al.* were able to correlate CEI growth and particle cracking during the first five cycles.[76] For identification of particle cracking they relied on SEM images. Fig. 20 shows SEM images of the LNO electrodes during initial charging with increasing electrode potentials, *i.e.* (A) pristine, (B) 3.8 V, (C) 4.1 V and (D) 4.2 V. The technique reveals that at higher voltage particle cracking occurs.

Transmission electron microscopy (TEM) enables to gain deeper insight at smaller length scales. However, unlike SEM, TEM often requires more elaborate sample preparation and is generally not designed to examine large number of samples. Fig. 21A shows one of the earliest TEM images of the SEI on Gr.[420] Today, cryogenic transmission electron microscopy (cryo-TEM) allows the study of sensitive chemical phases without damaging the interfacial layer,[421] allowing the microstructure of the SEI to be studied. For example, Huang *et al.* found that in carbon black||Li half cells, a predominantly amorphous SEI of approximately 2 nm forms on the carbon black during an initial C/10 cycle, as shown in Fig. 21B.[422] Extending TEM with

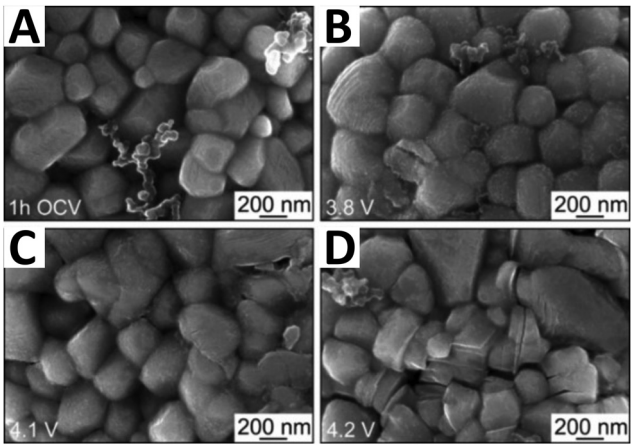

Fig. 20 Top view SEM images of the LNO cathode taken (A) after 1 h OCV and (B) after charging to ~3.8 V, (C) ~4.1 V and (D) ~4.2 V *vs.* Li^+|Li in the first cycle. Reprinted with permission from Schweidler *et al.*,[77] John Wiley and Sons, Copyright 2020.

electron energy-loss spectrocopy (EELS) also provides high resolution structural and chemical information.[423] For example, Chen *et al.*[222] obtained and analysed EELS spectral images of Si negative electrodes after cycling for a designed and a conventional electrolyte. The comparison of the images shows that the SEI of the designed electrolyte (Fig. 21C) is thinner compared to the traditional electrolyte (Fig. 21D). In addition, the LiF content near the particles of the designed electrolyte (Fig. 21E) is higher than that of the conventional electrolyte (Fig. 21F). Recent progress in establishing *in situ* TEM analyses of battery electrodes has been discussed in a review article by Yuan *et al.*[424]

The combination of SEM and TEM can provide interesting insights due to their distinctly different scopes and capabilities. For example, Bhattacharya *et al.* studied formation of SEI on Gr-based electrodes when they applied different voltage scan rates in a linear sweep voltammetry experiment.[425] SEM images showed a difference in layer morphology, with the SEI being more uniform and tubular.[425] By performing TEM measurements, the authors were then able to determine the microstructure of the formed SEI, which consisted of nanocrystalline domains within an amorphous structure.[420,425] Cheong *et al.* also used a combination of TEM and SEM to study the formation on the alternative negative electrode material, *i.e.* Co_3O_4 nanoparticles. By combining the datasets from both methods, changes in the SEI morphology became apparent.[75] TEM visualised the SEI layer after formation and after cycling and determined its thickness.[75] SEM, which covers a larger area, showed the SEI around the particles.[75]

When electron microscopes are equipped with energy-dispersive X-ray spectroscopy (EDX) capability, the elemental composition of samples can often be determined directly after imaging, making the technique even more valuable.[426] For example, among other analytical techniques, Stockhausen *et al.* used SEM and EDX. Results are shown in Fig. 22. While Gr surface did not show any significant structural changes as

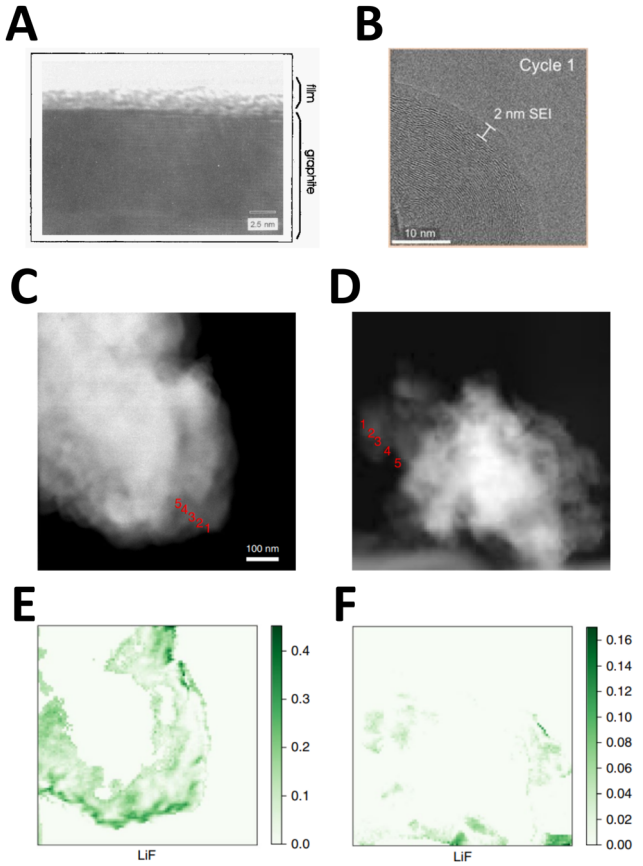

Fig. 21 (A) Early TEM micrograph of SEI on a discharged artificial graphite negative electrode. Reprinted with permission from Besenhard and Winter,[420] International Union of Pure and Applied Chemistry, Copyright 1998 (B) Cryo-TEM images of a carbon black after a single cycle in EC/DEC electrolyte. The image was taken in the fully delithiated state. Reprinted with permission from Huang *et al.*,[422] American Chemical Society, 2019. (C) and (D) are high-angle annular dark-field imaging images of Si particle surfaces with a designed electrolyte with 2.0 Mol $LiPF_6$ in tetrahydrofuran(THF)/2-methyltetrahydrofuran (MTHF) (mixTHF) 1 : 1 (C) and a conventional electrolyte with 1.0 Mol $LiPF_6$ in EC/DMC (D). The red numbers indicate the 5 positions at which the EELS spectral images were analysed, with 1 being at the layer surface and 5 being at the inner layer. The LiF distribution of the analysed area is shown in percentage for the designed electrolyte in (E) and for the conventional electrolyte in (F). Reprinted with permission from Chen *et al.*,[210] Springer Nature, 2020.

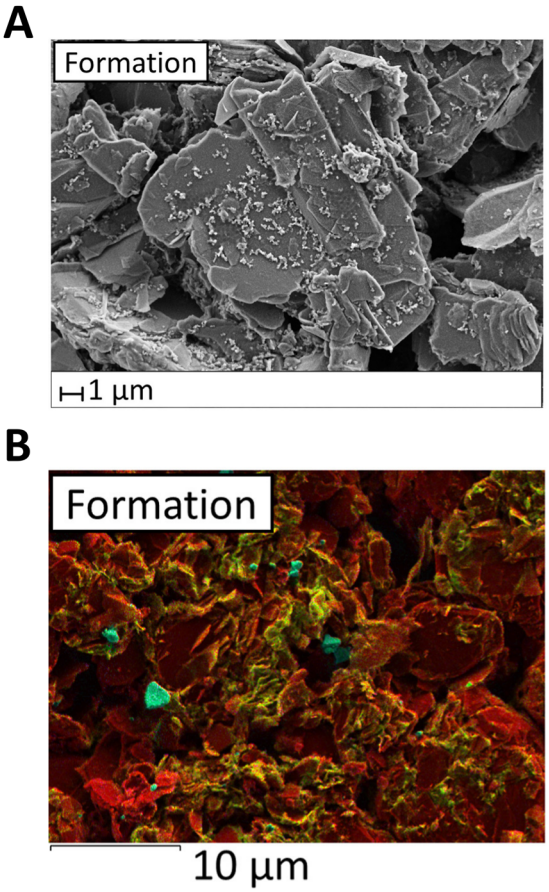

Fig. 22 SEM (A) and EDX (B) images of a graphite surface in NMC622||graphite cells with EC/DMC 1 : 1 + 3% VC electrolyte after formation, respectively. Reprinted with permission from Stockhausen *et al.*,[101] Elsivier, Copyright 2022.

shown in Fig. 22A, SEI deposits are visible on the Gr surface in the EDX as shown in Fig. 22B. The scope and limitations of electron microscopy in the context of LIB research have been reviewed by Wu *et al.*[426]

Atomic force microscopy (AFM) is an alternative method for morphological analysis, *e.g.* for determining the thickness of the SEI. Using special cell designs, the method can be applied *in situ*, as described for amorphous carbon,[427,428] HOPG-based electrodes,[52,428,429] MCMB[428] and Si-based electrodes.[222,430] As an example, the evolution of the SEI morphology on a thin layer of amorphous carbon during an initial charge with a consistent voltage scan rate is shown Fig. 23.[427] The AFM images show minor changes of the surface morphology at potentials higher than 1.5 V (Fig. 23B). The surface roughness and features exhibit their most significant changes between 0.8 and 0.6 V *vs.* Li/Li^+ (Fig. 23E and F) due to formation of organic decomposition products. During the remaining charge, the morphology changes at a slower rate. Such a potential dependent SEI growth of the SEI was observed is also observed for the other mentioned electrode types.

Furthermore, distinct variations in SEI growth behaviour were observed when different electrolytes were used. This highlights the relevance of AFM in the development of novel electrolytes and the elucidation of the structural evolution of the SEI. An overview of the application of AFM in the context of LIB research is given in the review by Weidong *et al.*[431]

While SEM and TEM are mostly complementary techniques as they cover significantly different length scales, AFM is a frequently used alternative and especially suitable for *in situ* analysis.

Spectroscopy-based techniques. To investigate the composition of interphase layers spectroscopy-based techniques are usually used.

XPS is a very surface sensitive and frequently applied technique that can be used to determine surface layer composition.

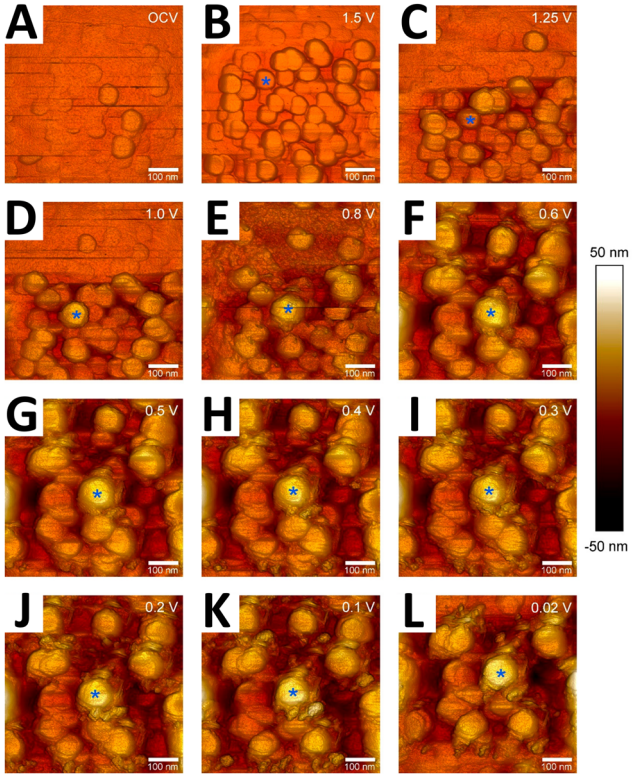

Fig. 23 Evolution of the surface morphology on a carbon model electrode and a 1 Mol $LiPF_6$ in EC/DEC 1 : 1 electrolyte obtained *via in situ* AFM during the initial charge with a constant voltage scan rate of 1 mV s^{-1}. The voltage scane was stopped and held at OCV (A), 1.5 V (B), 1.25 V (C), 1.0 V (D), 0.8 V (E), 0.6 V (F), 0.5 V (G), 0.4 V (H), 0.3 V (I), 0.2 V (J), 0.1 (K) and 0.02 V (L) *vs.* Li/Li+ for several minutes to gather the AFM data. The blue asterisk marks the same feature in troughput all images. Reprinted with permission from Steinhauer *et al.*,[427] American Chemical Society, 2017.

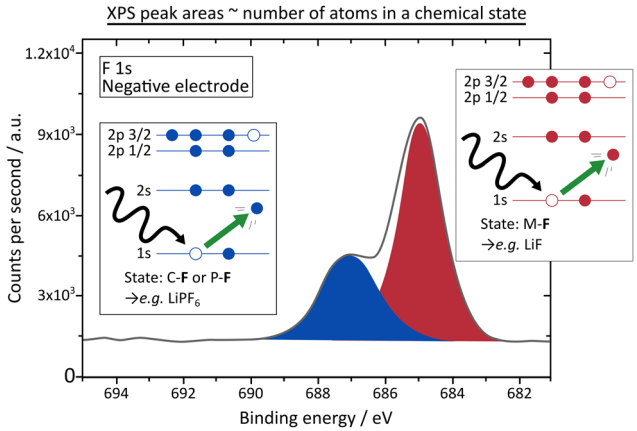

Fig. 24 An exemplary F 1s XP spectrum of a graphite-based negative electrode after formation illustrates one of the main assumptions underlying quantification in XPS: The spectrum contains two overlapping peaks, one from $LiPF_6$ and one from LiF, and the peak area is proportional to the number of atoms in each chemical state.

An example schematic of an F 1s XP spectrum is shown in Fig. 24 for a Gr-based negative electrode after formation. It is illustrated that each of the peaks of the overlapping areas can be assigned to a chemical state, *i.e.* $LiPF_6$ or LiF, on the surface. The area under each peak reflects the number of atoms in the respective chemical states. Thus, XPS enables both identification and quantification of chemical components.

By combining XPS with sputter depth profiling (SDP), it can also be used to measure thickness. For example, Mao *et al.* determined the layer thickness for electrode samples.[105] The chemical composition was monitored before and after parts of the layer had been removed by sputtering. This allowed the composition of the SEI to be determined and the thickness to be approximated. Several advanced XPS-based approaches have been developed to determine the thickness of the SEI based on depth profiles that rely on sputtering[432] or a variation of X-ray energy.[55] By measuring XPS at multiple positions spatial homogeneity of the SEI and CEI can be deduced.[433]

XPS is usually performed *ex situ*. However, efforts are being made to establish *in situ* XPS measurements and are summarised in the review by *Wi et al.*[434] Another recent development in photoelectron spectroscopy is the lab-scale hard X-ray photoelectron spectroscopy (HAXPES),[435] which uses X-rays of higher energy than conventional lab-scale XPS, thereby increasing the depth information. This allows thicker layers to be studied without the need for SDP, which is in particular relevant to study the formation of Si-based electrodes, which are known to form thicker SEI.[436]

Time-of-flight secondary ion mass spectrometry (ToF-SIMS) is an alternative technique for mapping of elements and chemical species. Due to its excellent lateral resolution, it provides valuable additional insights. For example, Veryovkin *et al.* used ToF-SIMS to analyse Gr-based negative electrodes before and after formation, as well as after long-term cycling.[437] It allowed them to observe distinct differences between the cycling protocols. However, the authors point out that the large number of data sets obtained with ToF-SIMS could not be evaluated in detail. This may be one reason why ToF-SIMS-based analyses of SEI are not yet as common as XPS analyses. An advantage of ToF-SIMS over XPS is the ability to make continuous measurements during depth profiling experiments, which allows to follow the compositional changes as the layer is removed.[438] ToF-SIMS has been shown to be very powerful in combination with XPS. Gauthier *et al.* analysed the surface layer formed on LTO-based electrodes.[439] While surface composition information obtained by the two approaches is mostly comparable, some results are also synergetic. For example, the observability of titanium in XPS, with an information depth of approximately 10 nm, allowed the sputtering depth of their ToF-SIMS experiments to be estimated. Furthermore, ToF-SIMS detected titanium-containing species on the positive electrode, which was not possible with XPS alone. Sui *et al.* used a combination of ToF-SIMS with SEM-EDX to study the surface properties.[440] This allowed them to map the elemental composition of a SEM image with EDX and scan the surface with the highly surface sensitive ToF-SIMS to obtain a high resolution map of surface species distribution.

When it comes to characterising the SEI and CEI using vibrational spectroscopy, such as Raman and Infrared (IR) spectroscopy, a recent review by Weiling *et al.* gives a comprehensive overview of the scope of each method.[441] They conclude that these techniques will play a key role to monitor chemical compounds, and highlight the importance of *in situ* techniques. Vibrational spectroscopy techniques certainly can add complementary information. This can be seen in very early studies by Aurbach *et al.*, where IR spectroscopy and XPS was used.[442] XPS showed that halides, such as LiF, were part of the layer, while IR spectroscopy enabled the authors to identify Li alkyl carbonates as the main components.

Several studies demonstrate the synergistic effect of sample-based characterisation, which can help to understand fundamental aspects of the interphase layers. For example, a broad combination of surface analytical methods was used by Bhattacharya *et al.*[189] Optical microscopy was used *operando* to monitor surface damage, SEM gave further insight into the morphology, EDX provided elemental distribution, TEM, XPS and Fourier-transform infrared spectroscopy (FTIR) each provided information on the chemical composition and structure. Also Lu *et al.* highlighted the importance of combined morphology and composition analysis.[93] They further included EIS in their analysis, which enabled to show that not only thickness, but also the composition of the SEI contributes to the measured impedance.

Surface analysis techniques are very important in characterising the formation process, as they provide a detailed insight into the composition, thickness, morphology, and heterogeneity of the interphase layers. However, each method has its advantages and disadvantages. Often only a combination of different methods provides the comprehensive picture needed to gain the mechanistic insight required for knowledge-based process optimisation.

Gas and electrolyte analysis techniques. During SEI and CEI formation, electrolyte components are consumed, and gases are formed as by-products of the reactions. Analysis of the evolved gases and changes in the electrolyte, *e.g.* quantification of the gas species produced and assessment of their (re)solubility, is important to gain a holistic understanding of the process.

Archimedes principle is an *in situ* method to determine the gas volume as result of formation cycling and was introduced by Aiken *et al.*[443] The technique was later used by Self *et al.*[175] and Leißing *et al.*[184,185] in combination with gas chromatography mass spectrometry (GC-MS) to identify the species generated when using different electrolyte additives during formation. By equipping commercial LIB cells with a gas sampling port, Schmiegel *et al.* were able to monitor the volume and nature of the evolving gas *in situ* at defined cell voltages.[444]

As gas evolution is closely linked to the decomposition reactions, the combination of surface and gas analysis can provide insight into the reactions and the build-up process during the formation step. For example, Ellis *et al.* used a combination of GC-MS, the gas volume determination *using* Archimedes principle and surface analysis using XPS analysis.[165] The authors showed measurable differences in surface composition when the cells were not degassed after formation, which could be attributed to follow-up reactions of the formation gases within the cell.

In addition, analysis of the electrolyte, *e.g.* by liquid chromatography (LC), can provide further insights into the underlaying degradation. Numerous studies have been carried out using, *e.g.* liquid ion, or with mass spectrometry. Comprehensive reviews of electrolyte analysis have been provided by Nowak *et al.*[445] and Stenzel *et al.*[446] Nuclear magnetic resonance (NMR) spectroscopy is a powerful analytical technique that has been widely used to understand degradation pathways in LIBs. *Ex situ* and, with special cell designs, *in situ* measurements are possible,[447] *e.g.* to study the ageing of electrolytes. A review and an overview of the historical development of NMR in the context of battery research has been provided by Hu *et al.*[448]

Gas analysis is most important for understanding the reaction mechanisms during. Since the gas is also involved in the reaction, it is important to get a detailed understanding of the gases produced, where GC-MS are suitable methods. Similarly, analysis of the electrolyte composition by NMR can contribute significantly to the understanding of the reaction processes. A complete picture requires identification of surface layer composition, electrolyte composition change, and gas evolution and composition.

***Post mortem* methods for Li plating detection.** An essential criterion for successful formation is the exclusion of Li plating.

Li plating is most commonly detected by optical inspection, *e.g.* visually or by microscope after opening the cell. Visual inspection is straightforward and reliable as no special equipment is required. Despite its simplicity, visual inspection is usually sufficient to judge whether Li plating has occurred during formation, as can be seen for two electrodes shown in Fig. 25. It can even give a rough estimate of the amount and therefore the severity of Li–metal deposits. Janakiraman *et al.* have written a comprehensive review of established methods for characterising Li plating in LIBs.[449]

A specific example of detection of plating in formation studies is given by Mao *et al.* who found a visual increase in plated Li for reduced formation time.[105] Only with very slow formation was no plating observed at all. After long-term cycling, which showed only minor differences between formation protocols, a smaller part of the electrodes appeared to be covered with Li. The authors concluded that some Li plating was reversible.

The *post-mortem* detection of Li plating is possible not only by optical examination but also by NMR spectroscopy. Münster *et al.* varied the formation C-rate between 0.2C and 2C.[132] After 2C formation, optical inspection showed that large parts of the Gr-based electrode were covered with deposited Li, which could also be confirmed by SEM images. Using NMR spectroscopy and inductively coupled plasma-optical emission spectroscopy (ICP-OES), the difference in the amount of plated Li was quantified to be up to 5% of the total capacity.

Glow discharge optical emission spectroscopy (GD-OES) can also be used to determine the depth-resolved elemental

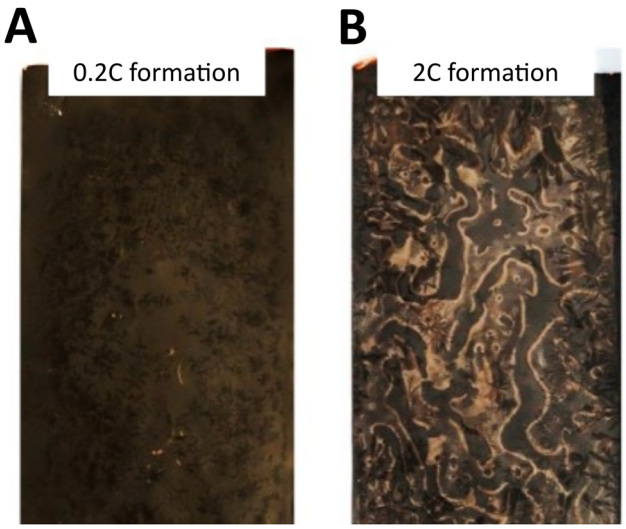

Fig. 25 Photographs of graphite-based negative electrodes from multi-layer pouch cells after formation at either (A) 0.2C or (B) 2.0C with clear differences in the visual amount of Li plated. Reprinted with permission from Münster *et al.*,[132] IOP Publishing, Copyright 2015.

composition of samples. GD-OES has been shown to be particularly useful for detection of Li on negative electrodes.[450] Ghanbari *et al.* studied differently aged Gr-based electrodes with GD-OES and were able to estimate the Li distribution of the samples.[451] They were also able to distinguish between different plating morphologies, *i.e.* island-like deposits *vs.* more homogeneous, layer-like coverage of the particles. This approach was later adapted and revised by Flügel *et al.* to be applicable to Si-Gr composite electrodes, where Li plating is less understood than for purely Gr-based negative electrodes.[452]

Li plating must be excluded during formation. Therefore, usually optical inspection is sufficient for formation studies. However, to effectively mitigate Li plating during formation, additional information on the plating morphology may be helpful to identify the root cause. This is where advanced techniques such as GF-OES can be useful.

Computer-aided process engineering

Computer-aided engineering techniques play an essential role in establishing knowledge-based process optimisation and design. For complex processes with many influencing factors such as the formation process, computational techniques offer the potential to reduce development costs and improve the process quality.

Since the formation process is affected on considerably different time and length scales, different modelling techniques must be used. Frequently used computational techniques, together with their typical length and time scales at which they are applied, are summarised in Fig. 26.

Wang *et al.* published a comprehensive review of modelling approaches for the SEI.[453] The review by Horstmann *et al.* focuses on multi-scale models.[42] Quantum mechanical methods used to investigate the main mechanisms involved in SEI reduction reactions of organic solvents are reviewed by Ramos-Sanchez *et al.*[454] Theoretical work on the CEI is summarised in a section in Xu's critical review.[275] Atkins *et al.* also devote a section to the simulation of interphases, discussing both interphase layers, *i.e.* SEI and CEI.[455]

This section highlights modelling approaches specifically related to the formation process. The section is structured according to the relevant areas of application, which are the decomposition reactions at the solid|liqud interfaces, interphase layer growth, interphase layer nanostructures and gas evolution.

Simulation of decomposition reactions at solid–liquid interfaces

Electrolyte decomposition occurs when the potential of the electrode is outside the electrochemical stability window of

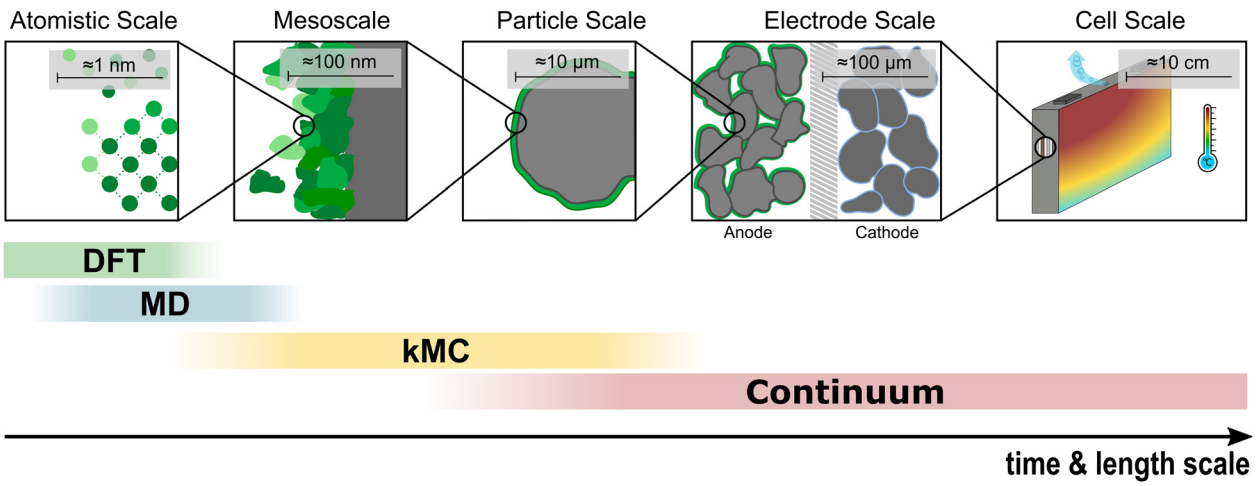

Fig. 26 Overview of the simulation methods used to depict phenomena during the formation process as well as their typical time and length scales. Adopted with permission from Röder *et al.*,[496] John Wiley and Sons, copyright 2019.

the electrolyte components. Computational methods can help to identify suitable electrolyte components and explain their decomposition mechanisms.

The electrochemical stability window of state-of-the-art electrolyte has been studied in many DFT simulations.[341,456–458] In addition, quantum chemistry (QC) calculations can be used to obtain binding energies and redox potentials of common salts, solvents and additives and to study the redox reactions.[459] Examples for computed reduction potentials are shown in Fig. 27. Such calculated values can be used as an initial assessment to screen and pre-select promising electrolyte components.

The reaction mechanisms of the formation process are very complex, making them difficult to describe mathematically. There are many possible reaction pathways, often involving multi-step reactions with many intermediates. AMID simulations were used to investigate reduction pathways. For example, the decomposition mechanisms of EC[163] and $LiPF_6$[460] in the electrolyte bulk and EC in the proximity of electrodes, *i.e.* Si[246,461] and Gr,[462] were investigated with this simulation method. Further, AMID simulations were used to compute redox potentials of additives.[463] AMID simulations have been also used to gain a better understanding of the reaction mechanisms at the positive electrode. For example, Leung studied the initial stages of EC decomposition on ideal $Li_{0.6}Mn_2O_2$ surfaces at constant potential using DFT and AMID.[169] Computerised reaction networks (CRN)[464] and their combination with machine learning techniques (CRN-ML)[465] can be used to construct large reactions networks from first principle calculations.

Combined DFT and AMID simulations were used to calculate electron transfer through SEI components,[461] thermodynamic and transport properties of electrolytes,[466,467] decomposition potentials of solvents[468] and additives.[463] Furthermore, these methods can be used to study the influence of the local solvent concentration,[293,469] the degree of lithiation[246] or the electrolyte composition at the interface.[286,470] These aspects must be considered together to predict the SEI composition.

There are two main tasks that computational methods can perform with respect to interfacial reactions. They can be used to quickly screen possible electrolyte components by examining their decomposition potentials. In addition, AMID simulations can be used to investigate complex reaction networks, even near the interface. The combination of these aspects may allow computational design of composition of the interphase layers.

Simulation of interphase layer growth

An essential property of the interphase layers is their ability to passivate against electrolyte decomposition. Passivation defines the continuous growth of the interphase layer and the associated capacity loss during formation and ageing. Furthermore, the CE of the LIB after formation is determined by the growth limiting properties of the interphase layers.

Continuum models can be used to describe the growth of interphase layers in a lumped fashion. These models usually simplify the reaction mechanisms and kinetics by reducing them to a single mechanism and assuming homogeneous interphase properties. The growth rate is limited by various passivation mechanisms. Understanding the growth limitation of the interphase layer is essential.[11]

Several transport mechanisms that determine the self-limiting nature of the SEI are discussed. These mechanisms are illustrated in Fig. 28 and were discussed by Horstmann *et al.* in their review on multi-scale models of the SEI growth in detail.[42] In general, these mechanisms are also applicable for the formation process. Equations and references for these mechanisms are summarized in Table 2.

The electron tunneling mechanism (ETM) originates from quantum mechanics, where it describes the possibility of an electron passing through a zone that is normally prevented by an energy barrier. The mechanism can be implemented using a modified Tafel equation.

The electron conduction mechanism (ECM) assumes that the rate is determined by the transport of charge-carrier driven by potential gradients across a dense SEI.[471] Colclasure *et al.*

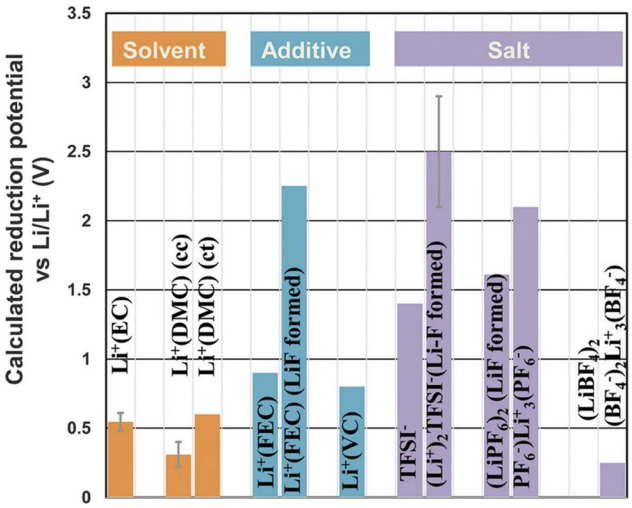

Fig. 27 Reduction potentials of electrolyte components according to the first principal simulation. Reprinted with permission from Wang *et al.*,[453] Springer Nature, Copyright 2018, who compiled the data of Delp *et al.*[459]

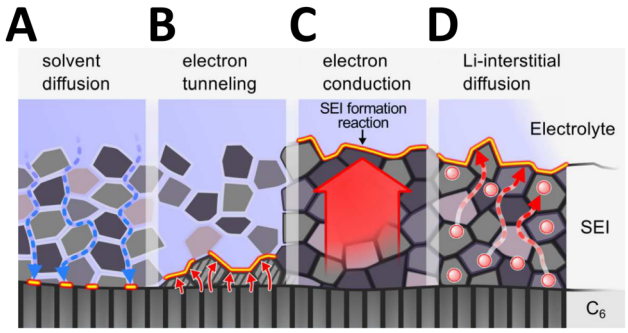

Fig. 28 Schematic of considered leakage mechanisms to reaction site enabling SEI growth. Reprinted with permission from Single *et al.*,[479] John Wiley and Sons, Copyright 2018.

Table 2 Summary of discussded continuum thermodynamic mesoscale SEI growth models. These models assume the SEI thickness, independent of its composition, to limit the ongoing passivation layer growth during operation. Due to their low computational cost, the models can be applied to simulate long-term growth, *i.e.* during storage or operation

		Parameters		
Mechanism	Equation	Symbol	Term	Unit
Electron tunneling (ETM)[476]	$i_{ET} = \kappa_{ET}\, i_0\, e^{\frac{-\alpha F \eta}{RT}}$	i_0	Exchange current denstity of the reduction reaction	A m^{-2}
		α	Reaction symmetry	—
		η	Overpotential	V
	$\kappa_{ET} = {\kappa_{ET}}^0 e^{-\beta L_{SEI}}$	T	Temperature	K
		${\kappa_{ET}}^0$	Reaction probability in direct contact	—
		β	Tunnelling barrier	m^{-1}
Electron conduction (ECM)[471,472]	$i_{EC} = \left(J_k - C_k \frac{\partial L_{SEI}}{\partial t}\right)$	J_k	Molar diffusion flux of species k	mol cm^{-2} s^{-1}
		c_k	Molar concentration of species k	mol m^{-3}
Solvent diffusion (SDM)[473]	$i_{SD} = F D_S \frac{\partial^2 c_s}{\partial z^2}$	D_s	Diffusion coefficient of the solvent	m^2 s^{-1}
		c_s	Solvent molar concentration	mol m^{-3}
		z	Coordinate variable	m
Interstitial diffusion (IDM)[479]	$i_{ID} = F \frac{D}{L_{SEI}} c_0 \left(\frac{-\phi F}{RT}\right)$	c_0	Average Li concentration in the SEI	mol m^{-3}
		D	Diffusion coefficient of the Li interstitials	m^2 s^{-1}
		ϕ	Potential of the active material *vs.* Li|Li$^+$	V
		T	Temperature	K

implemented this mechanisms in a single-particle model that includes reaction kinetics and transport of species within the SEI film.[472]

The solvent diffusion mechanism (SDM) assumes that the transport of the solvent or salt from the electrolyte bulk to the reaction site is the limiting factor in continuous SEI growth. The process is modelled by assuming Fick's law of diffusion for the solvent components.[473]

The diffusive interstitial mechanism (IDM) has been proposed by Shi *et al.*[474] Small radicals, such as Li atoms, are charge carriers. Shi *et al.* calculated the concentration of Li interstitials within a compact Li_2CO_3 layer to be between 4.9×10^9 and 2.3×10^{16} cm^{-3} depending on the electrode potential. The Li interstitials enable the propagation of decomposition reactions in the SEI layer.[42,342,474]

Several simulative and experimental studies suggest that the initial growth after the first atomic layer of SEI is established on the surface, is limited by ETM.[408,475,476] The tunneling barrier of SEI has been investigated in several studies. Lin *et al.* performed DFT simulations to calculate the electron tunnelling barrier of Li_2CO_3, Li_2O, and LiF and a Li metal electrode.[475] They concluded that the initial capacity loss is driven by ETM until a thickness of approximately 2–3 nm is reached, which was also found to change under compression/expansion.[475] Leung *et al.* concluded that electron tunnelling is sufficiently suppressed by a 7 Å insulating oxide SEI in a combined experimental and first-principles study.[477] A thickness of about 10 Å was calculated by Benitez *et al.* using AMID and DFT simulations to sufficiently block electron transport through pure LiF or Li_2O films on Si negative electrodes and varying degrees of lithiation by Benitez *et al.* using AMID and DFT simulations.[461]

Beyond the tunneling regime, knowledge of the limiting mechanism is less profound. Using the experimental long-term storage data at different electrode potentials published by Keil *et al.*,[383,478] Single *et al.* contrast the discussed mechanisms by comparing their plausibility.[479] The authors conclude that IDM is the only mechanism that adequately explains the experimentally observed dependencies.[479] The analysis of the same data was later extended to include the time dependence of the SEI growth mechanisms, focusing on the comparison between SDM and IDM.[480] It was shown that IDM explains both the SOC and time dependence, while SDM reproduces only one of these dependencies.[480] They conclude that IDM is the main driver for the SOC-dependent SEI growth.[480] This is in agreement with the DFT study by Soto *et al.*, which identified IDM as responsible for electron transfer.[342]

Schomburg *et al.* analysed SEI growth curves obtained during formation using DVA.[408] Using an SEI growth model that considers a concurrent ETM and IDM for two electrolytes, the model-based analysis indicated that the tunnelling barrier shifts as a function of electrolyte composition. It was also shown that the SEI growth obtained during a slow initial formation cycle cannot be explained by ETM alone. As shown recently, growth functions can be also identified with data driven models such as neural ordinary differential equations.[481]

A dependence on the current direction has been reported by Attia *et al.*[482] To describe this phenomenon, Das *et al.* introduced a model based on the assumption that the SEI can be considered as a mixed ion-electron conductor.[483] By this and by introducing a Li concentration dependence for the electronic conductivity in the SEI, the growth of the layer is promoted or suppressed depending on the lithiation current direction.

Typically, SEI growth models assume a solid layer of a single SEI species and a limiting transport mechanism. However, it is conceivable that the evolution of the SEI morphology may also influence the limiting transport processes. To investigate this possible influence, Single *et al.* introduced a one-dimensional framework that takes into account the porosity of the SEI.[484] This approach allows to simulate the evolution of SEI thickness and morphology along the interphase thickness

and incorporates different rate-limiting transport mechanisms, *i.e.* SDM in the SEI pores and IDM or ETM in the solid SEI phase.[484] The model predicts the often reported two-layer structure with a constant ratio between the thicknesses of the inner and porous outer layers.[484]

Growth models typically neglect mechanical stress. While these variables can be neglected for comparison in storage tests, they play an important role in formation cycling. Mai *et al.* modified a Pseudo 2D (P2D) battery model using finite-strain theory to account for the interplay between large electrochemical-mechanical deformations at the particle and electrode levels. This was used to model the influence of porosity changes on the mechanical stress of each cell component.[485] Kolzenberg *et al.* introduced a chemo-mechanical model that incorporates the mechanical-stress inducted SEI growth.[486] The model is in good qualitative agreement with the experimentally observed SEI cracking during lithiation and healing during delithiation of Si particles, leading to accelerated capacity fade during cyclic ageing.[486] However, the model has not yet been tested for formation cycling. Other continuum-level models that consider degradation mechanisms due to mechanical stress have been reviewed by Zhang.[205]

Model-based analysis of SEI properties after formation is also possible. Witt *et al.* have applied such an approach to investigate long-term evolution of the SEI properties.[487] The model comprises a P2D and SEI model capable of calculating EIS and electrochemical discharge curves.[487] This allows to determine physically insight such as SEI thickness or interfacial SEI|liquid interface area.

Simulation of SEI growth can be used to design formation cycling protocols. However, it remains a challenge to identify suitable growth limiting processes. The situation is even more complicated for materials with significant volume expansion, such as Si, because the mechanical properties of the interface layers must also be considered. The goal of the formation simulation methods discussed is to reduce the number of experiments required to design formation cycling protocols that are tailored to the material and cell design.

Simulation of interphase nanostructures

Due to the changing conditions and the different reactants and intermediates, several reactions compete during the initial formation, resulting in a heterogeneous structure, which was first introduced by Peled *et al.*[488,489] To obtain spatially resolved insights on the SEI structure, first-principle simulations and the kinetic Monte Carlo (kMC) method were used.[306,454,490–496]

Although first-principle studies provide spatially resolved information on the SEI and have made progress on the time scale,[497] they are still limited to the ns range and are therefore unable to describe complete formation cycles. Compared to *ab initio* simulations, kMC allows longer time scales to be simulated while preserving atomistic detail.[162,493,498]

Methekar *et al.* developed a 2D kMC model to theoretically investigate the effect of process parameters, such as charging voltage, current density and temperature, on the initial SEI layer formation and suggest that there is an optimal temperature to minimise initial capacity loss.[490] This model was extended by Ramos-Sanchez *et al.* to a three-dimensional coarse-grained kMC (CG-kMC) model, allowing them to track the growth rate as a function of layer thickness.[454] The model was used as an example to simulate the layer growth for a multi-step reduction of EC to LEDC using a fixed adsorption rate and DFT-based reaction rates.[454] Esmaeilpour *et al.* performed a simulation study of SEI formation using a 2D kMC model with reaction rates obtained from QC calculations.[306] Their simulation shows qualitatively good agreement with experimental observations of the SEI morphology for a solution-mediated growth scenario.[306] Similarly, based on reaction mechanisms obtained by AIMD and a stochastic analysis method that accelerates CRN-ML simulations,[494] Spotte-Smith *et al.* used a kMC model to perform a comprehensive study of the initial SEI formation and evolution for varying potentials and electron tunneling barriers.

Röder *et al.* dynamically couple a kMC surface film growth model with a macroscopic continuum battery model to simulate SEI formation.[495] In this way, the structure of the passivating film directly influences the reactions at the particle surface. In a first simulation study, they investigate the effect of two particle sizes on SEI formation for an electrolyte composed of EC and $LiPF_6$. The simulations show faster SEI growth on larger particles. In subsequent work, the same multiscale approach was extended by combining the kMC model with a P2D model and an advanced coupling method, allowing to account for distribution of concentrations and potentials.[492,496] The novel multiscale model was used to simulate various formation protocols. Simulation results are show in Fig. 29. While slow charging led to locally heterogenous structures and homogeneous distributions of species along the *x*-axis (Fig. 29A), the opposite was observed for fast charging protocols (Fig. 29B).[496]

In contrast to the continuum models used to simulate SEI growth, the models discussed in this section provide a detailed insight into the molecular structure of the interphase layer. They allow to combine insights from complex decomposition mechanisms and SEI growth mechanisms. Theoretically, it enables to reveal differences in the SEI structure without the need for sophisticated experimental surface characterization methods. The goal of these simulations is to tune the electrolyte choice and cycling protocol to achieve a desired interphase layer structure. However, it is usually not known how the ideal SEI and CEI should be composed to achieve long life and safety. These aspects need to be worked out in order for the methods to reach their full potential.

Simulation of gas evolution

Gas evolution affects the formation at different scales and is considered in different modelling approaches.

In first-principle and kMC simulations, gases are considered as products and reactants of the reactions. For example, Leung predicted the formation of CO gas when examining two-electron reduction pathways of EC and assuming fast electron tunneling.[163] In the case of slow electron tunneling, the reduction of EC was calculated to yield C_2H_4 and CO_2

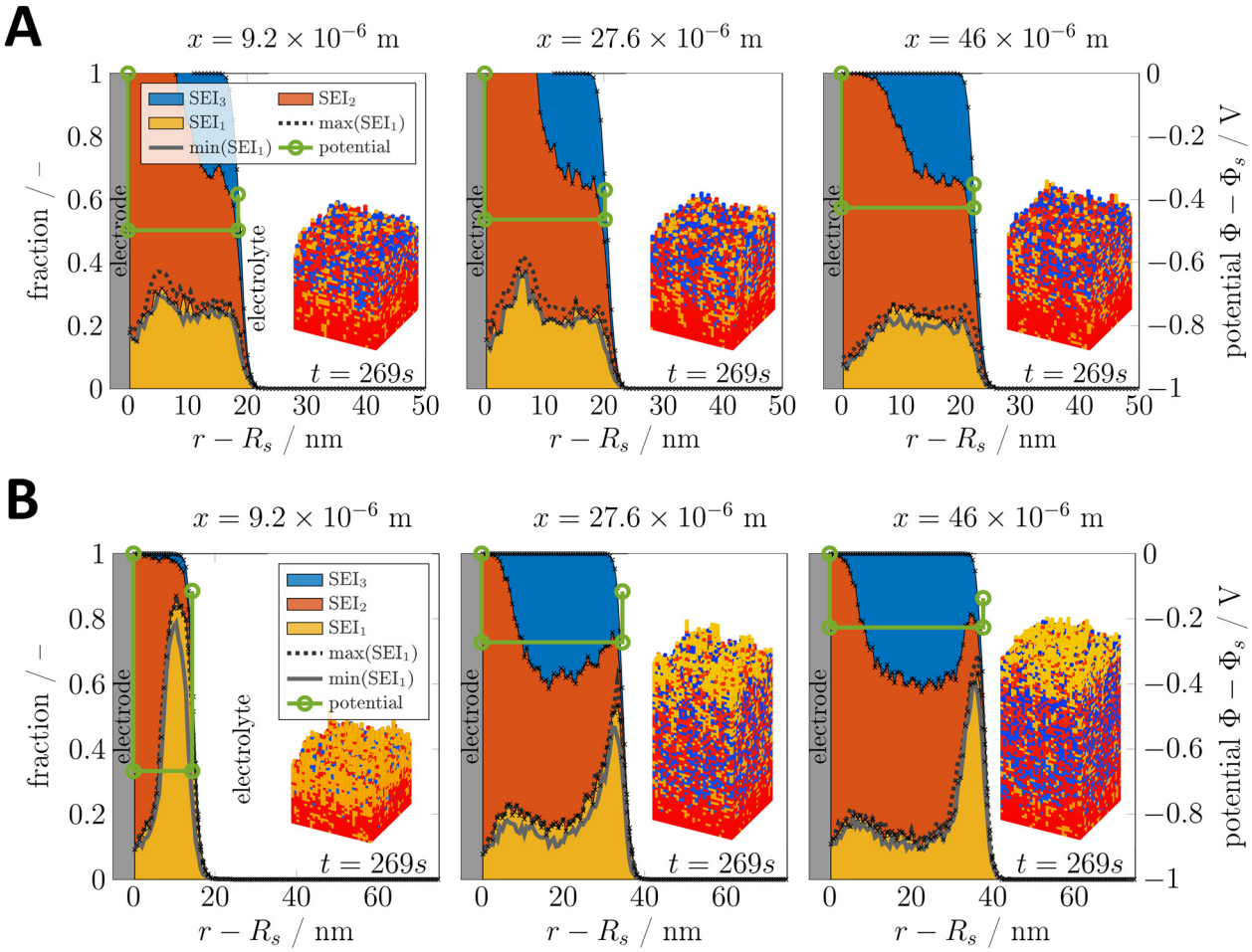

Fig. 29 Results of a multi-scale simulation of SEI growth. Shown are the composition and film structure of a kMC instance at t = 269 s during the first charge applying (A) a low C-rate of 0.07C and (B) a high C-rate of 2C at different positions x along the negative electrode thickness. The positions shown are left (x = 9.2 μm), middle (x = 27.6 μm) and right (x = 46 μm), which are close to the current collector, middle of the active material layer and close to the separator, respectively. In addition, the highest and lowest values for the species SEI$_1$ from four parallel kMC instances are shown. Finally, the potential at the electrode surface (s), left and right of the film (s) and the electrolyte (s) is shown. Reprinted permission from Röder *et al.*,[496] John Wiley and Sons, copyright 2019.

instead.[163] This is consistent with the findings of Alzate-Vargas *et al.* who reported the presence of C_2H_4 in the later stages of their simulation, covering the first 100 ns of SEI formation.[497] They also discuss the relevance of the consideration of gas molecules, as they did not observe the formation of gas bubbles.[497] However, given the uncertainties regarding potential entrapment, temporary influence of these molecules on SEI growth, or change in density they suggest to consider the gas molecules in the simulations.

Gas evolution and its effects on battery performance have been simulated in mechanistic continuum models. These models assume that the generated gas is inert and reduces the volume fraction of electrolyte. Seo *et al.* introduced a model that discusses how gas evolution from electrolyte decomposition and impurities causes swelling in Li-ion batteries.[499] Their model explains the non-linear increase in cell resistance with changes in volume fraction caused by gas evolution. They apply the model to study the effects of these changes on discharge curves and heat generation.[499] The P2D model has been extended by Rashid and Gupta to capture the combined effect of SEI formation and gas evolution on battery performance caused by cyclic degradation.[500] Here, both growing SEI and generated gases reduce the electrolyte volume fraction.

Although the modeling approaches presented have been applied to study long-term effects of gas evolution, they are also relevant to simulate gas evolution and its effects during formation. As discussed in this review, gas evolution is critical for fast formation processes. Therefore, the amount of gas produced and its transport through the cell during formation must be considered for the model-based design of formation protocols and in particular for the degassing steps. This aspect is currently poorly addressed in the literature.

Summary and discussion

In the following main insights into the influencing factors, the most relevant experimental and theoretical methods are

summarised and discussed. In addition, conclusions are drawn and a perspective on future directions is given.

Summary

This review systematically examines the main factors influencing the formation process. The electrochemical conditions, *i.e.* current and voltage, during the formation cycling and the electrolyte have been widely studied and have a significant influence. However, this review shows other important factors, such as the pressure, temperature, and degassing, as well as material and cell design aspects, are less frequently addressed, although they undoubtably influence the formation processes. By systematically reviewing the literature on these various aspects, it has become clear that the formation process is not independent of the material and the cell design, but that both aspects must be precisely coordinated. The main challenges posed by next-generation materials are related to the significant volume expansion, which requires a better understanding of the mechanical properties of the interphase layer and the influence of external and internal pressure. In addition, as the voltage window expands especially towards high-voltage positive electrodes, the formation process must consider both electrodes simultaneously, while development of new electrolytes additives are shown to be a promising approach to tune both electrodes independently.

Experimental methods suitable for studying the formation process are also reviewed. It is shown that a combination of non-destructive and destructive characterisation techniques can provide valuable insights into the formation process and quality parameters of battery cells. A combination of methods is required to deduce details on the interphase layer properties as a function of the structure and composition. Several techniques are presented and discussed, which can be used as a guide for a detailed study of relevant phenomena of interest.

Computer-aided engineering techniques have become essential for understanding and optimising the formation process. However, few of the available tools are systematically used to support process development. It is shown that the multitude of influential parameters affecting the process on different time and length scales is a key challenge. Different modelling techniques are reviewed that allow the representation of relevant formation process phenomena.

Discussion

Given the recognised importance of formation and its potential correlation with lifetime, safety and cost, systematic variation of formation protocols remains surprisingly scarce.

It was shown that single cycle formation protocols are a promising way to achieve faster formation procedures. However, a key challenge with single cycle protocols is that Li plating must be avoided, and formation may not be complete.

A common definition of when formation is complete is needed for systematic comparison and improvement. Otherwise, no comparison of formation time is possible. This, combined with the lack of systematic variation, limits our current understanding of these formation protocols. Based on our analysis of non-destructive characterisation techniques, we propose to use the CE and CR to evaluate the progression of the formation process. These values can be used to convolute the CEI and SEI contributions. Possibly the change in CE in two consecutive cycles can be used for a general material independent definition of the end of formation. However, measurement accuracy and measurement artefacts caused by electrode overhang in large cell formats are major challenges for this assessment. Therefore, the use of CE and CR alone may not be sufficient and must be accompanied by other methods such as EIS and self-discharge testing.

There is a well-established toolbox of experimental methods that can be used to characterize the influence of the formation process in detail. In this context, surface analysis techniques play a key role. It has been shown that a combination of different techniques is required to gain a comprehensive understanding of the interphase layers. The goal must be to select a comprehensive set of methods that can reveal composition, molecular structure, thickness, ion transport, and passivation capabilities. For example, without a comprehensive set of methods, it is not possible to deduce the difference between improved ionic conductivity and a thinner film.

Due to the large parameter space and time-intensive characterisation, computational approaches are promising to reveal multi-scale and multi-physical correlations or to pre-select promising material candidates, *e.g.* electrolyte additives. Although simulation studies have already contributed valuable insights to the current understanding of the formation process, it is striking that key influencing factors, such as pressure or gas evolution, are hardly investigated in theoretical work. While simulations have explored the factors influencing battery ageing, their application to the formation process is still limited. Similarly, gas evolution and transport at the electrode and cell level have not been extensively studied in theoretical work. However, gas distribution might be limiting factor for fast formation protocols and should therefore be investigated in more detail. Control of the gaseous species may even prove to be an active means of modifying the formation process, offering further potential for optimisation.

A major problem for knowledge-based optimisation of the formation process is that the relationships between process, structure, and performance are not fully understood yet, despite the progress in understanding key physical aspects and the effects of SEI species on cell performance. To adress this, further knowledge regarding the relationship between electrolyte components is essential, as also emphasised in other articles regarding ageing[89] and fast-charging.[501,502] To be able to actively form desired passivation layer, also systemtically acquiring more insights on the involved reactions and initial dynamic structural evolution is important.

A methodical comparison of theoretical and experimental work is required. This requires a temporal recording of different physical properties and ideally a quantitative comparison with simulation results. Tracking and comparing the temporal evolution of gaseous by-products could be a simple yet powerful method to parameterise and validate mathematical models.

Validation of the temporally and spatially resolved evolution of SEI structure and morphology appears more complex. However, EC-AFM, if possible, in combination with XPS images at selected time points, can provide useful and detailed information on the temporal evolution of the SEI, but is time consuming.

An improved multi-physical understanding also holds potential for model-based *operando* analysis of formation data for cell quality assessment. It has been shown that formation data can already be used for quality assessment and parameterisation of interphase growth models. Such approaches could even be considered as an integral part of the EOL, potentially leading to a reduction in manufacturing time and cost.

The limitation of commonly used small sample sizes needs to be addressed, particularly given the significant uncertainties associated with the handmade battery electrodes often used in academia. Valid evaluations of reject rates in relation to the formation protocol are often not possible in academia due to limited sample sizes. Larger sample sizes are essential to investigate the effect of the influencing factors and their interdependencies, particularly to assess the impact on battery ageing. The use of cells produced in larger production lines and larger sample sizes is one way to overcome this problem.

There is little information from industry on formation processes. This is likely to lead to differences between academic and industrial perspectives on the formation process, creating a research gap and limiting the transferability of research results to real production lines. Industry expertise and insight is needed to bridge the gap between academic studies and practical implementation.

Additional process, *e.g.* prelithiation or surface medication, should be investigated in more detail in the context of cell formation as they offer a possibility to influence of formation prior to the formation processes without compromising material and cell format choices. Prelithiation of the negative electrodes can compensate for initial irreversible capacity losses.[503] This showed promising improvements in cell quality and performance and should be carefully investigated to better understand its effect, particularly in terms of improved SEI formation for electrodes with increased Si content.[249] This is also interesting in terms of gassing, as the SEI is partially built before the actual formation cycle.

Finally, it has been shown that many of the current challenges are even more important for next generation materials such as Li, Si or high-voltage positive electrode materials. These materials are often associated with significant implications for the formation process design. A knowledge-based understanding and a systematic use of computational methods can significantly reduce time and cost for the development of material-tailored formation processes which improve the cells' sustainability, durability, and safety.

Conclusion

In this review, the current understanding of the formation process is presented, and the most relevant influencing factors are summarised and examined in detail.

Interdependencies between the electrochemical conditions during formation and the materials selected, as well as the lack of a standardised evaluation of formation, often make it difficult to directly compare existing studies, which sometimes prevents general conclusions from being drawn. Therefore, it is highlighted that a key challenge for a knowledge-based design

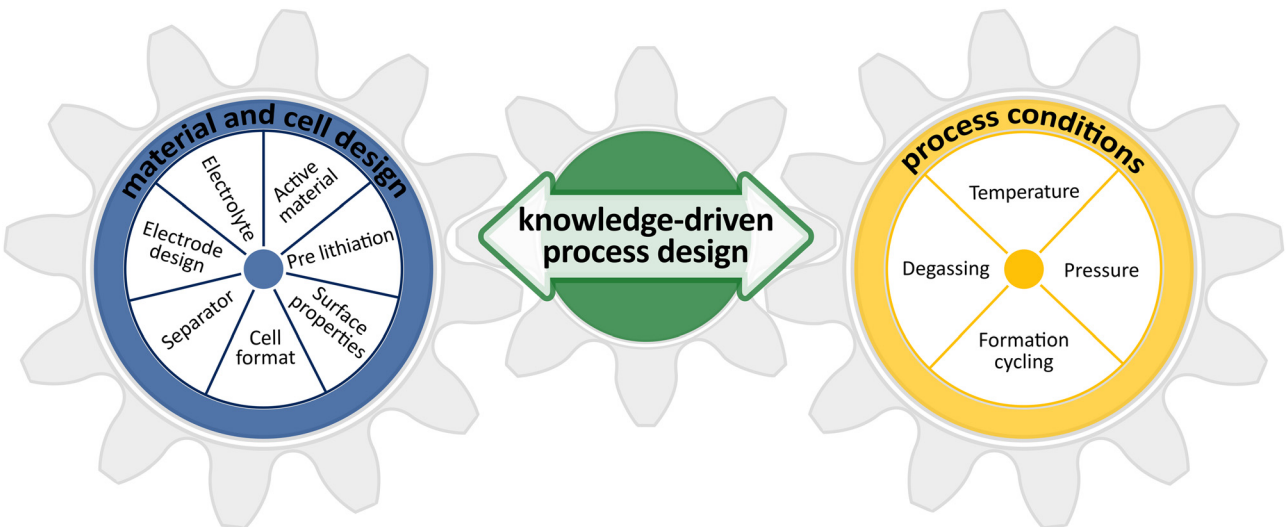

Fig. 30 Schematic summary of the factors influencing the forming process and their interaction. The influencing factors include the material and cell design, *i.e.* the electrolyte, the active material, a potential prelithiation, surface properties, the cell format, the separator and the electrode design, as well as process conditions, *i.e.* the temperature, the pressing pressure, forming cyclisation and degassing. The material and cell design aspects result from the previous design and production steps. The process parameters must be designed and optimised according to these aspects. Findings from the forming process must also be fed back to the material and cell design to exploit further optimisation potential. Mutual alignment, configuration and optimisation is therefore necessary to realise a holistic, knowledge-based process design of the formation process.

of the formation process lies in an interlocking of material and cell design on the one hand and the process design on the other hand. This is also illustrated in Fig. 30. The discussed experimental and theoretical methods must be applied systematically to reveal the mechanisms and then utilize the knowledge by computational process engineering.

Most important future perspectives are summarised below:

•There is no agreed criterion for when the formation process is complete. Therefore, a chemistry independent criterion for the end of formation is needed.

•Gas evolution during formation is high and affects the overall process dynamics. In some cases, degassing even plays a rate-limiting role. Degassing must therefore be considered as an active part of the formation process.

•The effect of passive materials, *i.e.* separator design, and cell formats, *i.e.* pouch or cylindrical cells, also influence the formation process and need to be investigated.

•A better understanding of the relationship between the SEI/CEI structure and the performance metrics is required.

•Different computational methods are available at different scales, covering the most relevant aspects of formation. They should be systematically combined to optimise the process.

•Systematic and standardised characterisation of battery cells after formation with sufficient sample quality and size is essential to allow meaningful comparison of different formation strategies and data-driven analysis.

•Next generation materials often increase the significance of the formation process. Thus, formation must be studied more extensively for these materials.

Reflecting on the current state and future directions of the formation process, further advances are needed at both the materials science and process engineering levels to tailor optimal formation processes to specific chemistries, cell formats and applications. More systematic research is needed to identify key relationships between the formation process and performance metrics, and to pave the way for novel, affordable, high quality, safe and sustainable cell generation with knowledge-driven formation process design.

Author contributions

Felix Schomburg: conceptualization, investigation, project administration, visualization, writing – original draft, writing – review & editing; Bastian Heidrich: conceptualization, investigation, writing – original draft, writing – review & editing; Sarah Wennemar: conceptualization, investigation, writing – original draft, Writing – review & editing; Robin Drees: conceptualization investigation, writing – original draft, writing – review & editing; Thomas Roth: conceptualization, investigation, writing – original draft, writing – review & editing; Michael Kurrat: funding acquisition, supervision; Heiner Heimes: funding acquisition, supervision; Andreas Jossen: funding acquisition, supervision, writing – review & editing; Martin Winter: funding acquisition, supervision, writing – review & editing; Jun Young Cheong: conceptualization, investigation, supervision, writing – original draft, writing – review & editing; Fridolin Röder: conceptualization, funding acquisition, investigation, project administration, supervision, writing – original draft, writing – review & editing.

Conflicts of interest

There are no conflicts to declare.

Acknowledgements

This work was supported by the project ''FormEL'' (03XP0296E) as part of the competence cluster ''ProZell'' by the Federal Ministry of Education and Research in Germany (BMBF). This work was also supported by the Deutsche Forschungsgemeinschaft (DFG, project number: 533115776). Only the authors are responsible for the content of this article.

References

1 G. E. Blomgren, *J. Electrochem. Soc.*, 2017, **164**, A5019–A5025.
2 A. K. Stephan, *Joule*, 2019, **3**, 2583–2584.
3 P. V. Kamat, *ACS Energy Lett.*, 2019, **4**, 2757–2759.
4 F. Duffner, N. Kronemeyer, J. Tübke, J. Leker, M. Winter and R. Schmuch, *Nat. Energy*, 2021, **6**, 123–134.
5 S. Zhang, S. Li and Y. Lu, *eScience*, 2021, **1**, 163–177.
6 J. T. Frith, M. J. Lacey and U. Ulissi, *Nat. Commun.*, 2023, **14**, 420.
7 H. Wan, J. Xu and C. Wang, *Nat. Rev. Chem.*, 2024, **8**, 30–44.
8 T. Kim, W. Song, D.-Y. Son, L. K. Ono and Y. Qi, *J. Mater. Chem. A*, 2019, **7**, 2942–2964.
9 M.-T. F. Rodrigues, G. Babu, H. Gullapalli, K. Kalaga, F. N. Sayed, K. Kato, J. Joyner and P. M. Ajayan, *Nat. Energy*, 2017, **2**.
10 J. Xiao, F. Shi, T. Glossmann, C. Burnett and Z. Liu, *Nat. Energy*, 2023, **8**, 329–339.
11 J. Amici, P. Asinari, E. Ayerbe, P. Barboux, P. Bayle-Guillemaud, R. J. Behm, M. Berecibar, E. Berg, A. Bhowmik, S. Bodoardo, I. E. Castelli, I. Cekic-Laskovic, R. Christensen, S. Clark, R. Diehm, R. Dominko, M. Fichtner, A. A. Franco, A. Grimaud, N. Guillet, M. Hahlin, S. Hartmann, V. Heiries, K. Hermansson, A. Heuer, S. Jana, L. Jabbour, J. Kallo, A. Latz, H. Lorrmann, O. M. Løvvik, S. Lyonnard, M. Meeus, E. Paillard, S. Perraud, T. Placke, C. Punckt, O. Raccurt, J. Ruhland, E. Sheridan, H. Stein, J.-M. Tarascon, V. Trapp, T. Vegge, M. Weil, W. Wenzel, M. Winter, A. Wolf and K. Edström, *Adv. Energy Mater.*, 2022, 2102785.
12 Y. Liu, R. Zhang, J. Wang and Y. Wang, *iScience*, 2021, **24**, 102332.
13 A. Kwade, W. Haselrieder, R. Leithoff, A. Modlinger, F. Dietrich and K. Droeder, *Nat Energy*, 2018, **3**, 290–300.
14 D. L. Wood, J. Li and C. Daniel, *J. Electrochem. Soc.*, 2015, **275**, 234–242.
15 M. Schönemann, *Multiscale Simulation Approach for Battery Production Systems*, Springer International Publishing, Cham, 1st edn, 2017.

16 F. Degen, M. Winter, D. Bendig and J. Tübke, *Nat. Energy*, 2023, **8**, 1284–1295.
17 D. L. Wood, J. Li and S. J. An, *Joule*, 2019, **3**, 2884–2888.
18 *Lithium-Ion Batteries: Basics and Applications*, ed. R. Korthauer, Springer Berlin Heidelberg, Berlin, Heidelberg, 2018.
19 R. Gogoana, M. B. Pinson, M. Z. Bazant and S. E. Sarma, *J. Electrochem. Soc.*, 2014, **252**, 8–13.
20 S. Davidsson Kurland, *Environ. Res. Commun.*, 2020, **2**, 12001.
21 M. Erakca, M. Baumann, W. Bauer, L. de Biasi, J. Hofmann, B. Bold and M. Weil, *iScience*, 2021, **24**, 102437.
22 O. Schmidt, M. Thomitzek, F. Röder, S. Thiede, C. Herrmann and U. Krewer, *J. Electrochem. Soc.*, 2020, **167**, 60501.
23 M. Thomitzek, O. Schmidt, F. Röder, U. Krewer, C. Herrmann and S. Thiede, *Procedia CIRP*, 2018, **72**, 346–351.
24 S. J. An, J. Li, C. Daniel, H. M. Meyer, S. E. Trask, B. J. Polzin and D. L. Wood, *ACS Appl. Mater. Interfaces*, 2017, **9**, 18799–18808.
25 S. J. An, J. Li, D. Mohanty, C. Daniel, B. J. Polzin, J. R. Croy, S. E. Trask and D. L. Wood, *J. Electrochem. Soc.*, 2017, **164**, A1195–A1202.
26 B. R. Long, S. G. Rinaldo, K. G. Gallagher, D. W. Dees, S. E. Trask, B. J. Polzin, A. N. Jansen, D. P. Abraham, I. Bloom, J. Bareño and J. R. Croy, *J. Electrochem. Soc.*, 2016, **163**, A2999–A3009.
27 J. Hagemeister, S. Stock, M. Linke, M. Fischer, R. Drees, M. Kurrat and R. Daub, *Energy Technol.*, 2022, **11**, 2200686.
28 E. Peled, *J. Electrochem. Soc.*, 1979, **126**, 2047–2051.
29 D. R. Gallus, R. Wagner, S. Wiemers-Meyer, M. Winter and I. Cekic-Laskovic, *Electrochim. Acta*, 2015, **184**, 410–416.
30 X. Fan, X. Ou, W. Zhao, Y. Liu, B. Zhang, J. Zhang, L. Zou, L. Seidl, Y. Li, G. Hu, C. Battaglia and Y. Yang, *Nat. Commun.*, 2021, **12**, 5320.
31 F. Friedrich, A. Kunz, A. Jossen and H. A. Gasteiger, *J. Electrochem. Soc.*, 2023, **170**, 50506.
32 F. Lin, I. M. Markus, D. Nordlund, T.-C. Weng, M. D. Asta, H. L. Xin and M. M. Doeff, *Nat. Commun.*, 2014, **5**, 3529.
33 N. D. Rago, J. K. Basco, A. Vu, J. Li, K. Hays, Y. Sheng, D. L. Wood and I. Bloom, *J. Power Sources*, 2019, **435**, 126548.
34 L. Guo, D. B. Thornton, M. A. Koronfel, I. E. L. Stephens and M. P. Ryan, *J. Phys. Energy*, 2021, **3**, 32015.
35 J. W. Braithwaite, A. Gonzales, G. Nagasubramanian, S. J. Lucero, D. E. Peebles, J. A. Ohlhausen and W. R. Cieslak, *J. Electrochem. Soc.*, 1999, **146**, 448–456.
36 S. Dai, J. Chen, Y. Ren, Z. Liu, J. Chen, C. Li, X. Zhang, X. Zhang and T. Zeng, *Int. J. Electrochem. Sci.*, 2017, **12**, 10589–10598.
37 F. German, A. Hintennach, A. LaCroix, D. Thiemig, S. Ostwald, F. Scheiba, M. J. Hoffmann and H. Ehrenberg, *J. Power Sources*, 2014, **264**, 100–107.
38 B. Garcia and M. Armand, *J. Electrochem. Soc.*, 2004, **132**, 206–208.
39 W. K. Behl and E. J. Plichta, *J. Electrochem. Soc.*, 1998, **72**, 132–135.
40 S. Zhang and T. Jow, *J. Electrochem. Soc.*, 2002, **109**, 458–464.
41 J. B. Goodenough and Y. Kim, *Chem. Mater.*, 2010, **22**, 587–603.
42 B. Horstmann, F. Single and A. Latz, *Curr. Opin. Electrochem.*, 2019, **13**, 61–69.
43 M. Winter, *Z. Phys. Chem.*, 2009, **223**, 1395–1406.
44 X.-G. Yang and C.-Y. Wang, *J. Electrochem. Soc.*, 2018, **402**, 489–498.
45 S. J. An, J. Li, C. Daniel, D. Mohanty, S. Nagpure and D. L. Wood, *Carbon*, 2016, **105**, 52–76.
46 H. Adenusi, G. A. Chass, S. Passerini, K. V. Tian and G. Chen, *Adv. Energy Mater.*, 2023, **13**, 2203307.
47 Q. Liu, W. Jiang, J. Xu, Y. Xu, Z. Yang, D.-J. Yoo, K. Z. Pupek, C. Wang, C. Liu, K. Xu and Z. Zhang, *Nat. Commun.*, 2023, **14**, 3678.
48 K. Kanamura, H. Tamura, S. Shiraishi and Z. Takehara, *J. Electrochem. Soc.*, 1995, **142**, 340–347.
49 K. Edström, M. Herstedt and D. P. Abraham, *J. Power Sources*, 2006, **153**, 380–384.
50 A. M. Andersson and K. Edström, *J. Electrochem. Soc.*, 2001, **148**, A1100.
51 M. Nie, D. Chalasani, D. P. Abraham, Y. Chen, A. Bose and B. L. Lucht, *J. Phys. Chem. C*, 2013, **117**, 1257–1267.
52 T. Liu, L. Lin, X. Bi, L. Tian, K. Yang, J. Liu, M. Li, Z. Chen, J. Lu, K. Amine, K. Xu and F. Pan, *Nat. Nanotechnol.*, 2019, **14**, 50–56.
53 G. Feng, H. Jia, Y. Shi, X. Yang, Y. Liang, M. H. Engelhard, Y. Zhang, C. Yang, K. Xu, Y. Yao, W. Xu and X. Shan, *Nat. Nanotechnol.*, 2023, **18**, 780–789.
54 M. N. Richard and J. R. Dahn, *J. Electrochem. Soc.*, 1999, **146**, 2068–2077.
55 S. Malmgren, K. Ciosek, M. Hahlin, T. Gustafsson, M. Gorgoi, H. Rensmo and K. Edström, *Electrochim. Acta*, 2013, **97**, 23–32.
56 G. V. Zhuang and P. N. Ross, *Electrochem. Solid-State Lett.*, 2003, **6**, A136.
57 A. Andersson, A. Henningson, H. Siegbahn, U. Jansson and K. Edström, *J. Electrochem. Soc.*, 2003, **119–121**, 522–527.
58 H. Yoshida, T. Fukunaga, T. Hazama, M. Terasaki, M. Mizutani and M. Yamachi, *J. Electrochem. Soc.*, 1997, **68**, 311–315.
59 D. Aurbach, B. Markovsky, A. Shechter, Y. Ein-Eli and H. Cohen, *J. Electrochem. Soc.*, 1996, **143**, 3809–3820.
60 A. Tornheim, S. E. Trask and Z. Zhang, *J. Electrochem. Soc.*, 2016, **163**, A1717–A1722.
61 A. J. Smith, J. C. Burns, D. Xiong and J. R. Dahn, *J. Electrochem. Soc.*, 2011, **158**, A1136–A1142.
62 E. M. Erickson, F. Schipper, T. R. Penki, J.-Y. Shin, C. Erk, F.-F. Chesneau, B. Markovsky and D. Aurbach, *J. Electrochem. Soc.*, 2017, **164**, A6341–A6348.
63 B. Heidrich, L. Pritzlaff, M. Börner, M. Winter and P. Niehoff, *J. Electrochem. Soc.*, 2022, **169**, 30533.
64 M. Ue, in *Lithium-Ion Batteries*, ed. M. Yoshio, R. J. Brodd and A. Kozawa, Springer New York, New York, NY, 2009, pp. 1–41.
65 K. Edström, T. Gustafsson and J. O. Thomas, *Electrochim. Acta*, 2004, **50**, 397–403.

66 R. Dedryvère, D. Foix, S. Franger, S. Patoux, L. Daniel and D. Gonbeau, *J. Phys. Chem. C*, 2010, **114**, 10999–11008.
67 H. Duncan, D. Duguay, Y. Abu-Lebdeh and I. J. Davidson, *J. Electrochem. Soc.*, 2011, **158**, A537–A545.
68 D. Ostrovskii, F. Ronci, B. Scrosati and P. Jacobsson, *J. Electrochem. Soc.*, 2001, **94**, 183–188.
69 N. Dupré, J.-F. Martin, J. Oliveri, P. Soudan, D. Guyomard, A. Yamada and R. Kanno, *J. Electrochem. Soc.*, 2009, **156**, C180.
70 D. Li, H. Li, D. Danilov, L. Gao, J. Zhou, R.-A. Eichel, Y. Yang and P. H. Notten, *J. Electrochem. Soc.*, 2018, **396**, 444–452.
71 N. Liu, H. Li, Z. Wang, X. Huang and L. Chen, *Electrochem. Solid-State Lett.*, 2006, **9**, A328.
72 M. Metzger, B. Strehle, S. Solchenbach and H. A. Gasteiger, *J. Electrochem. Soc.*, 2016, **163**, A798–A809.
73 R. Jung, M. Metzger, F. Maglia, C. Stinner and H. A. Gasteiger, *J. Electrochem. Soc.*, 2017, **164**, A1361–A1377.
74 D. J. Xiong, T. Hynes, L. D. Ellis and J. R. Dahn, *J. Electrochem. Soc.*, 2017, **164**, A3174–A3181.
75 J. Y. Cheong, J. H. Chang, S.-H. Cho, J.-W. Jung, C. Kim, K. S. Dae, J. M. Yuk and I.-D. Kim, *Electrochim. Acta*, 2019, **295**, 7–13.
76 S. Schweidler, M. Bianchini, P. Hartmann, T. Brezesinski and J. Janek, *Batteries Supercaps*, 2020, **3**, 1021–1027.
77 R. Ruess, S. Schweidler, H. Hemmelmann, G. Conforto, A. Bielefeld, D. A. Weber, J. Sann, M. T. Elm and J. Janek, *J. Electrochem. Soc.*, 2020, **167**, 100532.
78 P.-C. Tsai, B. Wen, M. Wolfman, M.-J. Choe, M. S. Pan, L. Su, K. Thornton, J. Cabana and Y.-M. Chiang, *Energy Environ. Sci.*, 2018, **11**, 860–871.
79 S. Kalnaus, K. Rhodes and C. Daniel, *J. Electrochem. Soc.*, 2011, **196**, 8116–8124.
80 X. H. Liu and J. Y. Huang, *Energy Environ. Sci.*, 2011, **4**, 3844.
81 X. H. Liu, L. Zhong, S. Huang, S. X. Mao, T. Zhu and J. Y. Huang, *ACS nano*, 2012, **6**, 1522–1531.
82 B. Han, Y. Zou, G. Xu, S. Hu, Y. Kang, Y. Qian, J. Wu, X. Ma, J. Yao, T. Li, Z. Zhang, H. Meng, H. Wang, Y. Deng, J. Li and M. Gu, *Energy Environ. Sci.*, 2021, **14**, 4882–4889.
83 J. Asenbauer, T. Eisenmann, M. Kuenzel, A. Kazzazi, Z. Chen and D. Bresser, *Sustainable Energy Fuels*, 2020, **4**, 5387–5416.
84 M. E. Spahr, T. Palladino, H. Wilhelm, A. Würsig, D. Goers, H. Buqa, M. Holzapfel and P. Novák, *J. Electrochem. Soc.*, 2004, **151**, A1383.
85 G. Assat, S. L. Glazier, C. Delacourt and J.-M. Tarascon, *Nat Energy*, 2019, **4**, 647–656.
86 D. J. Arnot, E. Allcorn and K. L. Harrison, *J. Electrochem. Soc.*, 2021, **168**, 110509.
87 J. R. Croy, K. G. Gallagher, M. Balasubramanian, Z. Chen, Y. Ren, D. Kim, S.-H. Kang, D. W. Dees and M. M. Thackeray, *J. Phys. Chem. C*, 2013, **117**, 6525–6536.
88 P. Verma, P. Maire and P. Novák, *Electrochim. Acta*, 2010, **55**, 6332–6341.
89 S. K. Heiskanen, J. Kim and B. L. Lucht, *Joule*, 2019, **3**, 2322–2333.
90 K. Zaghib, G. Nadeau and K. Kinoshita, *J. Electrochem. Soc.*, 2000, **147**, 2110.
91 J. A. Gilbert, I. A. Shkrob and D. P. Abraham, *J. Electrochem. Soc.*, 2017, **164**, A389–A399.
92 A. J. Smith and J. R. Dahn, *J. Electrochem. Soc.*, 2012, **159**, A290–A293.
93 P. Lu, C. Li, E. W. Schneider and S. J. Harris, *J. Phys. Chem. C*, 2014, **118**, 896–903.
94 S. S. Zhang, K. Xu and T. R. Jow, *Electrochim. Acta*, 2006, **51**, 1636–1640.
95 M. Steinhauer, S. Risse, N. Wagner and K. A. Friedrich, *Electrochim. Acta*, 2017, **228**, 652–658.
96 S. Solchenbach, X. Huang, D. Pritzl, J. Landesfeind and H. A. Gasteiger, *J. Electrochem. Soc.*, 2021, **168**, 110503.
97 R. Xu, Y. Yang, F. Yin, P. Liu, P. Cloetens, Y. Liu, F. Lin and K. Zhao, *J. Mech. Phys. Solids*, 2019, **129**, 160–183.
98 R. Xu, L. Scalco de Vasconcelos and K. Zhao, *J. Mater. Res.*, 2016, **31**, 2715–2727.
99 J. S. Edge, S. O'Kane, R. Prosser, N. D. Kirkaldy, A. N. Patel, A. Hales, A. Ghosh, W. Ai, J. Chen, J. Yang, S. Li, M.-C. Pang, L. Bravo Diaz, A. Tomaszewska, M. W. Marzook, K. N. Radhakrishnan, H. Wang, Y. Patel, B. Wu and G. J. Offer, *Phys. Chem. Chem. Phys.*, 2021, **23**, 8200–8221.
100 R. Stockhausen, A. Hofmann, L. Gehrlein, T. Bergfeldt, M. Müller, H. Ehrenberg and A. Smith, *J. Electrochem. Soc.*, 2021, **168**, 80504.
101 R. Stockhausen, L. Gehrlein, M. Müller, T. Bergfeldt, A. Hofmann, F. J. Müller, J. Maibach, H. Ehrenberg and A. Smith, *J. Power Sources*, 2022, **543**, 231842.
102 J. Landesfeind and H. A. Gasteiger, *J. Electrochem. Soc.*, 2019, **166**, A3079–A3097.
103 S. Uchida and T. Kiyobayashi, *Phys. Chem. Chem. Phys.*, 2021, **23**, 10875–10887.
104 A. Weng, P. Mohtat, P. M. Attia, V. Sulzer, S. Lee, G. Less and A. Stefanopoulou, *Joule*, 2021, **5**, 2971–2992.
105 C. Mao, S. J. An, H. M. Meyer, J. Li, M. Wood, R. E. Ruther and D. L. Wood, *J. Power Sources*, 2018, **402**, 107–115.
106 C. Huang, K. Huang, H. Wang, S. Liu and Y. Zeng, *J. Solid State Electrochem.*, 2011, **15**, 1987–1995.
107 S. Kranz, T. Kranz, T. Graubner, Y. Yusim, L. Hellweg and B. Roling, *Batteries Supercaps*, 2019, **2**, 1026–1036.
108 T. Jaumann, J. Balach, U. Langklotz, V. Sauchuk, M. Fritsch, A. Michaelis, V. Teltevskij, D. Mikhailova, S. Ostwald, M. Klose, G. Stephani, R. Hauser, J. Eckert and L. Giebeler, *Energy Storage Mater.*, 2017, **6**, 26–35.
109 N. Ogihara, Y. Igarashi, A. Kamakura, K. Naoi, Y. Kusachi and K. Utsugi, *Electrochim. Acta*, 2006, **52**, 1713–1720.
110 T. R. Jow, S. A. Delp, J. L. Allen, J.-P. Jones and M. C. Smart, *J. Electrochem. Soc.*, 2018, **165**, A361–A367.
111 S. Tu, B. Zhang, Y. Zhang, Z. Chen, X. Wang, R. Zhan, Y. Ou, W. Wang, X. Liu, X. Duan, L. Wang and Y. Sun, *Nat Energy*, 2023, **8**, 1365–1374.
112 J. Wen, Y. Yu and C. Chen, *Mat Express*, 2012, **2**, 197–212.
113 Q. Wang, P. Ping, X. Zhao, G. Chu, J. Sun and C. Chen, *J. Electrochem. Soc.*, 2012, **208**, 210–224.

114 P. G. Balakrishnan, R. Ramesh and T. Prem Kumar, *J. Electrochem. Soc.*, 2006, **155**, 401–414.
115 G. Park, H. Nakamura, Y. Lee and M. Yoshio, *J. Electrochem. Soc.*, 2009, **189**, 602–606.
116 Z. Zhang, D. Fouchard and J. R. Rea, *J. Electrochem. Soc.*, 1998, **70**, 16–20.
117 I. A. Profatilova, C. Stock, A. Schmitz, S. Passerini and M. Winter, *J. Electrochem. Soc.*, 2013, **222**, 140–149.
118 F. Baakes, D. Witt and U. Krewer, *Chem. Sci.*, 2023, **14**, 13783–13798.
119 A. Kampker, H. Heimes, C. Offermanns, S. Wennemar, T. Robben and N. Lackner, *WEVJ*, 2023, **14**, 96.
120 A Review of Process Innovations in the Cell Finishing of Lithium-Ion Batteries in Large-Scale Production, 2023.
121 A. Davoodabadi, J. Li, H. Zhou, D. L. Wood, T. J. Singler and C. Jin, *J. Energy Storage*, 2019, **26**, 101034.
122 J. Schnell, C. Nentwich, F. Endres, A. Kollenda, F. Distel, T. Knoche and G. Reinhart, *J. Power Sources*, 2019, **413**, 360–366.
123 A. Kampker, in *Elektromobilproduktion*, ed. A. Kampker, Springer Berlin Heidelberg, Berlin, Heidelberg, 2014, pp. 43–113.
124 K.-H. Pettinger, A. Kampker, C.-R. Hohenthanner, C. Deutskens, H. Heimes and A. Vom Hemdt, in *Lithium-Ion Batteries: Basics and Applications*, ed. R. Korthauer, Springer Berlin Heidelberg, Berlin, Heidelberg, 2018, pp. 211–226.
125 T. Aregay, Torque News, 2020 - 6:45am, **https://www.torquenews.com/11826/tesla-achieves-battery-breakthrough-here-are-manufacturing-advancements-made-it-possible**.
126 V. Müller, R. Kaiser, S. Poller, D. Sauerteig, R. Schwarz, M. Wenger, V. R. Lorentz and M. März, *J. Energy Storage*, 2017, **14**, 56–61.
127 S. Leroy, F. Blanchard, R. Dedryvère, H. Martinez, B. Carré, D. Lemordant and D. Gonbeau, *Surf. Interface Anal.*, 2005, **37**, 773–781.
128 P. Jankowski, W. Wieczorek and P. Johansson, *J. Mol. Model.*, 2017, **23**, 6.
129 B. Zhang, M. Metzger, S. Solchenbach, M. Payne, S. Meini, H. A. Gasteiger, A. Garsuch and B. L. Lucht, *J. Phys. Chem. C*, 2015, **119**, 11337–11348.
130 N. Legrand, B. Knosp, P. Desprez, F. Lapicque and S. Raël, *J. Electrochem. Soc.*, 2014, **245**, 208–216.
131 P. Wang de Yan, C. Wang, H. Ding, H. Dong, J. Wang, S. Wu, X. Cui, C. Li, D. Zhao and S. Li, *Appl. Surf. Sci.*, 2022, **596**, 153572.
132 P. Münster, M. Diehl, J. E. Frerichs, M. Börner, M. R. Hansen, M. Winter and P. Niehoff, *J. Power Sources*, 2021, **484**, 229306.
133 P. Münster, M. Winter and P. Niehoff, *J. Electrochem. Soc.*, 2022, **169**, 70525.
134 R. Nölle, K. Beltrop, F. Holtstiege, J. Kasnatscheew, T. Placke and M. Winter, *Mater. Today*, 2020, **32**, 131–146.
135 R. Drees, Model-based Design and Evaluation of Fast-Charging Strategies for Lithium-Ion Battery Formation and Cyclization, Technische Universität Braunschweig, Braunschweig, 2023.
136 S. Zhang, M. S. Ding, K. Xu, J. Allen and T. R. Jow, *Electrochem. Solid-State Lett.*, 2001, **4**, A206.
137 P. M. Attia, S. J. Harris and W. C. Chueh, *J. Electrochem. Soc.*, 2021, **168**, 50543.
138 B. K. Antonopoulos, C. Stock, F. Maglia and H. E. Hoster, *Electrochim. Acta*, 2018, **269**, 331–339.
139 H.-H. Lee, Y.-Y. Wang, C.-C. Wan, M.-H. Yang, H.-C. Wu and D.-T. Shieh, *J. Power Sources*, 2004, **134**, 118–123.
140 B. K. Antonopoulos, F. Maglia, F. Schmidt-Stein, J. P. Schmidt and H. E. Hoster, *Batteries Supercaps*, 2018, **1**, 110–121.
141 K. Xu, *Chem. Rev.*, 2014, **114**, 11503–11618.
142 O. Borodin, *Curr. Opin. Electrochem.*, 2019, **13**, 86–93.
143 L. Mickelson, H. Castro, E. Switzer and C. Friesen, *J. Electrochem. Soc.*, 2014, **161**, A2121–A2127.
144 S. Schweidler, L. de Biasi, A. Schiele, P. Hartmann, T. Brezesinski and J. Janek, *J. Phys. Chem. C*, 2018, **122**, 8829–8835.
145 E. Peled and S. Menkin, *J. Electrochem. Soc.*, 2017, **164**, A1703–A1719.
146 V. Sharova, Enhancing the performance of lithium batteries through the development of improved electrolyte formulation, formation protocol and graphite surface modification, Karlsruher Instituts für Technologie, 2018.
147 T. S. Pathan, M. Rashid, M. Walker, W. D. Widanage and E. Kendrick, *J. Phys. Energy*, 2019, **1**, 44003.
148 S. J. An, J. Li, Z. Du, C. Daniel and D. L. Wood, *J. Power Sources*, 2017, **342**, 846–852.
149 R. Drees, F. Lienesch and M. Kurrat, *Energy Technol.*, 2022, 2200868.
150 S.-H. Lee, *Appl. Surf. Sci.*, 2014, **322**, 64–70.
151 T. Phraewphiphat, A. Promwicha, P. Tammawat, P. Limthongkul, P. Chirawatkul and W. Kobsiriphat, *Solid State Ionics*, 2021, **370**, 115749.
152 Z. Zhang, J. Yang, W. Huang, H. Wang, W. Zhou, Y. Li, Y. Li, J. Xu, W. Huang, W. Chiu and Y. Cui, *Matter*, 2021, **4**, 302–312.
153 R. Drees, F. Lienesch and M. Kurrat, *J. Energy Storage*, 2021, **36**, 102345.
154 P.-C. J. Chiang, M.-S. Wu and J.-C. Lin, *Electrochem. Solid-State Lett.*, 2005, **8**, A423.
155 S. S. Zhang, K. Xu and T. R. Jow, *J. Electrochem. Soc.*, 2004, **130**, 281–285.
156 A. Moretti, V. Sharova, D. V. Carvalho, A. Boulineau, W. Porcher, I. de Meatza and S. Passerini, *Batteries Supercaps*, 2019, **2**, 240–247.
157 M. J. Lain, J. Brandon and E. Kendrick, *Batteries*, 2019, **5**, 64.
158 Z. Mao, M. Farkhondeh, M. Pritzker, M. Fowler and Z. Chen, *J. Electrochem. Soc.*, 2017, **164**, A3469–A3483.
159 Y. Li, X. Liu, L. Wang, X. Feng, D. Ren, Y. Wu, G. Xu, L. Lu, J. Hou, W. Zhang, Y. Wang, W. Xu, Y. Ren, Z. Wang, J. Huang, X. Meng, X. Han, H. Wang, X. He, Z. Chen, K. Amine and M. Ouyang, *Nano Energy*, 2021, **85**, 105878.
160 B. Michalak, H. Sommer, D. Mannes, A. Kaestner, T. Brezesinski and J. Janek, *Sci. Rep.*, 2015, **5**, 15627.

161 K.-S. Yun, S. J. Pai, B. C. Yeo, K.-R. Lee, S.-J. Kim and S. S. Han, *J. Phys. Chem. Lett.*, 2017, **8**, 2812–2818.
162 E. W. C. Spotte-Smith, R. L. Kam, D. Barter, X. Xie, T. Hou, S. Dwaraknath, S. M. Blau and K. A. Persson, *ACS Energy Lett.*, 2022, **7**, 1446–1453.
163 K. Leung, *Chem. Phys. Lett.*, 2013, **568–569**, 1–8.
164 D. J. Xiong, L. D. Ellis, R. Petibon, T. Hynes, Q. Q. Liu and J. R. Dahn, *J. Electrochem. Soc.*, 2017, **164**, A340–A347.
165 L. D. Ellis, J. P. Allen, L. M. Thompson, J. E. Harlow, W. J. Stone, I. G. Hill and J. R. Dahn, *J. Electrochem. Soc.*, 2017, **164**, A3518–A3528.
166 M. Raghibi, B. Xiong, S. Phadke and M. Anouti, *Electrochim. Acta*, 2020, **362**, 137214.
167 M. R. Wagner, P. R. Raimann, A. Trifonova, K.-C. Moeller, J. O. Besenhard and M. Winter, *Electrochem. Solid-State Lett.*, 2004, **7**, A201.
168 K. H. Lee, E. H. Song, J. Y. Lee, B. H. Jung and H. S. Lim, *J. Electrochem. Soc.*, 2004, **132**, 201–205.
169 K. Leung, *J. Phys. Chem. C*, 2012, **116**, 9852–9861.
170 B. D. McCloskey, D. S. Bethune, R. M. Shelby, G. Girishkumar and A. C. Luntz, *J. Phys. Chem. Lett.*, 2011, **2**, 1161–1166.
171 S. Meini, N. Tsiouvaras, K. U. Schwenke, M. Piana, H. Beyer, L. Lange and H. A. Gasteiger, *Phys. Chem. Chem. Phys.*, 2013, **15**, 11478–11493.
172 J. Liu, P. Bian, J. Li, W. Ji, H. Hao and A. Yu, *J. Power Sources*, 2015, **286**, 380–387.
173 B. Strehle, S. Solchenbach, M. Metzger, K. U. Schwenke and H. A. Gasteiger, *J. Electrochem. Soc.*, 2017, **164**, A2513–A2526.
174 K. U. Schwenke, S. Solchenbach, J. Demeaux, B. L. Lucht and H. A. Gasteiger, *J. Electrochem. Soc.*, 2019, **166**, A2035–A2047.
175 J. Self, C. P. Aiken, R. Petibon and J. R. Dahn, *J. Electrochem. Soc.*, 2015, **162**, A796–A802.
176 X. Teng, C. Zhan, Y. Bai, L. Ma, Q. Liu, C. Wu, F. Wu, Y. Yang, J. Lu and K. Amine, *ACS Appl. Mater. Interfaces*, 2015, **7**, 22751–22755.
177 M. Holzapfel, A. Würsig, W. Scheifele, J. Vetter and P. Novák, *J. Electrochem. Soc.*, 2007, **174**, 1156–1160.
178 R. Bernhard, M. Metzger and H. A. Gasteiger, *J. Electrochem. Soc.*, 2015, **162**, A1984–A1989.
179 R. Jung, P. Strobl, F. Maglia, C. Stinner and H. A. Gasteiger, *J. Electrochem. Soc.*, 2018, **165**, A2869–A2879.
180 D. J. Xiong, L. D. Ellis, K. J. Nelson, T. Hynes, R. Petibon and J. R. Dahn, *J. Electrochem. Soc.*, 2016, **163**, A3069–A3077.
181 D. B. Thornton, B. J. V. Davies, S. B. Scott, A. Aguadero, M. P. Ryan and I. E. L. Stephens, *Angew. Chem.*, 2024, **136**, e202315357.
182 C. Mao, R. E. Ruther, L. Geng, Z. Li, D. N. Leonard, H. M. Meyer, R. L. Sacci and D. L. Wood, *ACS Appl. Mater. Interfaces*, 2019, **11**, 43235–43243.
183 L. Bläubaum, P. Röse, L. Schmidt and U. Krewer, *ChemSusChem*, 2021, **14**, 2943–2951.
184 M. Leißing, F. Horsthemke, S. Wiemers-Meyer, M. Winter, P. Niehoff and S. Nowak, *Batteries Supercaps*, 2021, **4**, 1344–1350.
185 J. Henschel, C. Peschel, S. Klein, F. Horsthemke, M. Winter and S. Nowak, *Angew. Chem.*, 2020, **132**, 6184–6193.
186 L. Wen, Z. Wu, P. Zhao, J. Liang, H. Luo, G. Liu and F. Li, *J. Electrochem. Soc.*, 2019, **166**, A5033–A5037.
187 J. Cannarella and C. B. Arnold, *J. Power Sources*, 2014, **245**, 745–751.
188 H. H. Heimes, C. Offermanns, A. Mohsseni, H. Laufen, U. Westerhoff, L. Hoffmann, P. Niehoff, M. Kurrat, M. Winter and A. Kampker, *Energy Technol.*, 2020, **8**, 1900118.
189 S. Bhattacharya, A. R. Riahi and A. T. Alpas, *Carbon*, 2014, **67**, 592–606.
190 Y.-B. He, Z.-Y. Tang, Q.-S. Song, H. Xie, Y.-G. Liu and Q. Xu, *J. Electrochem. Soc.*, 2008, **155**, A481.
191 S.-B. Lee and S.-I. Pyun, *Carbon*, 2002, **40**, 2333–2339.
192 L. D. Ellis, J. P. Allen, I. G. Hill and J. R. Dahn, *J. Electrochem. Soc.*, 2018, **165**, A1529–A1536.
193 W. Li, B. Song and A. Manthiram, *Chem. Soc. Rev.*, 2017, **46**, 3006–3059.
194 M. Hu, X. Pang and Z. Zhou, *J. Electrochem. Soc.*, 2013, **237**, 229–242.
195 W. Xue, M. Huang, Y. Li, Y. G. Zhu, R. Gao, X. Xiao, W. Zhang, S. Li, G. Xu, Y. Yu, P. Li, J. Lopez, D. Yu, Y. Dong, W. Fan, Z. Shi, R. Xiong, C.-J. Sun, I. Hwang, W.-K. Lee, Y. Shao-Horn, J. A. Johnson and J. Li, *Nat Energy*, 2021, **6**, 495–505.
196 J. Zhang, H. Zhang, S. Weng, R. Li, D. Lu, T. Deng, S. Zhang, L. Lv, J. Qi, X. Xiao, L. Fan, S. Geng, F. Wang, L. Chen, M. Noked, X. Wang and X. Fan, *Nat. Commun.*, 2023, **14**, 2211.
197 M. Weiling, C. Lechtenfeld, F. Pfeiffer, L. Frankenstein, D. Diddens, J.-F. Wang, S. Nowak and M. Baghernejad, *Adv. Energy Mater.*, 2023, **14**, 2303568.
198 C. K. Chan, H. Peng, G. Liu, K. McIlwrath, X. F. Zhang, R. A. Huggins and Y. Cui, *Nat. Nanotechnol.*, 2008, **3**, 31–35.
199 H. Wu and Y. Cui, *Nano Today*, 2012, **7**, 414–429.
200 J. Shin, T.-H. Kim, Y. Lee and E. Cho, *Energy Storage Mater.*, 2020, **25**, 764–781.
201 F. Shi, Z. Song, P. N. Ross, G. A. Somorjai, R. O. Ritchie and K. Komvopoulos, *Nat. Commun.*, 2016, **7**, 11886.
202 G. Yang, S. Frisco, R. Tao, N. Philip, T. H. Bennett, C. Stetson, J.-G. Zhang, S.-D. Han, G. Teeter, S. P. Harvey, Y. Zhang, G. M. Veith and J. Nanda, *ACS Energy Lett.*, 2021, **6**, 1684–1693.
203 S. Ko, X. Han, T. Shimada, N. Takenaka, Y. Yamada and A. Yamada, *Nat. Sustainable*, 2023, **6**, 1705–1714.
204 F. An, H. Zhao, W. Zhou, Y. Ma and P. Li, *Sci. Rep.*, 2019, **9**, 14108.
205 S. Zhang, *npj Comput. Mater.*, 2017, **3**, 7.
206 D. Martín-Yerga, D. C. Milan, X. Xu, J. Fernández-Vidal, L. Whalley, A. J. Cowan, L. J. Hardwick and P. R. Unwin, *Angew. Chem., Int. ed.*, 2022, **61**, e202207184.
207 C. Stetson, M. Schnabel, Z. Li, S. P. Harvey, C.-S. Jiang, A. Norman, S. C. DeCaluwe, M. Al-Jassim and A. Burrell, *ACS Energy Lett.*, 2020, **5**, 3657–3662.
208 L. Zhang, Y. Qin, Y. Liu, Q. Liu, Y. Ren, A. N. Jansen and W. Lu, *J. Electrochem. Soc.*, 2018, **165**, A2102–A2107.

209 Z. Liu, Q. Yu, Y. Zhao, R. He, M. Xu, S. Feng, S. Li, L. Zhou and L. Mai, *Chem. Soc. Rev.*, 2019, **48**, 285–309.
210 H. Ghassemi, M. Au, N. Chen, P. A. Heiden and R. S. Yassar, *ACS Nano*, 2011, **5**, 7805–7811.
211 C.-M. Wang, X. Li, Z. Wang, W. Xu, J. Liu, F. Gao, L. Kovarik, J.-G. Zhang, J. Howe, D. J. Burton, Z. Liu, X. Xiao, S. Thevuthasan and D. R. Baer, *Nano Lett.*, 2012, **12**, 1624–1632.
212 B. Key, R. Bhattacharyya, M. Morcrette, V. Seznéc, J.-M. Tarascon and C. P. Grey, *J. Am. Chem. Soc.*, 2009, **131**, 9239–9249.
213 W. Xu, J. Wang, F. Ding, X. Chen, E. Nasybulin, Y. Zhang and J.-G. Zhang, *Energy Environ. Sci.*, 2014, **7**, 513–537.
214 J.-F. Ding, Y.-T. Zhang, R. Xu, R. Zhang, Y. Xiao, S. Zhang, C.-X. Bi, C. Tang, R. Xiang, H. S. Park, Q. Zhang and J.-Q. Huang, *Green Energy Environ.*, 2023, **8**, 1509–1530.
215 D. Lin, Y. Liu and Y. Cui, *Nat. Nanotechnol.*, 2017, **12**, 194–206.
216 J. Liu, Z. Bao, Y. Cui, E. J. Dufek, J. B. Goodenough, P. Khalifah, Q. Li, B. Y. Liaw, P. Liu, A. Manthiram, Y. S. Meng, V. R. Subramanian, M. F. Toney, V. V. Viswanathan, M. S. Whittingham, J. Xiao, W. Xu, J. Yang, X.-Q. Yang and J.-G. Zhang, *Nat Energy*, 2019, **4**, 180–186.
217 B. Liu, J.-G. Zhang and W. Xu, *Joule*, 2018, **2**, 833–845.
218 J. Wagner-Henke, D. Kuai, M. Gerasimov, F. Röder, P. B. Balbuena and U. Krewer, *Nat. Commun.*, 2023, **14**, 6823.
219 X. He, D. Bresser, S. Passerini, F. Baakes, U. Krewer, J. Lopez, C. T. Mallia, Y. Shao-Horn, I. Cekic-Laskovic, S. Wiemers-Meyer, F. A. Soto, V. Ponce, J. M. Seminario, P. B. Balbuena, H. Jia, W. Xu, Y. Xu, C. Wang, B. Horstmann, R. Amine, C.-C. Su, J. Shi, K. Amine, M. Winter, A. Latz and R. Kostecki, *Nat. Rev. Mater.*, 2021, **6**, 1036–1052.
220 B. Horstmann, J. Shi, R. Amine, M. Werres, X. He, H. Jia, F. Hausen, I. Cekic-Laskovic, S. Wiemers-Meyer, J. Lopez, D. Galvez-Aranda, F. Baakes, D. Bresser, C.-C. Su, Y. Xu, W. Xu, P. Jakes, R.-A. Eichel, E. Figgemeier, U. Krewer, J. M. Seminario, P. B. Balbuena, C. Wang, S. Passerini, Y. Shao-Horn, M. Winter, K. Amine, R. Kostecki and A. Latz, *Energy Environ. Sci.*, 2021, **14**, 5289–5314.
221 Q.-K. Zhang, X.-Q. Zhang, J. Wan, N. Yao, T.-L. Song, J. Xie, L.-P. Hou, M.-Y. Zhou, X. Chen, B.-Q. Li, R. Wen, H.-J. Peng, Q. Zhang and J.-Q. Huang, *Nat. Energy*, 2023, **8**, 725–735.
222 J. Chen, X. Fan, Q. Li, H. Yang, M. R. Khoshi, Y. Xu, S. Hwang, L. Chen, X. Ji, C. Yang, H. He, C. Wang, E. Garfunkel, D. Su, O. Borodin and C. Wang, *Nat. Energy*, 2020, **5**, 386–397.
223 X. Zheng, L. Huang, W. Luo, H. Wang, Y. Dai, X. Liu, Z. Wang, H. Zheng and Y. Huang, *ACS Energy Lett.*, 2021, **6**, 2054–2063.
224 Z. Yu, P. E. Rudnicki, Z. Zhang, Z. Huang, H. Celik, S. T. Oyakhire, Y. Chen, X. Kong, S. C. Kim, X. Xiao, H. Wang, Y. Zheng, G. A. Kamat, M. S. Kim, S. F. Bent, J. Qin, Y. Cui and Z. Bao, *Nat. Energy*, 2022, **7**, 94–106.
225 Z. Yu, H. Wang, X. Kong, W. Huang, Y. Tsao, D. G. Mackanic, K. Wang, X. Wang, W. Huang, S. Choudhury, Y. Zheng, C. V. Amanchukwu, S. T. Hung, Y. Ma, E. G. Lomeli, J. Qin, Y. Cui and Z. Bao, *Nat. Energy*, 2020, **5**, 526–533.
226 X.-Q. Zhang, X.-B. Cheng, X. Chen, C. Yan and Q. Zhang, *Adv. Funct. Mater.*, 2017, **27**, 1605989.
227 Y. Liu, D. Lin, Y. Li, G. Chen, A. Pei, O. Nix, Y. Li and Y. Cui, *Nat. Commun.*, 2018, **9**, 3656.
228 W. Li, H. Yao, K. Yan, G. Zheng, Z. Liang, Y.-M. Chiang and Y. Cui, *Nat. Commun.*, 2015, **6**, 7436.
229 Y. Lu, Z. Tu and L. A. Archer, *Nat. Mater.*, 2014, **13**, 961–969.
230 A. Le Ma, A. Buckel, A. Hofmann, L. Nyholm and R. Younesi, *Adv. Sci.*, 2023, e2306771.
231 A. Buckel, C. A. Hall, A. Le Ma, L. O. S. Colbin, H. Eriksson, R. Mogensen and R. Younesi, *Batteries Supercaps*, 2023, e202300533.
232 J. Sun, I. E. Gunathilaka, L. A. O'Dell, P. C. Howlett and M. Forsyth, *J. Electrochem. Soc.*, 2023, **554**, 232298.
233 X. Cui, F. Tang, C. Li, Y. Zhang, P. Wang, S. Li and X. Ye, *Energy Technol.*, 2017, **5**, 549–556.
234 S. H. Ng, C. Vix-Guterl, P. Bernardo, N. Tran, J. Ufheil, H. Buqa, J. Dentzer, R. Gadiou, M. E. Spahr, D. Goers and P. Novák, *Carbon*, 2009, **47**, 705–712.
235 R. Fong, U. von Sacken and J. R. Dahn, *J. Electrochem. Soc.*, 1990, **137**, 2009–2013.
236 M. E. Spahr, D. Goers, W. Märkle, J. Dentzer, A. Würsig, H. Buqa, C. Vix-Guterl and P. Novák, *Electrochim. Acta*, 2010, **55**, 8928–8937.
237 W. Märkle, C.-Y. Lu and P. Novák, *J. Electrochem. Soc.*, 2011, **158**, A1478.
238 D. Goers, M. E. Spahr, A. Leone, W. Märkle and P. Novák, *Electrochim. Acta*, 2011, **56**, 3799–3808.
239 N. Zhang, A. Eldesoky, R. A. Dressler and J. R. Dahn, *J. Electrochem. Soc.*, 2023, **170**, 70517.
240 D. Xiong, J. C. Burns, A. J. Smith, N. Sinha and J. R. Dahn, *J. Electrochem. Soc.*, 2011, **158**, A1431.
241 D. Aurbach, K. Gamolsky, B. Markovsky, Y. Gofer, M. Schmidt and U. Heider, *Electrochim. Acta*, 2002, **47**, 1423–1439.
242 T. Placke, V. Siozios, S. Rothermel, P. Meister, C. Colle and M. Winter, *Z. Phys. Chem.*, 2015, **229**, 1451–1469.
243 M. Tang, K. Miyazaki, T. Abe and J. Newman, *J. Electrochem. Soc.*, 2012, **159**, A634–A641.
244 S. Müllner, T. Held, T. Tichter, P. Rank, D. Leykam, W. Jiang, T. Lunkenbein, T. Gerdes and C. Roth, *J. Electrochem. Soc.*, 2023, **170**, 70523.
245 P. Ganesh, P. R. C. Kent and D. Jiang, *J. Phys. Chem. C*, 2012, **116**, 24476–24481.
246 J. M. La. Martinez de Hoz, K. Leung and P. B. Balbuena, *ACS Appl. Mater. Interfaces*, 2013, **5**, 13457–13465.
247 J. Sun, L. Huang, G. Xu, S. Dong, C. Wang and G. Cui, *Mater. Today*, 2022, **58**, 110–118.
248 X. Liu, Z. Wu, L. Xie, L. Sheng, J. Liu, L. Wang, K. Wu and X. He, *Energy Environ. Mater.*, 2023, **6**, e12501.

249 C. Yang, H. Ma, R. Yuan, K. Wang, K. Liu, Y. Long, F. Xu, L. Li, H. Zhang, Y. Zhang, X. Li and H. Wu, *Nat Energy*, 2023, **8**, 703–713.
250 F. Wang, B. Wang, J. Li, B. Wang, Y. Zhou, D. Wang, H. Liu and S. Dou, *ACS Nano*, 2021, **15**, 2197–2218.
251 V. L. Chevrier, L. Liu, R. Wohl, A. Chandrasoma, J. A. Vega, K. W. Eberman, P. Stegmaier and E. Figgemeier, *J. Electrochem. Soc.*, 2018, **165**, A1129–A1136.
252 E. Esen, M. Mohrhardt, P. Lennartz, I. de Meatza, M. Schmuck, M. Winter and E. Paillard, *Mater. Today Chem.*, 2023, **30**, 101587.
253 Y. Sun, H.-W. Lee, Z. W. Seh, N. Liu, J. Sun, Y. Li and Y. Cui, *Nat Energy*, 2016, **1**, 15008.
254 D. Witt, D. Wilde, F. Baakes, F. Belkhir, F. Röder and U. Krewer, *Energy Technol.*, 2021, **9**, 2000989.
255 D. H. Jeon, *Energy Storage Mater.*, 2019, **18**, 139–147.
256 F. J. Günter, C. Burgstaller, F. Konwitschny and G. Reinhart, *J. Electrochem. Soc.*, 2019, **166**, A1709–A1714.
257 S. N. Lauro, J. N. Burrow and C. B. Mullins, *eScience*, 2023, **3**, 100152.
258 V. de Lauri, L. Krumbein, S. Hein, B. Prifling, V. Schmidt, T. Danner and A. Latz, *ACS Appl. Energy Mater.*, 2021, **4**, 13847–13859.
259 J. Keilhofer, L. W. F. Schaffranka, A. Wuttke, F. J. Günter, L. Hille, F. A. Dorau and R. Daub, *Energy Technol.*, 2023, **11**, 2200869.
260 J. Kriegler, L. Hille, S. Stock, L. Kraft, J. Hagemeister, J. B. Habedank, A. Jossen and M. F. Zaeh, *Appl. Energy*, 2021, **303**, 117693.
261 L. Hille, H.-C. Toepper, C. Schriever, J. Kriegler, J. Keilhofer, M. P. Noecker and M. F. Zaeh, *J. Electrochem. Soc.*, 2022, **169**, 60518.
262 N. Dunlap, D. B. Sulas-Kern, P. J. Weddle, F. Usseglio-Viretta, P. Walker, P. Todd, D. Boone, A. M. Colclasure, K. Smith, B. J. Tremolet de Villers and D. P. Finegan, *J. Electrochem. Soc.*, 2022, **537**, 231464.
263 L.-L. Lu, Y.-Y. Lu, Z.-X. Zhu, J.-X. Shao, H.-B. Yao, S. Wang, T.-W. Zhang, Y. Ni, X.-X. Wang and S.-H. Yu, *Sci. Adv.*, 2022, **8**, eabm6624.
264 R. Schmuch, R. Wagner, G. Hörpel, T. Placke and M. Winter, *Nat. Energy*, 2018, **3**, 267–278.
265 K. Xu, *Chem. Rev.*, 2004, **104**, 4303–4417.
266 X. Fan and C. Wang, *Chem. Soc. Rev.*, 2021, **50**, 10486–10566.
267 B. Flamme, G. Rodriguez Garcia, M. Weil, M. Haddad, P. Phansavath, V. Ratovelomanana-Vidal and A. Chagnes, *Green Chem.*, 2017, **19**, 1828–1849.
268 S. S. Zhang, *J. Electrochem. Soc.*, 2006, **162**, 1379–1394.
269 W. Zhao, Y. Ji, Z. Zhang, M. Lin, Z. Wu, X. Zheng, Q. Li and Y. Yang, *Curr. Opin. Electrochem.*, 2017, **6**, 84–91.
270 A. M. Haregewoin, A. S. Wotango and B.-J. Hwang, *Energy Environ. Sci.*, 2016, **9**, 1955–1988.
271 V. Aravindan, J. Gnanaraj, S. Madhavi and H.-K. Liu, *Chem. Eur. J.*, 2011, **17**, 14326–14346.
272 S. Lei, Z. Zeng, S. Cheng and J. Xie, *Battery Energy*, 2023, **2**, 20230018.
273 D. Zhang, L. Li, W. Zhang, M. Cao, H. Qiu and X. Ji, *Chinese Chem. Lett.*, 2023, **34**, 107122.
274 U. S. Meda, L. Lal and P. Garg, *J. Energy Storage*, 2022, **47**, 103564.
275 J. Xu, *Nano-Micro Lett.*, 2022, **14**, 166.
276 V. S. K. Sungjemmenla, C. B. Soni, V. Kumar and Z. W. Seh, *Energy Technol.*, 2022, **10**, 2200421.
277 H. Wang, X. Li, F. Li, X. Liu, S. Yang and J. Ma, *Electrochem. Commun.*, 2021, **122**, 106870.
278 S. Leroy, H. Martinez, R. Dedryvère, D. Lemordant and D. Gonbeau, *Appl. Surf. Sci.*, 2007, **253**, 4895–4905.
279 M. Nie and B. L. Lucht, *J. Electrochem. Soc.*, 2014, **161**, A1001–A1006.
280 B. S. Parimalam and B. L. Lucht, *J. Electrochem. Soc.*, 2018, **165**, A251–A255.
281 P. Yan, M. Shevchuk, C. Wölke, F. Pfeiffer, D. Berghus, M. Baghernejad, G.-V. Röschenthaler, M. Winter and I. Cekic-Laskovic, *Small Struct.*, 2023, 2300425.
282 M. Nie, D. P. Abraham, D. M. Seo, Y. Chen, A. Bose and B. L. Lucht, *J. Phys. Chem. C*, 2013, **117**, 25381–25389.
283 R. Petibon, L. Madec, D. W. Abarbanel and J. R. Dahn, *J. Electrochem. Soc.*, 2015, **300**, 419–429.
284 X. Fan, L. Chen, X. Ji, T. Deng, S. Hou, J. Chen, J. Zheng, F. Wang, J. Jiang, K. Xu and C. Wang, *Chem*, 2018, **4**, 174–185.
285 Z. Shadike, H. Lee, O. Borodin, X. Cao, X. Fan, X. Wang, R. Lin, S.-M. Bak, S. Ghose, K. Xu, C. Wang, J. Liu, J. Xiao, X.-Q. Yang and E. Hu, *Nat. Nanotechnol.*, 2021, **16**, 549–554.
286 O. Borodin, X. Ren, J. Vatamanu, A. von Wald Cresce, J. Knap and K. Xu, *Acc. Chem. Res.*, 2017, **50**, 2886–2894.
287 D. Aurbach, *J. Electrochem. Soc.*, 2000, **89**, 206–218.
288 V. Ponnuchamy, S. Mossa and I. Skarmoutsos, *J. Phys. Chem. C*, 2018, **122**, 25930–25939.
289 H. Haghkhah, B. Ghalami Choobar and S. Amjad-Iranagh, *J. Mol. Model.*, 2020, **26**, 220.
290 A. L. Michan, M. Leskes and C. P. Grey, *Chem. Mater.*, 2016, **28**, 385–398.
291 H. Ota, Y. Sakata, A. Inoue and S. Yamaguchi, *J. Electrochem. Soc.*, 2004, **151**, A1659.
292 D. M. Seo, S. Reininger, M. Kutcher, K. Redmond, W. B. Euler and B. L. Lucht, *J. Phys. Chem. C*, 2015, **119**, 14038–14046.
293 T. Li and P. B. Balbuena, *Chem. Phys. Lett.*, 2000, **317**, 421–429.
294 J. Jones, M. Anouti, M. Caillon-Caravanier, P. Willmann and D. Lemordant, *Fluid Phase Equilib.*, 2009, **285**, 62–68.
295 J. Jones, M. Anouti, M. Caillon-Caravanier, P. Willmann, P.-Y. Sizaret and D. Lemordant, *Fluid Phase Equilib.*, 2011, **305**, 121–126.
296 P. Sayavong, W. Zhang, S. T. Oyakhire, D. T. Boyle, Y. Chen, S. C. Kim, R. A. Vilá, S. E. Holmes, M. S. Kim, S. F. Bent, Z. Bao and Y. Cui, *J. Am. Chem. Soc.*, 2023, **145**, 12342–12350.
297 K. Tasaki and S. J. Harris, *J. Phys. Chem. C*, 2010, **114**, 8076–8083.

298 K. Tasaki, A. Goldberg, J.-J. Lian, M. Walker, A. Timmons and S. J. Harris, *J. Electrochem. Soc.*, 2009, **156**, A1019.
299 D. T. Boyle, W. Huang, H. Wang, Y. Li, H. Chen, Z. Yu, W. Zhang, Z. Bao and Y. Cui, *Nat Energy*, 2021, **6**, 487–494.
300 C. H. Lee, J. A. Dura, A. LeBar and S. C. DeCaluwe, *J. Electrochem. Soc.*, 2019, **412**, 725–735.
301 C. Jin, Y. Huang, L. Li, G. Wei, H. Li, Q. Shang, Z. Ju, G. Lu, J. Zheng, O. Sheng and X. Tao, *Nat. Commun.*, 2023, **14**, 8269.
302 S. M. Wood, C. Fang, E. J. Dufek, S. C. Nagpure, S. V. Sazhin, B. Liaw and Y. S. Meng, *Adv. Energy Mater.*, 2018, **8**.
303 R. Yazami and Y. Reynier, *Electrochim. Acta*, 2002, **47**, 1217–1223.
304 Y.-F. Tian, S.-J. Tan, C. Yang, Y.-M. Zhao, D.-X. Xu, Z.-Y. Lu, G. Li, J.-Y. Li, X.-S. Zhang, C.-H. Zhang, J. Tang, Y. Zhao, F. Wang, R. Wen, Q. Xu and Y.-G. Guo, *Nat. Commun.*, 2023, **14**, 7247.
305 K. Ushirogata, K. Sodeyama, Z. Futera, Y. Tateyama and Y. Okuno, *J. Electrochem. Soc.*, 2015, **162**, A2670–A2678.
306 M. Esmaeilpour, S. Jana, H. Li, M. Soleymanibrojeni and W. Wenzel, *Adv. Energy Mater.*, 2023, 2203966.
307 O. Borodin, G. V. Zhuang, P. N. Ross and K. Xu, *J. Phys. Chem. C*, 2013, **117**, 7433–7444.
308 C.-C. Su, M. He, R. Amine, T. Rojas, L. Cheng, A. T. Ngo and K. Amine, *Energy Environ. Sci.*, 2019, **12**, 1249–1254.
309 R. W. Schmitz, P. Murmann, R. Schmitz, R. Müller, L. Krämer, J. Kasnatscheew, P. Isken, P. Niehoff, S. Nowak, G.-V. Röschenthaler, N. Ignatiev, P. Sartori, S. Passerini, M. Kunze, A. Lex-Balducci, C. Schreiner, I. Cekic-Laskovic and M. Winter, *Prog. Solid State Chem.*, 2014, **42**, 65–84.
310 K. Kim, D. Hwang, S. Kim, S. O. Park, H. Cha, Y.-S. Lee, J. Cho, S. K. Kwak and N.-S. Choi, *Adv. Energy Mater.*, 2020, **10**, 2000012.
311 J.-P. Schmiegel, R. Nölle, J. Henschel, L. Quach, S. Nowak, M. Winter, F. Glorius and T. Placke, *Cell Rep. Phys. Sci.*, 2021, **2**, 100327.
312 D. Y. Wang, J. Xia, L. Ma, K. J. Nelson, J. E. Harlow, D. Xiong, L. E. Downie, R. Petibon, J. C. Burns, A. Xiao, W. M. Lamanna and J. R. Dahn, *J. Electrochem. Soc.*, 2014, **161**, A1818–A1827.
313 S. Dalavi, P. Guduru and B. L. Lucht, *J. Electrochem. Soc.*, 2012, **159**, A642–A646.
314 L. Chen, K. Wang, X. Xie and J. Xie, *J. Electrochem. Soc.*, 2007, **174**, 538–543.
315 J. C. Burns, R. Petibon, K. J. Nelson, N. N. Sinha, A. Kassam, B. M. Way and J. R. Dahn, *J. Electrochem. Soc.*, 2013, **160**, A1668–A1674.
316 V. Winkler, G. Kilibarda, S. Schlabach, D. V. Szabó, T. Hanemann and M. Bruns, *J. Phys. Chem. C*, 2016, **120**, 24706–24714.
317 F. Lindgren, C. Xu, L. Niedzicki, M. Marcinek, T. Gustafsson, F. Björefors, K. Edström and R. Younesi, *ACS Appl. Mater. Interfaces*, 2016, **8**, 15758–15766.
318 N.-S. Choi, K. H. Yew, K. Y. Lee, M. Sung, H. Kim and S.-S. Kim, *J. Electrochem. Soc.*, 2006, **161**, 1254–1259.
319 Y. Li, F. Lian, L. Ma, C. Liu, L. Yang, X. Sun and K. Chou, *Electrochim. Acta*, 2015, **168**, 261–270.
320 H. Nakai, T. Kubota, A. Kita and A. Kawashima, *J. Electrochem. Soc.*, 2011, **158**, A798–A801.
321 S.-K. Jeong, M. Inaba, R. Mogi, Y. Iriyama, T. Abe and Z. Ogumi, *Langmuir*, 2001, **17**, 8281–8286.
322 C. Xu, F. Lindgren, B. Philippe, M. Gorgoi, F. Björefors, K. Edström and T. Gustafsson, *Chem. Mater.*, 2015, **27**, 2591–2599.
323 J. M. La Martínez de Hoz and P. B. Balbuena, *Phys. Chem. Chem. Phys.*, 2014, **16**, 17091–17098.
324 W. Zhao, G. Zheng, M. Lin, W. Zhao, D. Li, X. Guan, Y. Ji, G. F. Ortiz and Y. Yang, *J. Electrochem. Soc.*, 2018, **380**, 149–157.
325 B. Yang, H. Zhang, L. Yu, W. Fan and D. Huang, *Electrochim. Acta*, 2016, **221**, 107–114.
326 K.-E. Kim, J. Y. Jang, I. Park, M.-H. Woo, M.-H. Jeong, W. C. Shin, M. Ue and N.-S. Choi, *Electrochem. Commun.*, 2015, **61**, 121–124.
327 S. Tan, Z. Shadike, J. Li, X. Wang, Y. Yang, R. Lin, A. Cresce, J. Hu, A. Hunt, I. Waluyo, L. Ma, F. Monaco, P. Cloetens, J. Xiao, Y. Liu, X.-Q. Yang, K. Xu and E. Hu, *Nat. Energy*, 2022, **7**, 484–494.
328 Q. Lei, T. Yang, X. Zhao, W. Fan, W. Wang, L. Yu, S. Guo, X. Zuo, R. Zeng and J. Nan, *J. Electroanal. Chem.*, 2019, **846**, 113141.
329 C. Wang, L. Yu, W. Fan, J. Liu, L. Ouyang, L. Yang and M. Zhu, *ACS Appl. Energy Mater*, 2018, **1**, 2647–2656.
330 S. Klein, P. Harte, J. Henschel, P. Bärmann, K. Borzutzki, T. Beuse, S. van Wickeren, B. Heidrich, J. Kasnatscheew, S. Nowak, M. Winter and T. Placke, *Adv. Energy Mater.*, 2021, **11**, 2003756.
331 S. Klein, P. Harte, S. van Wickeren, K. Borzutzki, S. Röser, P. Bärmann, S. Nowak, M. Winter, T. Placke and J. Kasnatscheew, *Cell Rep. Phys. Sci.*, 2021, **2**, 100521.
332 J.-G. Han, J. B. Lee, A. Cha, T. K. Lee, W. Cho, S. Chae, S. J. Kang, S. K. Kwak, J. Cho, S. Y. Hong and N.-S. Choi, *Energy Environ. Sci.*, 2018, **11**, 1552–1562.
333 A. Ghaur, C. Peschel, I. Dienwiebel, L. Haneke, L. Du, L. Profanter, A. Gomez-Martin, M. Winter, S. Nowak and T. Placke, *Adv. Energy Mater.*, 2023, **13**, 2203503.
334 S. Park, S. Y. Jeong, T. K. Lee, M. W. Park, H. Y. Lim, J. Sung, J. Cho, S. K. Kwak, S. Y. Hong and N.-S. Choi, *Nat. Commun.*, 2021, **12**, 838.
335 D. S. Hall, J. Li, K. Lin, N. Stakheiko, J. Baltazar and J. R. Dahn, *J. Electrochem. Soc.*, 2019, **166**, A793–A801.
336 D. S. Hall, T. Hynes and J. R. Dahn, *J. Electrochem. Soc.*, 2018, **165**, A2961–A2967.
337 B. Koo, J. Lee, Y. Lee, J. K. Kim and N.-S. Choi, *Electrochim. Acta*, 2015, **173**, 750–756.
338 W. Song, J. Harlow, E. Logan, H. Hebecker, M. Coon, L. Molino, M. Johnson, J. Dahn and M. Metzger, *J. Electrochem. Soc.*, 2021, **168**, 90503.

339 D. Y. Wang, N. N. Sinha, R. Petibon, J. C. Burns and J. R. Dahn, *J. Electrochem. Soc.*, 2014, **251**, 311–318.
340 D. Y. Wang and J. R. Dahn, *J. Electrochem. Soc.*, 2014, **161**, A1890–A1897.
341 Y. Wang, S. Nakamura, K. Tasaki and P. B. Balbuena, *J. Am. Chem. Soc.*, 2002, **124**, 4408–4421.
342 F. A. Soto, Y. Ma, J. M. La Martinez de Hoz, J. M. Seminario and P. B. Balbuena, *Chem. Mater.*, 2015, **27**, 7990–8000.
343 L. D. Gibson and J. Pfaendtner, *Phys. Chem. Chem. Phys.*, 2020, **22**, 21494–21503.
344 J. Tan, J. Matz, P. Dong, J. Shen and M. Ye, *Adv. Energy Mater.*, 2021, **11**, 2100046.
345 Y. Yuan, F. Wu, Y. Bai, Y. Li, G. Chen, Z. Wang and C. Wu, *Energy Storage Mater.*, 2019, **16**, 411–418.
346 J. Pan, Y.-T. Cheng and Y. Qi, *Phys. Rev. B: Condens. Matter Mater. Phys.*, 2015, **91**, 134116.
347 H. Yildirim, A. Kinaci, M. K. Y. Chan and J. P. Greeley, *ACS Appl. Mater. Interfaces*, 2015, **7**, 18985–18996.
348 Y. Zhu, X. He and Y. Mo, *ACS Appl. Mater. Interfaces*, 2015, **7**, 23685–23693.
349 L. Suo, W. Xue, M. Gobet, S. G. Greenbaum, C. Wang, Y. Chen, W. Yang, Y. Li and J. Li, *Proc. Natl. Acad. Sci. U. S. A.*, 2018, **115**, 1156–1161.
350 G. M. Hobold, J. Lopez, R. Guo, N. Minafra, A. Banerjee, Y. Shirley Meng, Y. Shao-Horn and B. M. Gallant, *Nat Energy*, 2021, **6**, 951–960.
351 N. Lingappan, W. Lee, S. Passerini and M. Pecht, *Renewable Sustainable Energy Rev.*, 2023, **187**, 113726.
352 C. Man, P. Jiang, K. Wong, Y. Zhao, C. Tang, M. Fan, W. Lau, J. Mei, S. Li, H. Liu and D. Hui, *J. Mater. Chem. A*, 2014, **2**, 11980–11986.
353 M. F. Lagadec, R. Zahn and V. Wood, *J. Electrochem. Soc.*, 2018, **165**, A1829–A1836.
354 M. Frankenberger, M. Trunk, S. Seidlmayer, A. Dinter, J. Dittloff, L. Werner, R. Gernhäuser, Z. Revay, B. Märkisch, R. Gilles and K.-H. Pettinger, *Batteries*, 2020, **6**, 21.
355 D. Beck, P. Dechent, M. Junker, D. U. Sauer and M. Dubarry, *Energies*, 2021, **14**, 3276.
356 G. Bridgewater, M. J. Capener, J. Brandon, M. J. Lain, M. Copley and E. Kendrick, *Batteries*, 2021, **7**, 38.
357 N. Li, L. Fu and K. Jiang, *EC*, 2020, **37**, 1195–1211.
358 Y. Xiang, M. Tao, X. Chen, P. Shan, D. Zhao, J. Wu, M. Lin, X. Liu, H. He, W. Zhao, Y. Hu, J. Chen, Y. Wang and Y. Yang, *Nat. Commun.*, 2023, **14**, 177.
359 K. H. Min, S. M. Hwang, J. Cho, T. Jung, J. S. Son, C. Han, H. S. Lee, B. T. Yang, H. S. Baik, S. J. Jung, S. H. Kim, K. H. Song, S. H. Park and B. G. Kim, *US Pat.*, US2013244095 (A1), 2013.
360 S. Cho, *KR Pat.*, KR20170022391 (A), 2015.
361 H.-J. Park, M.-H. Kim, J.-S. Bae, E.-K. Lee, J.-W. Heo and S.-H. Hong, *KR Pat.*, KR20180062835 (A), 2016.
362 B. Lindemann and J. Gatz, *DE Pat.*, DE102017223231 (A1), 2017.
363 M. Yoshio, R. J. Brodd and A. Kozawa, *Lithium-Ion Batteries*, Springer New York, New York, NY, 2009.
364 J. T. Warner, *Lithium-Ion Battery Chemistries: A Primer*, Elsevier, 2019.
365 F. Dai and M. Cai, *Commun. Mater.*, 2022, 3.
366 D. Schreiner, T. Zünd, F. J. Günter, L. Kraft, B. Stumper, F. Linsenmann, M. Schüßler, R. Wilhelm, A. Jossen, G. Reinhart and H. A. Gasteiger, *J. Electrochem. Soc.*, 2021, **168**, 30507.
367 B. Gyenes, D. A. Stevens, V. L. Chevrier and J. R. Dahn, *J. Electrochem. Soc.*, 2015, **162**, A278–A283.
368 J. Wilhelm, S. Seidlmayer, P. Keil, J. Schuster, A. Kriele, R. Gilles and A. Jossen, *J. Electrochem. Soc.*, 2017, **365**, 327–338.
369 T. Roth, L. Streck, A. Graule, P. Niehoff and A. Jossen, *J. Electrochem. Soc.*, 2023, **170**, 20502.
370 M. Azzam, M. Ehrensberger, R. Scheuer, C. Endisch and M. Lewerenz, *Energies*, 2023, **16**, 3889.
371 T. Roth, L. Streck, N. Mujanovic, M. Winter, P. Niehoff and A. Jossen, *J. Electrochem. Soc.*, 2023, **170**, 80524.
372 J. P. Christophersen, Battery Test Manual For Electric Vehicles, Revision 3, 2015.
373 J. F. Plumeyer, N. Menebröker, H. Clever, L. Kokozinski, S. Wessel, H. H. Heimes and A. Kampker, *A Review of Process Innovations in the Cell Finishing of Lithium-Ion Batteries in Large-Scale Production*, Hannover: publish-Ing, 2023.
374 X. Li, X. Sun, X. Hu, F. Fan, S. Cai, C. Zheng and G. D. Stucky, *Nano Energy*, 2020, **77**, 105143.
375 F. Yang, D. Wang, Y. Zhao, K.-L. Tsui and S. J. Bae, *Energy*, 2018, **145**, 486–495.
376 R. Fathi, J. C. Burns, D. A. Stevens, H. Ye, C. Hu, G. Jain, E. Scott, C. Schmidt and J. R. Dahn, *J. Electrochem. Soc.*, 2014, **161**, A1572–A1579.
377 A. J. Smith, J. C. Burns, S. Trussler and J. R. Dahn, *J. Electrochem. Soc.*, 2010, **157**, A196.
378 A. Tornheim and D. C. O'Hanlon, *J. Electrochem. Soc.*, 2020, **167**, 110520.
379 J. Xiao, Q. Li, Y. Bi, M. Cai, B. Dunn, T. Glossmann, J. Liu, T. Osaka, R. Sugiura, B. Wu, J. Yang, J.-G. Zhang and M. S. Whittingham, *Nat Energy*, 2020, **5**, 561–568.
380 B. D. Adams, J. Zheng, X. Ren, W. Xu and J.-G. Zhang, *Adv. Energy Mater.*, 2018, **8**, 1702097.
381 F. Röder and S. Ramasubramanian, *Energy Technol*, 2022, **10**, 2200627.
382 A. J. Smith, J. C. Burns, X. Zhao, D. Xiong and J. R. Dahn, *J. Electrochem. Soc.*, 2011, **158**, A447.
383 P. Keil, S. F. Schuster, J. Wilhelm, J. Travi, A. Hauser, R. C. Karl and A. Jossen, *J. Electrochem. Soc.*, 2016, **163**, A1872–A1880.
384 A. H. Zimmerman, *IEEE Aerosp. Electron. Syst. Mag.*, 2004, **19**, 19–24.
385 L. Streck, T. Roth, P. Keil, B. Strehle, S. Ludmann and A. Jossen, *J. Electrochem. Soc.*, 2023, **170**, 40520.
386 H. Liao, B. Huang, Y. Cui, H. Qin, X. Liu and H. Xu, *J. Energy Storage*, 2022, **55**, 105431.
387 B. Epding, B. Rumberg, H. Jahnke, I. Stradtmann and A. Kwade, *J. Energy Storage*, 2019, **22**, 249–256.

388 A. Karger, J. Schmitt, C. Kirst, J. P. Singer, L. Wildfeuer and A. Jossen, *J. Electrochem. Soc.*, 2023, **578**, 233208.
389 M. Gaberšček, *Nat. Commun.*, 2021, **12**, 6513.
390 J. Li, E. Murphy, J. Winnick and P. A. Kohl, *J. Electrochem. Soc.*, 2001, **102**, 302–309.
391 C. Plank, T. Rüther, L. Jahn, M. Schamel, J. P. Schmidt, F. Ciucci and M. A. Danzer, *J. Electrochem. Soc.*, 2023, 233845.
392 U. Krewer, F. Röder, E. Harinath, R. D. Braatz, B. Bedürftig and R. Findeisen, *J. Electrochem. Soc.*, 2018, **165**, A3656–A3673.
393 T. Rüther, M. Schamel, C. Plank, F. Schomburg, F. Röder and M. A. Danzer, *J. Electrochem. Soc.*, 2023, **587**, 233677.
394 V. Müller, R. Kaiser, S. Poller and D. Sauerteig, *J. Energy Storage*, 2018, **15**, 256–265.
395 M. Petzl and M. A. Danzer, *J. Electrochem. Soc.*, 2014, **254**, 80–87.
396 S. E. J. O'Kane, I. D. Campbell, M. W. J. Marzook, G. J. Offer and M. Marinescu, *J. Electrochem. Soc.*, 2020, **167**, 90540.
397 A. Weng, J. B. Siegel and A. Stefanopoulou, *Front. Energy Res.*, 2023, **11**, 1087269.
398 S. Ludwig, I. Zilberman, M. F. Horsche, T. Wohlers and A. Jossen, *J. Electrochem. Soc.*, 2021, **490**, 229523.
399 S. Ludwig, M. Steinhardt and A. Jossen, *Batteries*, 2022, **8**, 60.
400 F. Leng, C. M. Tan and M. Pecht, *Sci. Rep.*, 2015, **5**, 12967.
401 W. Waag, S. Käbitz and D. U. Sauer, *Appl. Energy*, 2013, **102**, 885–897.
402 M. Ecker, J. B. Gerschler, J. Vogel, S. Käbitz, F. Hust, P. Dechent and D. U. Sauer, *J. Electrochem. Soc.*, 2012, **215**, 248–257.
403 M. J. Lacey, *ChemElectroChem*, 2017, **4**, 1997–2004.
404 D. Andre, M. Meiler, K. Steiner, C. Wimmer, T. Soczka-Guth and D. U. Sauer, *J. Electrochem. Soc.*, 2011, **196**, 5334–5341.
405 A. Barai, K. Uddin, W. D. Widanage, A. McGordon and P. Jennings, *Sci. Rep.*, 2018, **8**, 21.
406 G. Zampardi and F. La Mantia, *Batteries Supercaps*, 2020, **3**, 672–697.
407 T. Waldmann, A. Iturrondobeitia, M. Kasper, N. Ghanbari, F. Aguesse, E. Bekaert, L. Daniel, S. Genies, I. J. Gordon, M. W. Löble, E. de Vito and M. Wohlfahrt-Mehrens, *J. Electrochem. Soc.*, 2016, **163**, A2149–A2164.
408 F. Schomburg, R. Drees, M. Kurrat, M. A. Danzer and F. Röder, *Energy Technol.*, 2022, 2200688.
409 I. Bloom, A. N. Jansen, D. P. Abraham, J. Knuth, S. A. Jones, V. S. Battaglia and G. L. Henriksen, *J. Electrochem. Soc.*, 2005, **139**, 295–303.
410 I. Bloom, J. Christophersen and K. Gering, *J. Electrochem. Soc.*, 2005, **139**, 304–313.
411 I. Bloom, J. P. Christophersen, D. P. Abraham and K. L. Gering, *J. Electrochem. Soc.*, 2006, **157**, 537–542.
412 I. Bloom, L. K. Walker, J. K. Basco, D. P. Abraham, J. P. Christophersen and C. D. Ho, *J. Electrochem. Soc.*, 2010, **195**, 877–882.
413 S. Schindler and M. A. Danzer, *J. Electrochem. Soc.*, 2017, **343**, 226–236.
414 C. R. Birkl, M. R. Roberts, E. McTurk, P. G. Bruce and D. A. Howey, *J. Electrochem. Soc.*, 2017, **341**, 373–386.
415 L. B. Chen, J. Y. Xie, H. C. Yu and T. H. Wang, *J. Appl. Electrochem.*, 2009, **39**, 1157–1162.
416 J. E. Morales-Ugarte, E. Bolimowska, H. Rouault, J. Santos-Peña, C. C. Santini and A. Benayad, *J. Phys. Chem. C*, 2018, **122**, 18223–18230.
417 T. Momma, T. Yokoshima, H. Nara, Y. Gima and T. Osaka, *Electrochim. Acta*, 2014, **131**, 195–201.
418 B. Heidrich, M. Stamm, O. Fromm, J. Kauling, M. Börner, M. Winter and P. Niehoff, *J. Electrochem. Soc.*, 2023, **170**, 10530.
419 G. M. Hobold, K.-H. Kim and B. M. Gallant, *Energy Environ. Sci.*, 2023, **16**, 2247–2261.
420 J. O. Besenhard and M. Winter, *Pure Appl. Chem.*, 1998, **70**, 603–608.
421 T. S. Ortner, *Commun. Chem.*, 2021, **4**, 79.
422 W. Huang, P. M. Attia, H. Wang, S. E. Renfrew, N. Jin, S. Das, Z. Zhang, D. T. Boyle, Y. Li, M. Z. Bazant, B. D. McCloskey, W. C. Chueh and Y. Cui, *Nano Lett.*, 2019, **19**, 5140–5148.
423 F. Hofer, F. P. Schmidt, W. Grogger and G. Kothleitner, *IOP Conf. Ser.: Mater. Sci. Eng.*, 2016, **109**, 12007.
424 Y. Yuan, K. Amine, J. Lu and R. Shahbazian-Yassar, *Nat. Commun.*, 2017, **8**, 15806.
425 S. Bhattacharya and A. T. Alpas, *Carbon*, 2012, **50**, 5359–5371.
426 J. Wu, M. Fenech, R. F. Webster, R. D. Tilley and N. Sharma, *Sustainable Energy Fuels*, 2019, **3**, 1623–1646.
427 M. Steinhauer, M. Stich, M. Kurniawan, B.-K. Seidlhofer, M. Trapp, A. Bund, N. Wagner and K. A. Friedrich, *ACS Appl. Mater. Interfaces*, 2017, **9**, 35794–35801.
428 S. Y. Luchkin, S. A. Lipovskikh, N. S. Katorova, A. A. Savina, A. M. Abakumov and K. J. Stevenson, *Sci. Rep.*, 2020, **10**, 8550.
429 A. v Cresce, S. M. Russell, D. R. Baker, K. J. Gaskell and K. Xu, *Nano Lett.*, 2014, **14**, 1405–1412.
430 I. Yoon, D. P. Abraham, B. L. Lucht, A. F. Bower and P. R. Guduru, *Adv. Energy Mater.*, 2016, **6**, 1600099.
431 W. Zhao, W. Song, L.-Z. Cheong, D. Wang, H. Li, F. Besenbacher, F. Huang and C. Shen, *Ultramicroscopy*, 2019, **204**, 34–48.
432 P. Niehoff, S. Passerini and M. Winter, *Langmuir*, 2013, **29**, 5806–5816.
433 B. Heidrich, M. Börner, M. Winter and P. Niehoff, *J. Energy Storage*, 2021, **44**, 103208.
434 S. Wi, V. Shutthanandan, B. M. Sivakumar, S. Thevuthasan, V. Prabhakaran, S. Roy, A. Karakoti and V. Murugesan, *J. Vac. Sci. Technol., A*, 2022, **40**, 10808.
435 C. Kalha, N. K. Fernando, P. Bhatt, F. O. L. Johansson, A. Lindblad, H. Rensmo, L. Z. Medina, R. Lindblad, S. Siol, L. P. H. Jeurgens, C. Cancellieri, K. Rossnagel, K. Medjanik, G. Schönhense, M. Simon, A. X. Gray, S. Nemšák, P. Lömker, C. Schlueter and A. Regoutz, *J. Phys.: Condens.Matter*, 2021, **33**, 233001.

436 B. T. Young, C. C. Nguyen, A. Lobach, D. R. Heskett, J. C. Woicik and B. L. Lucht, *J. Mater. Res.*, 2019, **34**, 97–106.
437 I. V. Veryovkin, C. E. Tripa, A. V. Zinovev, S. V. Baryshev, Y. Li and D. P. Abraham, *Nucl. Instrum. Methods Phys. Res., Sect. B*, 2014, **332**, 368–372.
438 Z.-Y. Wu, L. Deng, J.-T. Li, S. Zanna, A. Seyeux, L. Huang, S.-G. Sun, P. Marcus and J. Światowska, *Batteries*, 2022, **8**, 271.
439 N. Gauthier, C. Courrèges, J. Demeaux, C. Tessier and H. Martinez, *Appl. Surf. Sci.*, 2020, **501**, 144266.
440 T. Sui, B. Song, J. Dluhos, L. Lu and A. M. Korsunsky, *Nano Energy*, 2015, **17**, 254–260.
441 M. Weiling, F. Pfeiffer and M. Baghernejad, *Adv. Energy Mater.*, 2022, **12**, 2202504.
442 D. Aurbach, M. L. Daroux, P. W. Faguy and E. Yeager, *J. Electrochem. Soc.*, 1987, **134**, 1611–1620.
443 C. P. Aiken, J. Xia, D. Y. Wang, D. A. Stevens, S. Trussler and J. R. Dahn, *J. Electrochem. Soc.*, 2014, **161**, A1548–A1554.
444 J.-P. Schmiegel, M. Leißing, F. Weddeling, F. Horsthemke, J. Reiter, Q. Fan, S. Nowak, M. Winter and T. Placke, *J. Electrochem. Soc.*, 2020, **167**, 60516.
445 S. Nowak and M. Winter, *J. Electrochem. Soc.*, 2015, **162**, A2500–A2508.
446 Y. Stenzel, F. Horsthemke, M. Winter and S. Nowak, *Separations*, 2019, **6**, 26.
447 S. Wiemers-Meyer, M. Winter and S. Nowak, *Phys. Chem. Chem. Phys.*, 2017, **19**, 4962–4966.
448 J. Z. Hu, N. R. Jaegers, M. Y. Hu and K. T. Mueller, *J. Phys.: Condens.Matter*, 2018, **30**, 463001.
449 U. Janakiraman, T. R. Garrick and M. E. Fortier, *J. Electrochem. Soc.*, 2020, **167**, 160552.
450 H. Takahara, M. Shikano and H. Kobayashi, *J. Electrochem. Soc.*, 2013, **244**, 252–258.
451 N. Ghanbari, T. Waldmann, M. Kasper, P. Axmann and M. Wohlfahrt-Mehrens, *J. Phys. Chem. C*, 2016, **120**, 22225–22234.
452 M. Flügel, K. Richter, M. Wohlfahrt-Mehrens and T. Waldmann, *J. Electrochem. Soc.*, 2022, **169**, 50533.
453 A. Wang, S. Kadam, H. Li, S. Shi and Y. Qi, *npj Comput Mater*, 2018, **4**, 15.
454 G. Ramos-Sanchez, F. A. Soto, J. M. La Martinez de Hoz, Z. Liu, P. P. Mukherjee, F. El-Mellouhi, J. M. Seminario and P. B. Balbuena, *J. Electrochem. Energy Convers. Storage*, 2016, **13**, 031002.
455 D. Atkins, E. Ayerbe, A. Benayad, F. G. Capone, E. Capria, I. E. Castelli, I. Cekic-Laskovic, R. Ciria, L. Dudy, K. Edström, M. R. Johnson, H. Li, J. M. G. Lastra, M. L. de Souza, V. Meunier, M. Morcrette, H. Reichert, P. Simon, J.-P. Rueff, J. Sottmann, W. Wenzel and A. Grimaud, *Adv. Energy Mater.*, 2022, **12**, 2102687.
456 X. Zhang, J. K. Pugh and P. N. Ross, *J. Electrochem. Soc.*, 2001, **148**, E183–E188.
457 L. Xing, O. Borodin, G. D. Smith and W. Li, *J. Phys. Chem. A*, 2011, **115**, 13896–13905.
458 T. A. Barnes, J. W. Kaminski, O. Borodin and T. F. Miller, *J. Phys. Chem. C*, 2015, **119**, 3865–3880.
459 S. A. Delp, O. Borodin, M. Olguin, C. G. Eisner, J. L. Allen and T. R. Jow, *Electrochim. Acta*, 2016, **209**, 498–510.
460 Y. Okamoto, *J. Electrochem. Soc.*, 2013, **160**, A404–A409.
461 L. Benitez, D. Cristancho, J. M. Seminario, J. M. La Martinez de Hoz and P. B. Balbuena, *Electrochim. Acta*, 2014, **140**, 250–257.
462 K. Leung and J. L. Budzien, *Phys. Chem. Chem. Phys.*, 2010, **12**, 6583–6586.
463 Y. Okamoto and Y. Kubo, *ACS omega*, 2018, **3**, 7868–7874.
464 S. M. Blau, H. D. Patel, E. W. C. Spotte-Smith, X. Xie, S. Dwaraknath and K. A. Persson, *Chem. Sci.*, 2021, **12**, 4931–4939.
465 X. Xie, E. W. Clark Spotte-Smith, M. Wen, H. D. Patel, S. M. Blau and K. A. Persson, *J. Am. Chem. Soc.*, 2021, **143**, 13245–13258.
466 O. Borodin and G. D. Smith, *J. Phys. Chem. B*, 2009, **113**, 1763–1776.
467 P. Ganesh, D. Jiang and P. R. C. Kent, *J. Phys. Chem. B*, 2011, **115**, 3085–3090.
468 O. Borodin, M. Olguin, C. E. Spear, K. W. Leiter and J. Knap, *Nanotechnology*, 2015, **26**, 354003.
469 J. M. La Martinez de Hoz, F. A. Soto and P. B. Balbuena, *J. Phys. Chem. C*, 2015, **119**, 7060–7068.
470 L. Xing, J. Vatamanu, O. Borodin, G. D. Smith and D. Bedrov, *J. Phys. Chem. C*, 2012, **116**, 23871–23881.
471 M. Broussely, S. Herreyre, P. Biensan, P. Kasztejna, K. Nechev and R. Staniewicz, *J. Power Sources*, 2001, **97–98**, 13–21.
472 A. M. Colclasure, K. A. Smith and R. J. Kee, *Electrochim. Acta*, 2011, **58**, 33–43.
473 H. J. Ploehn, P. Ramadass and R. E. White, *J. Electrochem. Soc.*, 2004, **151**, A456.
474 S. Shi, P. Lu, Z. Liu, Y. Qi, L. G. Hector, H. Li and S. J. Harris, *J. Am. Chem. Soc.*, 2012, **134**, 15476–15487.
475 Y.-X. Lin, Z. Liu, K. Leung, L.-Q. Chen, P. Lu and Y. Qi, *J. Power Sources*, 2016, **309**, 221–230.
476 M. Tang, S. Lu and J. Newman, *J. Electrochem. Soc.*, 2012, **159**, A1775–A1785.
477 K. Leung, Y. Qi, K. R. Zavadil, Y. S. Jung, A. C. Dillon, A. S. Cavanagh, S.-H. Lee and S. M. George, *J. Am. Chem. Soc.*, 2011, **133**, 14741–14754.
478 P. Keil and A. Jossen, *J. Electrochem. Soc.*, 2017, **164**, A6066–A6074.
479 F. Single, A. Latz and B. Horstmann, *ChemSusChem*, 2018, **11**, 1950–1955.
480 L. Köbbing, A. Latz and B. Horstmann, *J. Electrochem. Soc.*, 2023, **561**, 232651.
481 S. Ramasubramanian, F. Schomburg and F. Röder, *Electrochim. Acta*, 2024, **473**, 143479.
482 P. M. Attia, S. Das, S. J. Harris, M. Z. Bazant and W. C. Chueh, *J. Electrochem. Soc.*, 2019, **166**, E97–E106.
483 S. Das, P. M. Attia, W. C. Chueh and M. Z. Bazant, *J. Electrochem. Soc.*, 2019, **166**, E107–E118.

484 F. Single, B. Horstmann and A. Latz, *J. Electrochem. Soc.*, 2017, **164**, E3132–E3145.
485 W. Mai, A. Colclasure and K. Smith, *J. Electrochem. Soc.*, 2019, **166**, A1330–A1339.
486 L. Kolzenberg, A. Latz and B. Horstmann, *Batteries Supercaps*, 2022, **5**, e202100216.
487 D. Witt, F. Röder and U. Krewer, *Batteries Supercaps*, 2022, **5**, e202200067.
488 E. Peled, D. Golodnitsky and G. Ardel, *J. Electrochem. Soc.*, 1997, **144**, L208–L210.
489 E. Peled, D. Bar Tow, A. Merson, A. Gladkich, L. Burstein and D. Golodnitsky, *J. Power Sources*, 2001, **97–98**, 52–57.
490 R. N. Methekar, P. W. C. Northrop, K. Chen, R. D. Braatz and V. R. Subramanian, *J. Electrochem. Soc.*, 2011, **158**, A363.
491 F. Hao, Z. Liu, P. B. Balbuena and P. P. Mukherjee, *J. Phys. Chem. C*, 2017, **121**, 26233–26240.
492 F. Röder, R. D. Braatz and U. Krewer, *26th European Symposium on Computer Aided Process Engineering*, Elsevier, 2016, vol. 38, pp. 157–162.
493 M. Gerasimov, F. A. Soto, J. Wagner, F. Baakes, N. Guo, F. Ospina-Acevedo, F. Röder, P. B. Balbuena and U. Krewer, *J. Phys. Chem. C*, 2023, **127**, 4872–4886.
494 D. Barter, E. W. C. Spotte-Smith, N. S. Redkar, A. Khanwale, S. Dwaraknath, K. A. Persson and S. M. Blau, *Digital Discovery*, 2023, **2**, 123–137.
495 F. Röder, R. D. Braatz and U. Krewer, *J. Electrochem. Soc.*, 2017, **164**, E3335–E3344.
496 F. Röder, V. Laue and U. Krewer, *Batteries Supercaps*, 2019, **2**, 248–265.
497 L. Alzate-Vargas, S. M. Blau, E. W. C. Spotte-Smith, S. Allu, K. A. Persson and J.-L. Fattebert, *J. Phys. Chem. C*, 2021, **125**, 18588–18596.
498 E. M. Gavilán-Arriazu, M. P. Mercer, D. E. Barraco, H. E. Hoster and E. P. M. Leiva, *Prog. Energy*, 2021, **3**, 42001.
499 J. H. Seo, J. Park, G. Plett and A. M. Sastry, *Electrochem. Solid-State Lett*, 2010, **13**, A135.
500 M. Rashid and A. Gupta, *ECS Electrochem. Lett.*, 2014, **3**, A95–A98.
501 Y. Zou, Z. Cao, J. Zhang, W. Wahyudi, Y. Wu, G. Liu, Q. Li, H. Cheng, D. Zhang, G.-T. Park, L. Cavallo, T. D. Anthopoulos, L. Wang, Y.-K. Sun and J. Ming, *Adv. Mater.*, 2021, **33**, e2102964.
502 F. Hao, A. Verma and P. P. Mukherjee, *J. Mater. Chem. A*, 2018, **6**, 19664–19671.
503 W. Porcher and S. Lyonnard, *Nat. Energy*, 2023, **8**, 649–650.